EXPERIMENTAL INVESTIGATION ON PERFORMANCE AND EMISSIONS OF AN AUTOMOTIVE DIESEL ENGINE FUELLED WITH BIOFUELS

By
Ing. Theodoros G. Vlachos

Dissertation Submitted to the Doctorate School
of the Politecnico di Torino in Partial Fulfillment of the
Requirements for the Degree of

DOCTOR OF PHYLOSOPHY IN ENERGETICS
AT THE POLITECNICO DI TORINO

Tutor
Prof. Millo Federico

Scientific Committee
Prof. Ferraro Carlo Vincenzo
Prof. Onorati Angelo
Prof. Postrioti Lucio

May 2013

Φιλοκαλοῦμεν τε γὰρ μετ’ εὐτελείας
καὶ φιλοσοφοῦμεν ἄνευ μαλακίας

For we are lovers of the beautiful,
yet simple in our tastes,
and we cultivate the mind without loss of manliness

Thucydides,
History of the Peloponnesian War
"Funeral Oration of Pericles"

Translated by Benjamin Jowett,
Clarendon Press, 1900

Acknowledgments

This research was financially supported by MIUR (Ministero dell'Istruzione, dell'Università e della Ricerca) under the Cofin2009 Program “Analysis of last generation biodiesel fuel blends effects on performance and emissions of automotive common rail small displacement diesel engines”.

The valuable support from General Motors Powertrain Europe is also gratefully acknowledged. Special thanks, in particular, to Mr. Claudio Ciaravino for his constant support and his valuable suggestions.

Abstract

Biodiesel is the biofuel most commonly used in Europe, covering approximately 80% of the biofuel market. However, the relationship between biofuel industry and food prices push towards the adoption of new generation biodiesels which could minimize the impact of biofuels production on human food chain. Biodiesel sourced from non-edible seed oils like Jatropha Curcas could therefore be a viable solution for biodiesel production, since allows green cover to wasteland. More recently, also Hydrotreated Vegetable Oil (HVO), obtained by means of a refinery-based process that converts vegetable oils into paraffinic hydrocarbons, has been gaining an increasing attention.

The effects of using high percentage blends of ultra low sulphur diesel and biofuels (FAME and HVO) in a Euro 5 small displacement passenger car diesel engine on combustion process, full load performance and part load emissions have been evaluated in this work. Moreover, a characterization of Particulate Matter (PM) in terms of mass, chemical composition and particles number and size distribution was assessed as well.

The impacts that fuels with different physical and chemical properties may have on injection, combustion and on ECU calibration process were evaluated by means of specific tests campaign involving different injection timings under part load operation. Results highlighted that the implementation of models for blending detection, on engines ECUs, could be of crucial importance for a wider usage of biofuels in transportation sector.

In addition, the effects on engine torque were analyzed, for both a standard ECU calibration (i.e. without any special tuning for the different fuel characteristics) and for a specifically adjusted ECU calibration obtained by properly increasing the injected fuel quantities to compensate for the lower Lower Heating Value (LHV) of the biofuels: with the latter, the same torque levels measured under diesel operation could be observed with the biodiesel too, with lower smoke levels, thus highlighting the potential for maintaining the same level of performance while achieving substantial emissions benefits.

Moreover, the effects of biodiesel blends on brake specific fuel consumption and on engine-out exhaust emissions (CO_2, CO, HC, NO_x and smoke) were also evaluated at several part load operating conditions, representative of the New European Driving Cycle (NEDC). Both standard and specific calibrations were evaluated, highlighting an average rise of fuel consumption in good agreement with LHV decrease, at same fuel conversion efficiency and CO_2 emissions. A decrease of NO_x emissions when using a specifically adjusted engine calibration, along with a considerable smoke emission reduction were observed as well.

Due to increasing concerns about the hazardous effects that particulate matter could have on human health, PM emissions were evaluated under normal engine operating mode at part load operation. PM gravimetric analysis at medium and high load operating points showed a good correlation with soot measurements carried out by means of standard laboratory equipment (i.e. smokemeters). On the contrary, at low loads, the same instrument underestimated the Soluble Organic Fraction (SOF) fraction of PM especially when biofuel was used. Thermo-gravimetric analysis confirmed the outcomes from gravimetric analysis: the significance of standard measurements which are commonly carried out during the engine calibration activity should be carefully considered when biofuels are adopted.

Finally, the assessment of the toxicological potential of PM when HVO and Rapeseed Methyl Ester (RME) were used was carried out. Results highlighted that PM from HVO had a higher mutagenic effect respect to PM emissions obtained with other fuels.

List of Abbreviations

ACEA	Association des Constructeurs Européens d'Automobiles
BMEP	Brake Mean Effective Pressure
BSCO	Brake Specific CO
BSFC	Brake Specific Fuel Consumption
BSHC	Brake Specific HC
BSNO_x	Brake Specific NO_x
BTDC	Before Top Dead Center
CAFE	Corporate Average Fuel Economy
CARB	California Air Resources Board
CO	Carbon Monoxide
CR	Compression Ratio
DI	Direct Injection
DME	Dymethyl Ether
DOC	Diesel Oxidation Catalyst
DPF	Diesel Particulate Filter
DR	Dilution Ratio
DT	Dwell Time
ECU	Engine Control Unit
EGR	Exhaust Gas Recirculation
EPA	Environmental Protection Agency
ET	Energizing Time
ETP	Energy Technology Perspectives

EU	European Union
FA	Fatty Acid
FAME	Fatty Acid Methyl Ester
FSN	Filter Smoke Number
FT	Fischer-Tropsch synthesis process
GHG	Greenhouse Gases
HC	Unburned Hydrocarbons
HCCI	Homogeneous Charge Compression Ignition
HD	Heavy Duty
HEV	Hybrid Electric Vehicle
HRR	Heat Release Rate
HSDI	High Speed Direct Injection
HVO	Hydrotreated Vegetable Oil
IEA	International Energy Agency
ILUC	Indirect Land Use Change
IMEP	Indicated Mean Effective Pressure
JME	Jatropha Methyl Ester
LD	Light Duty
LDT	Light Duty Truck
LEV	Low Emission Vehicle
LHV	Lower Heating Value
LNT	Lean NO_x Trap
LTC	Low Temperature Combustion
MFB50	50% Mass Fraction Burned
mpg	Miles per gallons
MR	Mutagenicity Ratio
NEDC	New European Driving Cycle
NO_x	Nitrogen Oxides
OECD	Organization for Economic Co-operation Development
OEM	Original Equipment Manufacturer
PCCI	Premixed Combustion Compression Ignition
PM	Particulate Matter
PMP	Particulate Matter Programme
PN	Particle Number
ppm	Part per Million
RME	Rapeseed Methyl Ester
RN	Net Revertants
rpm	Revolution per minutes
SCR	Selective Catalytic Reduction
SME	Soy Methyl Ester

SMPS	Scanning Mobility Particle Sizer
SOF	Soluble Organic Fraction
SoI	Start of Injection
SULEV	Super Ultra Low Emission Vehicle
TAG	Triacylglycerols
TDC	Top Dead Center
TGA	Thermogravimetric Analysis
ULSD	Ultra Low Sulfur Diesel
VGT	Variable Geometry Turbocharger
WG	Waste Gate

List of Figures

Figure 1.1 CO2 reduction from Light-Duty Vehicles Under ACEA Agreement (Dieselnet, Emission Standards - Europe - Cars GHG - ACEA Agreements 2010) .. 9
Figure 1.2 Road map for NOx and PM emissions reduction, technological steps . 12
Figure 1.3 Global biofuel production 2000-2010 (source: IEA, 2010a)...................... 14
Figure 1.4 Share of biofuels in road transport energy consumption (March, 2012 WEC/Enerdata).. 15
Figure 1.5 Global energy use in the transport sector (left) and use of biofuels in different transport modes (right) in 2050 (BLUE Map Scenario).............................. 16
Figure 1.6 Contribution of biofuels to GHG emissions reduction in the transport sector 17
Figure 1.7 Biofuel demand by region 2010-50... 17
Figure 1.8 The transesterification reaction 18
Figure 1.9 HVO production process... 19
Figure 2.1 Distillation curves of tested fuels 24
Figure 2.2 Distillation curves for the diesel reference fuel and for the RME and HVO B30 blends 27
Figure 2.3 Viscosity vs. temperature for the diesel reference fuel and for the RME and HVO B30 blends.. 28
Figure 2.4 Scheme of the experimental test rig 29
Figure 2.5 Sweep of the start of the main injection.. 33

Figure 2.6 Partial flow dilution tunnel scheme 34
Figure 2.7 Sample mass loss as a function of sample temperature 37
Figure 2.8 Two stage dilution system (top); scheme of the first stage dilutor (bottom) 39
Figure 2.9 Particle number and size distribution comparison for long and short transfer line, 2000 rpm and 5 bar BMEP engine operating point 40
Figure 3.1 Full load engine performance with standard ECU calibration (left) and specific calibration (right) with all the tested fuels 46
Figure 3.2 Cylinder pressure trace and injector signal for all fuels at 1250 rpm and full load (standard calibration). 46
Figure 3.3 Intake manifold pressure during full load tests with standard (left) and specific (right) calibration and all fuels 46
Figure 3.4 Fuel conversion efficiency at full load for all fuels: standard calibration (left), specific calibration (right) 47
Figure 3.5 FSN reduction at full load for biodiesel blends compared to diesel: standard calibration (left), specific calibration (right) 47
Figure 3.6 Full load engine performance with diesel, RME B30 and HVO B30: standard calibration (left), specific calibration (right) 48
Figure 3.7 Fuel conversion efficiency at full load for all fuels: standard calibration (left), specific calibration (right) 49
Figure 3.8 Filter Smoke Numbers reduction for biofuels respect to diesel at full load with standard calibration 49
Figure 3.9 Accelerator pedal position for all fuels; standard calibration on the left and specific calibration on the right 51
Figure 3.10 Main injection energizing time for all fuels; standard calibration on the left and specific calibration on the right 51
Figure 3.11 Trapped air mass per cylinder for all fuels; standard calibration on the left and specific calibration on the right 51
Figure 3.12 Boost pressure for all fuels; standard calibration on the left and specific calibration on the right 52
Figure 3.13 EGR rate for all fuels; standard calibration on the left and specific calibration on the right 52
Figure 3.14 Relative air to fuel ratio (λ) for all fuels; standard calibration on the left and specific calibration on the right 52

Figure 3.15 Start of main injection for all fuels; standard calibration on the left and specific calibration on the right........ 53
Figure 3.16 50% of fuel mass burned for all fuels; standard calibration on the left and specific calibration on the right........ 53
Figure 3.17 Rail pressure for all fuels; standard calibration on the left and specific calibration on the right........ 53
Figure 3.18 Indicating analysis for the 1500 [rpm] @ 2 [bar] BMEP engine op. point for diesel, JME (B30) and JME (B100): in-cylinder pressure, heat release rate and injection pattern (top, figures a and b), heat release rate and mass fraction burned (bottom, figures c and d). 55
Figure 3.19 Indicating analysis for the 2000 [rpm] @ 5 [bar] BMEP engine op. point for diesel, JME (B30) and JME (B100): in-cylinder pressure, heat release rate and injection pattern (top portion, figures a and b), heat release rate and mass fraction burned (bottom, figures c and d)........ 56
Figure 3.20 Indicating analysis for the 2500 [rpm] @ 8 [bar] BMEP engine op. point for diesel, JME (B30) and JME (B100): in-cylinder pressure, heat release rate and injection pattern (top, figures a and b), heat release rate and mass fraction burned (bottom, figures c and d). 57
Figure 3.21 Brake Specific Fuel Consumption (BSFC): standard calibration (left), specific calibration (right)........ 60
Figure 3.22 Fuel conversion efficiency: standard calibration (left), specific calibration (right)........ 60
Figure 3.23 Brake Specific CO_2 emissions (engine outlet): standard calibration (left), specific calibration (right)........ 60
Figure 3.24 Brake Specific CO emissions (engine outlet): standard calibration (left), specific calibration (right)........ 61
Figure 3.25 Brake Specific HC emissions (engine outlet): standard calibration (left), specific calibration (right)........ 61
Figure 3.26 Brake Specific NO_x emissions (engine outlet): standard calibration (left), specific calibration (right)........ 61
Figure 3.27 FSN (engine outlet): standard calibration (left), specific calibration (right) 62
Figure 3.28 Soot–BSNO_x trade-off comparison at 1500 [rpm], 2 [bar] BMEP........ 62
Figure 3.29 Soot–BSNO_x trade-off comparison at 2000 [rpm], 5 [bar] BMEP......... 63
Figure 3.30 Soot–BSNO_x trade-off comparison at 2500 [rpm], 8 [bar] BMEP.......... 63

Figure 3.31 BSFC at part load 66
Figure 3.32 Fuel conversion efficiency at part load 67
Figure 3.33 $BSCO_2$ emissions at part load 67
Figure 3.34 BSCO emissions at part load 67
Figure 3.35 BSHC emissions at part load 68
Figure 3.36 $BSNO_x$ emissions at part load 68
Figure 3.37 Filter Smoke Number at part load 68
Figure 3.38 Combustion noise at part load 69
Figure 3.39 In-cylinder pressure, heat release rate, mass fraction burned and injector signal traces at 1500 rpm, 2 bar BMEP 69
Figure 3.40 Soot-$BSNO_x$ trade-off for at 2000 rpm, 5 bar BMEP for all fuels 69
Figure 3.41 BSCO-$BSNO_x$ trade-off at 2000 rpm, 5 bar BMEP for all fuels 70
Figure 3.42 Indicating analysis for the 1500 [rpm] @ 2 [bar] BMEP engine op. point for diesel, RME (B30) and HVO (B30) at SoI=5.7 deg BTDC (calibration point) without EGR (left column) and with EGR (right column): in-cylinder pressure, heat release rate and injection pattern (top), heat release rate and mass fraction burned (bottom) 72
Figure 3.43 Indicating analysis for the 1500 [rpm] @ 2 [bar] BMEP engine op. point for diesel, RME (B30) and HVO (B30) at SoI=2.7 deg BTDC without EGR (left column) and with EGR (right column): in-cylinder pressure, heat release rate and injection pattern (top), heat release rate and mass fraction burned (bottom). 73
Figure 3.44 Indicating analysis for the 1500 [rpm] @ 2 [bar] BMEP engine op. point for diesel, RME (B30) and HVO (B30) at SoI=7.7 deg BTDC without EGR (left column) and with EGR (right column): in-cylinder pressure, heat release rate and injection pattern (top), heat release rate and mass fraction burned (bottom). 74
Figure 3.45 BSFC with all fuels and SoI at 1500 rpm @ 2 bar BMEP: without EGR (left), with EGR (right) 74
Figure 3.46 Fuel conversion efficiency with all fuels and SoI at 1500 rpm @ 2 bar BMEP: without EGR (left), with EGR (right) 75
Figure 3.47 BSCO with all fuels and SoI at 1500 rpm @ 2 bar BMEP: without EGR (left), with EGR (right) 75
Figure 3.48 BSHC with all fuels and SoI at 1500 rpm @ 2 bar BMEP: without EGR (left), with EGR (right) 75
Figure 3.49 $BSNO_x$ with all fuels and SoI at 1500 rpm @ 2 bar BMEP: without EGR (left), with EGR (right) 76

Figure 4.1 PM specific emissions for all op. points and evaluated fuels. 78
Figure 4.2 Correlation between specific PM emissions and smoke, BSFC, BSHC for all fuels and tested operating points 79
Figure 4.3 BSHC versus relative air fuel ratio at 1500 rpm @ 2 bar BMEP 80
Figure 4.4 Specific PM emissions obtained by using AVL and MIRA models 81
Figure 4.5 Breakdown analysis of PM emissions according to AVL and MIRA model 82
Figure 4.6 Particulate matter chemical composition for three tested fuel at 1500 rpm @ 2 bar BMEP load condition... 83
Figure 4.7 Particulate matter chemical composition for three tested fuel at 1500 rpm @ 5 bar BMEP load condition... 83
Figure 4.8 Particulate matter chemical composition for three tested fuel at 1500 rpm @ 8 bar BMEP load condition... 84
Figure 4.9 EGR rate of three fuels at thermo-gravimetric analysis........................... 84
Figure 4.10 Comparison of five SMPS scans measured at the engine outlet for the 2000 rpm @ 5 bar BMEP engine operating point 86
Figure 4.11 PN distribution at 1500 rpm @ 2 bar BMEP: semi-log graph (left), log-log graph (right) 87
Figure 4.12 Soot-λ tradeoff curve with all fuels at 1500 rpm @ 2 bar BMEP 88
Figure 4.13 Soot-λ tradeoff curve with all fuels at 1500 rpm @ 5 bar BMEP 88
Figure 4.14 PN distribution at 1500 rpm @ 5 bar BMEP: semi-log graph (left), log-log graph (right) 89
Figure 4.15 PN distribution at 1500 rpm @ 8 bar BMEP: semi-log graph (left), log-log graph (right) 89
Figure 4.16 PN and size distributions with diesel, RME and JME (B30 and B100) at 2500 rpm @ 8 bar BMEP 90
Figure I.1. An example aof a typical chemical composition of PM 110
Figure I.2 Comparison between MIRA and AVL methods 112

List of Tables

Table 1.1 EU Emission Standards for Passenger Cars (Dieselnet, Emissions Standards - Europe - Cars and Light Trucks. 2011)........ 7
Table 1.2 Tier 2 Emission Standards (Dieselnet, Emissions Standards - USA - Cars and Light-Duty Trucks - Tier 2. 2011)........ 8
Table 1.3 CAFE fuel economy standards........ 10
Table 2.1 Properties of neat fuels........ 23
Table 2.2 Composition of neat fuels........ 24
Table 2.3 Main fuel properties........ 26
Table 2.4 Main characteristics of the engines under test........ 30
Table 2.5 Main characteristics of the after-treatment system........ 30
Table 2.6 Part load operating points........ 31
Table 2.7 Test matrix of start of injection (SOI) sweep tests........ 32
Table 2.8: Gravimetric analysis operating points........ 35
Table 2.9 Test conditions and parameters used during gravimetric tests........ 35
Table 2.10 TGA test procedure........ 37
Table 2.11 Particle size and number distribution test matrix........ 41
Table 2.12 Samples specifications........ 41
Table 3.1 Trade-off tests EGR rates [%]........ 64
Table 4.1 Statistic calculations performed by the Aerosol Instrument Manager® Software........ 86

Table 4.2 Relative A/F ratios and EGR rates levels for all fuels at 1500 rpm @ 2 bar BMEP 87
Table 4.3 Number of revertants with different mutagens for all the tested samples (red fonts are referred to toxic activity) 92
Table 4.4 Mutagenicity ratio and net revertants number for all fuels 93

Table of Contents

Abstract...I

List of Abbreviations...III

List of Figures...VII

List of Tables...XIII

Table of Contents...XV

Introduction...1

Chapter 1 – Diesel Emissions Control Technologies Review...5
  1.1 Introduction...5
  1.2 Regulatory Trends...6
  1.3 Engine Developments...10
  1.4 The growing role of biofuels...14
    1.4.1 Biofuels in the global energy scene...14
      1.4.1.1 The EU biofuels policy and regulatory landscape...15
      1.4.1.2 Energy independence through increased production of biofuels...15
    1.4.2 Future trend...16
  1.5 Renewable diesel fuel...17
    1.5.1 Traditional biodiesel (FAME)...18

1.5.2 Hydrotreated vegetable oil (HVO) 19

Chapter 2 – Experimental Apparatus & Test Procedures 21
2.1 Introduction 21
2.2 Evaluated Fuels 22
2.2.1 Biodiesel feedstock comparison 22
2.2.2 Fatty Acid Methyl Esters and Hydrotreated Vegetable Oil comparison 25
2.3 Engine and test rig description 28
2.4 Full load performance and part load emissions characterization 30
2.4.1 Test procedure 30
2.5 Analysis of the sensitivity of the different fuels to engine calibration 32
2.5.1 Test procedure 32
2.6 PM gravimetric analysis 33
2.6.1 Experimental setup 33
2.6.2 Test procedure 34
2.7 PM chemical composition (TGA) analysis 36
2.7.1 Experimental setup 36
2.7.2 TGA test procedure 36
2.8 PM particles number and size distribution analysis 37
2.8.1 Experimental setup 37
2.8.1.1 Measuring system 37
2.8.1.2 Sampling system 38
2.8.2 Test procedure 40
2.9 Mutagenicity analysis of PM emissions 41
2.9.1 Test procedure 41

Chapter 3 – Full Load Performance And Part Load Emissions Assessment 43
3.1 Introduction 43
3.2 Results analysis and discussion 44
3.2.1 Full load performance 44
3.2.1.1 Biodiesel feedstock comparison 44
3.2.1.2 FAME vs HVO characterization 47
3.2.2 Part load emission characterization 49
3.2.2.1 Biodiesel feedstock comparison 49
3.2.2.2 HVO characterization 64
3.2.3 Analysis of the sensitivity of the different fuels to engine calibration ... 70

Chapter 4 – Particulate Matter characterization 77
4.1 Introduction 77
4.2 Results analysis and discussion 78
4.2.1 PM gravimetric and chemical composition analysis 78
4.2.2 Particle size and number distribution 84
4.2.3 PM mutagenic characterization 90

Conclusions 95

Bibliography 99

List of Publications 105

Appendix I – PM estimation on the basis of FSN measurements 109
I.1 Introduction 109
I.2 AVL relationship 110
I.3 MIRA relationship 111
I.4 AVL and MIRA methods comparison 111

Introduction

Biofuels have been widely investigated in recent years, since they can provide interesting opportunities in terms of reductions of both Greenhouse Gases (GHG) and Particulate Matter (PM) emissions, as well as in terms of energy sources diversification. In particular, the usage of trans-esterified vegetable oils for fuelling diesel engines (often referred to as biodiesel, or FAME, Fatty Acid Methyl Ester), generally in blend with fossil fuels, has been increasingly spreading, thanks to its chemical and physical properties which are quite similar to those of fossil diesel fuels. In 2009 European directive 2009/28/EC introduced a new target for the European Union (EU) member states concerning the share of energy from renewable sources in all forms of transport; in particular, a target of at least 10% of the final energy consumption in the transportation sector should be achieved by 2020.

Nevertheless, in the fourth quarter of 2012, the European Commission published a proposal to limit the use of food-based biofuels and to include Indirect Land Use Change (ILUC) emissions when assessing the greenhouse gas effect of biofuels. The use of food-based biofuels to meet the 10% renewable energy target of should be limited to 5%. In order to meet the 10% target, biodiesel sourced by non-edible sources (i.e. algae, industrial waste, straw, animal manure, sewage sludge, palm oil mill effluent, crude glycerin, non-food cellulosic and ligno-cellulosic materials) have to be studied and developed.

Moreover, Asian countries are exploring biodiesel sourced from non-edible seed oils like Jatropha Curcas, a wild plant which can grow in arid, semiarid and wasteland; therefore, Jatropha Methyl Ester (JME) represents a viable solution for biodiesel production, since allows green cover to wasteland. However, unsaturated FAMEs such as Rapeseed Methyl Ester (RME) or Soy Methyl Ester (SME), are known to adversely impact on fuel oxidation stability, and FAME percentages that can be blended into automotive diesel fuel is currently limited in Europe to 7% on a volume basis, although higher percentages, up to 30% are currently being considered, even if they might require special care to prevent engine oil dilution, injectors coking and deposits formation in the fuel injection system.

More recently, also Hydrotreated Vegetable Oil (HVO), obtained by means of a refinery-based process that converts vegetable oils into paraffinic hydrocarbons, has been gaining an increasing attention, since being sulphur and aromatics free, and having a high cetane number its combustion characteristics are particularly attractive. In addition, thanks to the lack of unsaturated compounds also its oxidation stability has been demonstrated to be better than that of FAME. Finally, additional advantages in terms of environmental impact of the HVO production process have been highlighted, showing a good potential in terms of GHG emissions reduction, as well as the possibility of producing HVO in existing oil refineries without the need for additional chemicals such as methanol which is required for FAME production, or for the storage of by-products such as glycerol.

High Speed Direct Injection (HSDI) Diesel engines are nowadays spreading in the global market of passenger cars, thanks to undoubted advantages such as higher efficiency (lower fuel consumption and CO_2 emissions), drivability, durability and reliability. Increasing concerns regarding the two main pollutants from Diesel engines, NO_x and PM, started a progressive process of tightening of emission limits; Tier 2 (USA) and Euro5b/6 (Europe) emissions regulations will definitively bring down NO_x and PM, with also the introduction of new limitations such as, for instance, on particles number (PN) emissions.

Although the effects of biofuels (paraffinic and esters) on engine emissions have already been investigated by several researchers and a plethora of studies concerning the effects of FAME can be found in literature, only few studies have been carried out on last generation automotive engines, as the one which was adopted for the present work. Experimental activities reported in literature are usually carried out running the engine with the original, diesel oriented, ECU calibration; a specifically adjusted ECU calibration optimized for alternative fuels is rarely used and the possible decrease of engine torque output is often recovered by increasing the torque demand through an increase of the accelerator pedal position, thus simulating a switch of the supplied fuel. An extension of the investigations to modern engines and after-treatment systems, which may include advanced combustion technologies and closed loop combustion controls seems therefore to be necessary in order to fully understand the effects of both FAME and HVO usage.

Therefore, the aim of the present work is the analysis of the effects of using blended (30% vol.) and neat renewable diesel fuel, obtained from Rapeseed Methyl Ester (RME), Jatropha Methyl Ester (JME) and Hydrotreated Vegetable Oil (HVO), in a Euro 5 small displacement passenger car diesel engine, featuring advanced combustion technologies and closed loop combustion controls. Moreover due to increasing concerns about PM effects on human health a detail characterization of PM produced by different fuels in term of mass, chemical composition and particles number and size distribution was carried out as well.

In the *First Chapter* a review of the recent developments on Diesel emission control technologies and legislations limits is given, in order to summarize the evolution of emission control technologies over the last decade. Moreover a survey related to the usage of biodiesel is proposed.

The *Second Chapter* collects a detailed description of the experimental setups that have been prepared for each experimental investigation, which will be useful in understanding the following results.

In the *Third Chapter* the analysis of the effects that biofuels may have on full load performance and on emissions during part load operation will be presented; in addition the effects that different fuels may have on the combustion process are discussed as well.

Finally, in the *Fourth Chapter*, a characterization of PM emitted when fuelling the engine with both conventional and renewable diesel fuels in terms of mass, chemical composition, particles number and size distribution and of mutagenic potential will be given.

Chapter 1 – Diesel Emissions Control Technologies Review

1.1 Introduction

In this chapter, due to the target of the present work which is focused on the characterization of the effects of using biodiesel blends in a Euro 5 small displacement passenger car diesel engine, featuring advanced combustion technologies and closed loop combustion controls, a brief overview about the progress of the regulations on Diesel pollutant emissions will be given, moving subsequently to an overall description of latest Diesel emissions control technologies, presenting some of the newer technologies for in-cylinder emissions reduction and giving way to a more detailed description on the evolution of biofuel usage over the last years.

1.2 Regulatory Trends

Regulations regarding emission limits are the drivers which today, as well as in the past, force vehicles manufacturers to continuously introduce and develop new technologies for the control of pollutant species. For this reason it is important to give an overall picture of emission standards evolution within last decades in the major markets in the world, *i.e.* European and USA markets, in order to highlight the steps that led to the development and introduction of different emission control technologies. It should be here pointed out that the discussion will be focused on the description of the regulatory evolution regarding Diesel engines for light duty (LD) applications.

Emission regulations in European countries for LD applications were first introduced in the '70 with Directive 70/220/EEC which, over the years, has been amended several times up to 2004, while in 2007 this Directive has been repealed and replaced by Regulation 715/2007 (usually referred to as Euro 5/6). Some of the important regulatory steps implementing emission standards for Diesel engines for LD vehicles are summarized in Table 1.1.

Emissions, which are tested over the cold start test referred to as the New European Driving Cycle (NEDC), were progressively reduced, from the introduction of Euro 1 up to the current Euro 5 standard; referring to future Euro 6 standard, which will be effective from September 2014, it is possible to observe a progressive tightening of emission limits, especially for PM and NO_x. The Euro 5/6 standards introduce a new PM mass emission measurement method developed by the UN/ECE Particulate Measurement Programme (PMP) and adjusts the PM mass emission limits to account for differences in results using the old and the new method; more important, from Euro 5b a new particle number (PN) emission limit, in addition to the mass-based limits, has been set due to increasing concerns about PM health and environmental effects related to the number of emitted particles (2008/692/EC July 18, 2008).

Emission standards adopted in the USA for Diesel engines for LD applications differ significantly from the European picture, due to the fact that regulations are fuel neutral, meaning that no distinctions are made in terms of pollutant emissions between gasoline and Diesel engines; Federal Standards for engines and vehicles, including emission standards for greenhouse gas (GHG) emissions, are established by the US Environmental Protection Agency (EPA).

Two categories of standards have been defined for LD vehicles in 1990; Tier 1 Tier 2 emission standards are structured into 8 permanent and 3 temporary certification levels of different stringency, called "*certification bins*", and an average fleet standard for NO_x emissions, as reported in Table 1.2. Vehicle manufacturers have a choice to certify particular vehicles to any of the available bins, but with the clause that the average NO_x emissions of the entire LD vehicle fleet sold by each manufacturer has to meet the average NO_x standard corresponding to certification Bin #5. The temporary certification bins reported in Table 1.2 with more relaxed emission limits were available in the phase-in period and expired after the 2008 model year.

Table 1.1 EU Emission Standards for Passenger Cars (Dieselnet, Emissions Standards - Europe - Cars and Light Trucks. 2011)

Stage	Date	CO	HC	HC+NO_x	NO_x	PM	PN
				g/km			*#/km*
Euro 1	1992.07	2.72	-	0.97	-	0.14	-
Euro 2, IDI	1996.01	1.00	-	0.7	-	0.08	-
Euro 2, DI	1996.01	1.00	-	0.9	-	0.10	-
Euro 3	2000.01	0.64	-	0.56	0.50	0.05	-
Euro 4	2005.01	0.50	-	0.30	0.25	0.025	-
Euro 5a	2009.09	0.50	-	0.23	0.18	0.005	-
Euro 5b	2011.09	0.50	-	0.23	0.18	0.005	$6x10^{11}$
Euro 6	2014.09	0.50	-	0.17	0.08	0.005	$6x10^{11}$

In addition to the Federal Standards, each State has the right to adopt its own emission regulations. Regulations enforced by the State of California are often more stringent than the federal rules; States adopting the California standards include Arizona (2012 model year), Connecticut, Maine, Maryland, Massachusetts, New Jersey, New Mexico (2011 model year), New York, Oregon, Pennsylvania, Rhode Island, Vermont, and Washington, as well as the District of Columbia. Engine and vehicle emission regulations are adopted by the California Air Resources Board (CARB), a regulatory body within the California EPA. Low Emission Vehicle (LEV) California emissions standards, whose structure is quite similar to Federal Standards, followed an evolution from Tier 1/LEV (up to 2003), to LEV II (phased-in in the period 2004-2010), to the final LEV III (proposed in 2010 and phased-in through model years 2014-2022); for each of the emission standards, manufacturers must meet increasingly tighter fleet average targets, more stringent than for Federal Standards. Details on the modification proposed by CARB for LEV II emission standards are well summarized in (Johnson 2011).

Table 1.2 Tier 2 Emission Standards (Dieselnet, Emissions Standards - USA - Cars and Light-Duty Trucks - Tier 2. 2011)

Bin #	NMHC	CO	NO_x	PM	HCHO
			g/mi		
Temporary Bins					
11	0.280	7.3	0.9	0.12	0.032
10	0.156	4.2	0.6	0.08	0.018
9	0.090	4.2	0.3	0.06	0.018
Permanent Bins					
8	0.125	4.2	0.20	0.02	0.018
7	0.090	4.2	0.15	0.02	0.018
6	0.090	4.2	0.10	0.01	0.018
5	0.090	4.2	0.07	0.01	0.018
4	0.070	2.1	0.04	0.01	0.011
3	0.055	2.1	0.03	0.01	0.011
2	0.010	2.1	0.02	0.01	0.004
1	0.000	0.000	0.000	0.000	0.000

From a general point of view, looking at the increasing tightening of emission limits for both the European and the American standards, it possible to observe that the trend is to force the adoption of emission controlling technologies, whether they are in-cylinder or after-treatment, which could significantly bring down tailpipe emissions from mobile sources.

Besides the reduction of pollutant emissions described so far, vehicles fuel economy has gained a lot of attention through years, becoming today a worldwide important topic of discussion; not only pollutant emissions have to be controlled, but also fuel consumption should be kept within regulated limits, which somehow highlights the global efforts to increase as much as possible the internal combustion engine efficiency and to reduce the emission of CO_2, which is the best known greenhouse gas (GHG).

In Europe, in order to control GHG emissions from the transportation sector, the European Commission signed in 1998-99 a voluntary agreement with the European Automobile Manufacturers Association (ACEA) to reduce CO_2 emissions; the major provisions of the subscribed agreement were a 25% reduction in CO_2 emissions from the 1995 level, setting a target of 140 g/km to be reached by 2008, and the possibility to extend the agreement to 120 g CO_2/km by 2012, as shown in Figure 1.1. Even though significant CO_2 emission reductions were achieved in the initial years, the ACEA was not able to reach the 140 g/km target by 2008; the European Commission decided thus in 2009 to turn the voluntary agreement into a mandatory CO_2 emission regulation from new LD vehicles.

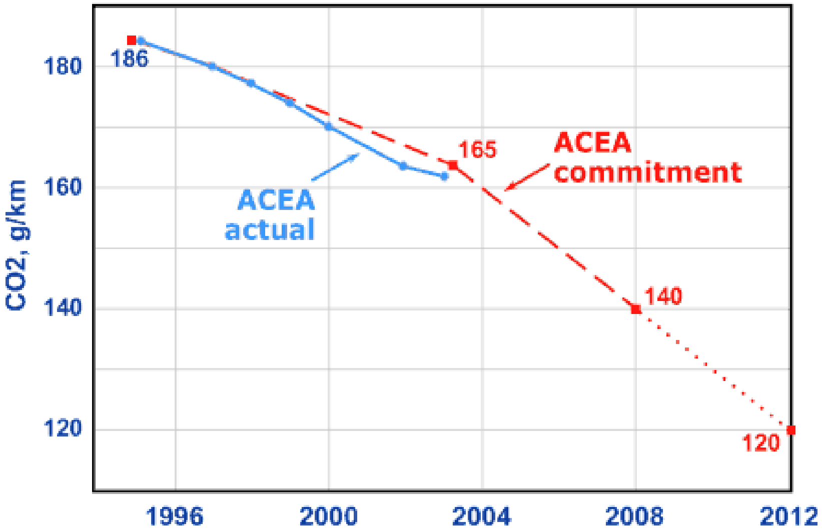

Figure 1.1 CO_2 reduction from Light-Duty Vehicles Under ACEA Agreement (Dieselnet, Emission Standards - Europe - Cars GHG - ACEA Agreements 2010)

For passenger cars, CO_2 emission targets were adopted in April 2009, setting a fleet-average medium-term CO_2 emission target of 130 g/km to be reached by 2015, and a long-term target of 95 g CO_2/km to be reached from 2020; the regulation is phased-in over the period from 2012 to 2015, where manufacturers must meet their average CO_2 emission targets in 65% of their fleets in 2012, 75% in 2013, 80% in 2014 and 100% from 2015. Besides incentives obtained respecting the targets, significant penalties will be applied to manufacturers which will not fulfill the limits; after a period (2012-2018) of progressively increasing fees, starting from 2019 manufacturers will pay €95 per vehicle for each g/km of CO_2 exceeding the target.

In USA the Corporate Average Fuel Economy (CAFE) standards for passenger cars and light duty trucks (LDT) was first established back in 1975 as part of the Energy Policy Conservation Act promoted as a response to the oil crisis of the early '70; the CAFE regulation requires each car manufacturer to meet a standard for the sales-weighted fuel economy, expressed in miles per gallon (mpg), for the entire fleet of vehicles sold in the USA in each model year. Table 1.3 summarizes the limits in mpg over the last 15 years, even though fuel economy standards were applied since 1978 (not reported here for the sake of brevity).

Table 1.3 CAFE fuel economy standards

Year	Cars	Light Trucks	Year	Cars	Light Trucks
1995	27.5	20.6	2007	27.5	22.2
1996	27.5	20.7	2008	27.5	22.5
2005	27.5	21.0	2009	27.5	23.1
2006	27.5	21.6	2010	27.5	23.5

In addition to CAFE standards, California adopted in 2002 a dedicated regulation, becoming effective from 2006 and phased-in over the period 2009-2016, aiming the control of emissions of GHG from motor vehicles in California; the average reduction of GHG should be about 22% in 2012 and 30% in 2016, compared to model year 2004 vehicles.

As it can be noticed from Table 1.3, few efforts have been done in USA with the aim to promote fuel economy, especially in the segment of passenger cars; however, recently the CAFE program has been modified for light-duty trucks application in order to tighten the existing limits. Moreover, CARB is proposing new LD CO_2 standards as part of the LEV III emission standards, resulting in an effective 20-25% tightening of current CO_2 emission standards (Johnson 2010).

An interesting analysis with the aim to illustrate the cost-effectiveness of the diesel in meeting CO_2 regulations has been carried out by (Körfer 2009); in his work Körfer compared the costs of bringing both a gasoline and a Diesel medium-size Euro 5 car to compliance with the 2020 European CO_2 requirements, finding that with Diesel engines it was possible not only to save money in terms of initial investment, but it was also possible to take advantages from the surplus in terms of g CO_2/km with respect to the legislation limits.

In conclusion, even though more stringent emission standards are being applied all over the world, looking at the future the emphasis of regulations is progressively shifting towards the attainment of CO_2 or fuel economy regulations, which could pave the way for the diffusion, also within the USA market, of Diesel powered LD vehicles.

1.3 Engine Developments

Progresses in emissions regulations (*i.e.* from emerging Super Ultra Low Emission Vehicle (SULEV) standards in California), evolution of the market and upcoming fuel economy requirements are making great pressure on the Diesel engine, especially if considering the continuous evolution of advanced gasoline concepts and Hybrid Electric Vehicles (HEV). Diesel engine developers are responding to the challenge focusing on the reduction of fuel consumption while maintaining good performance; this is mainly achieved through the adoption of very sophisticated combustion designs and control on the engine.

Thanks to advances in turbocharging and fuel injection technologies, engine downsizing is today a very effective method to bring down engine fuel consumption without sacrificing engine performance; exhaust gas recirculation (EGR) control, two-stage turbocharging, closed-loop combustion control, advanced swirl concepts realized through variable valve actuation are other key technologies for the achievement of further improvements (Johnson 2009).

Figure 1.2 shows the evolution of European emission regulations from Euro 4 up to Euro 6 in terms of NO_x and Particulate Matter emissions; as it can be noticed the achievement of very low emission levels can be attained only through a synergic combination of different technologies involving both engine and after-treatment developments.

Engine technology developments have been widely documented in literature over the last decades. (Czarnowski 2008) showed that the adoption of low pressure loop EGR and series turbocharging can lead to the achievement of both low engine-out NO_x and fuel consumption levels, as also reported from (Mattes 2008); more complicated engine layouts were explored by (Joergl 2008) (Dorenkamp 2008), with both low and high pressure EGR and dual stage turbocharging which can bring engine-out NO_x down to Euro 6 levels.

From a more scientific point of view, downsized prototype diesel engines are reaching very high levels in specific power and Indicated Mean Effective Pressure (IMEP) (Köerfer 2008); however, even though downsizing and downspeeding of the engine can give undoubted benefits in terms of fuel consumption, an increase up to 50% in engine-out NO_x could be reached. On production engines, downsizing enables great savings in fuel consumption, but appropriate measures should be taken in order to compensate for the unavoidable increase of engine-out NO_x; (Körfer 2009) well described an innovative approach in engine design, where a mix of advanced engine technologies such as new swirl concepts, EGR control, high pressure electronically controlled injection system and sophisticated combustion chamber design, led to a 17% reduction in fuel consumption, with at the same time a 50% reduction in engine-out NO_x and a 10% reduction in engine-out PM, when downsizing to a 1.6 liters a Euro 4 midsize passenger car a 2.0 liters Diesel engine. Another interesting analysis was carried out by (Tatur 2010), who showed that in order to meet US EPA Tier 2 Bin 5 standards a range of different technology options should be evaluated. Upper class passenger cars would need high pressure injection systems (injection pressure higher than 2000 bar, with piezoelectric injectors), 2-stage turbocharging, together with a selective catalytic reduction (SCR) system for NO_x control; on the other hand, lower class passenger cars could meet the target with 1450-1800 bar injectors, and variable geometry turbochargers (VGT), together with a lean NO_x traps (LNT) system for NO_x reduction, while medium-size passenger cars would need a mix of these technologies.

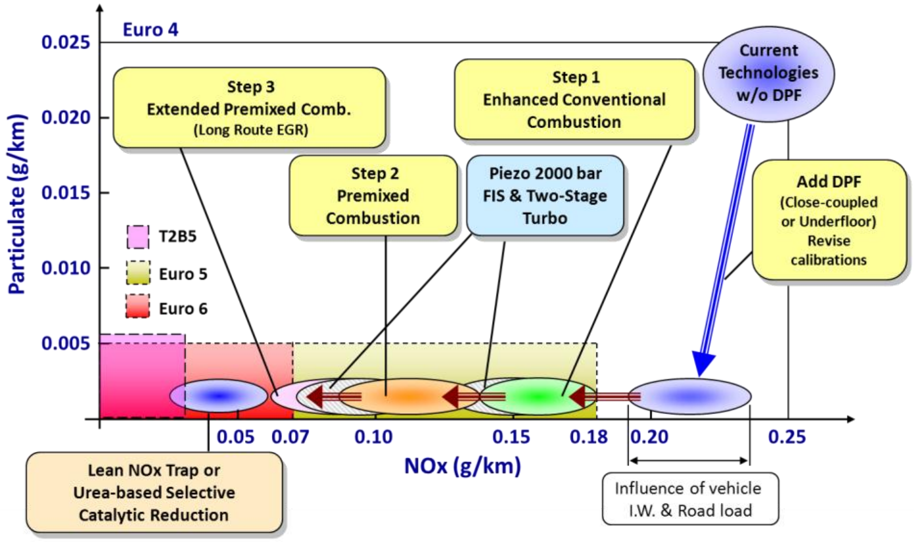

Figure 1.2 Road map for NOx and PM emissions reduction, technological steps

As far as compression ratio (CR) is concerned, decreasing of diesel engine CR could lead to a reduction of frictional losses and NO_x, as reported by (Tomoda 2010); lower compression ratios compromise thermodynamic efficiency and could result in poor cold start, especially in cold ambient conditions or at high altitude. The issue could be address by redesigning the bowl, adding more holes to the injector to get more air entrainment, and increasing the number of pilot injections. More recently, similar observations have been showed by (Sakono 2011).

On the other hand, advance combustion regimes have been widely investigated, with the aim to reduce emission of NO_x and PM which are more critical for diesel engines; Low Temperature Combustion (LTC) modes, which cover a number of advanced combustion strategies, including Homogeneous Charge Compression Ignition (HCCI) or Premixed Charge Compression Ignition (PCCI), seem to be very promising in this context, but often present as a drawback an increase in CO and HC emissions. NO_x emissions decrease thanks to the significant reduction of thermal NO formation process due to lower combustion temperature, while PM emissions decrease thanks to significantly lower soot formation rate resulting also from the combustion temperature lowering (Tao 2005); conversely, higher CO emissions can result from both formation increase (under-mixed fuel-rich regions at high loads, over-mixed, fuel-lean regions at low loads (Mueller 2005)) and slower oxidation of CO to CO_2 due to lower combustion temperature (Bhave 2006), while HC emissions can increase due to several factors such as, for instance, long spray penetration, which leads to wall impingement and, due to lower combustion peak temperature at low loads, to quenching at combustion chamber surfaces, and presence of significant amount of fuel in lean zones prone to escaping the burning process and leading to unburned HC emissions.

In addition to pollutant emissions, it should be taken into account that in premixed LTC combustion, the combustion rate is not directly linked to the injection rate, which means that combustion cannot be controlled by the injection rate; advanced combustion regimes are characterized by a more intense premixed portion of the combustion, which present as a drawback the combustion noise. In conventional diesel engines combustion noise was decreased significantly thanks to the advent of common rail injection systems and the ability to use pilot injection in order to reduce the pressure gradient associated with premixed burning; for these reasons LTC modes can be operated nowadays only under low load engine operating conditions, through a synergic exploitation of the flexibility given by the common rail injection system and advanced EGR and turbocharger technologies, while still keeping a more conventional combustion regime under medium-high loads operating conditions.

Finally, in recent years Diesel engines are moving towards hybridization, trying to make unique synergies on emissions between diesel engines and electrification, that may give them a relative advantage over similar steps with gasoline engines.

A detailed analysis has been carried out by (Cisternino 2010), who evaluated a second generation mild hybrid architecture on a 1.9 liter Euro 4 engine in dynamometer testing; the hybrid system utilized stop-start functionality for idle reduction and assist on starts and accelerations, while also enabling energy recuperation during decelerations. The analysis showed that fuel consumption can drop by 10%; meanwhile, CO emissions fall by 80%, while HC drops 20%, thanks to hotter DOC (Diesel Oxidation Catalyst) temperatures which may result of less idling. On the other hand NO_x is reduced by 15% thanks to milder transients phase which do not involve high load operating conditions.

A similar analysis was carried out by (Krüger 2010) on a 1.6 liter engine; the low-load hybrid assist was found to match very well with the high-load efficiencies of diesel engine, which allowed to reach a near uniform fuel consumption in urban and highway driving conditions, with a 20% reduction of fuel consumption with respect to conventional diesel engine on certification test cycles. Furthermore, also in this case CO and HC emissions were reduced by 75%, thanks also to lower engine-out emissions, in addition to faster DOC light-off.

1.4 The growing role of biofuels

The global biofuel industry has been witnessing rapid growth over the past few years in the backdrop of depleting fossil fuels and degradation of environmental conditions. Since the second half of the 20th century, amid concerns about rising oil prices and greenhouse gas emissions from fossil fuels, the term biofuel has largely come to mean bioethanol and biodiesel. Therefore, many economies have turned their attention towards biofuels. Many countries are also supporting the biofuel industry in the form of subsidies and tax incentives which keep the biofuel producing companies profitable. Even governments of various countries have implemented mandatory biofuel blend with the conventional fuel to increase its demand.

1.4.1 Biofuels in the global energy scene

According to official statistics of International Energy Agency (IEA), global production of biofuels – liquid and gaseous fuels derived from biomass – has been growing steadily over the last decade from 16 billion liters in 2000 to more than 100 billion liters in 2010 (Figure 1.3). Today, biofuels provide around 3% of total road transport fuel globally (on an energy basis) and considerably higher shares are achieved in certain countries. Brazil, for instance, met about 23% of its road transport fuel demand in 2008 with biofuels. In the United States, the share was 4% of road transport fuel and in the European Union (EU) around 3% in 2008. Figure 1.4 shows the share of biofuels in road transport energy consumption in the world. This has encouraged many countries to advance their biofuels development plans and increase production targets. It is widely expected that globally production of biofuels will continue growing in the coming years.

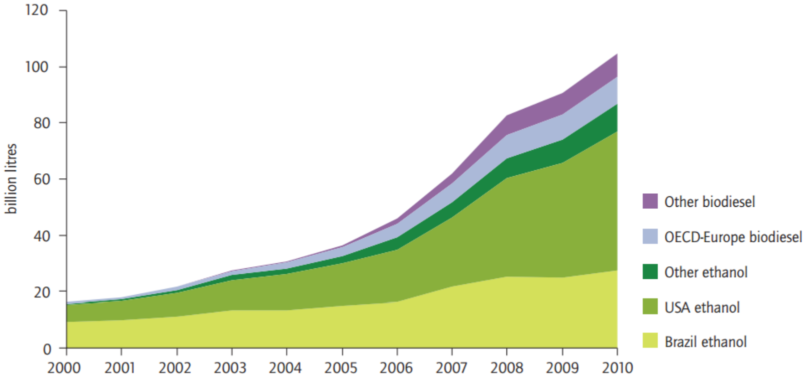

Figure 1.3 Global biofuel production 2000-2010 (source: IEA, 2010a)

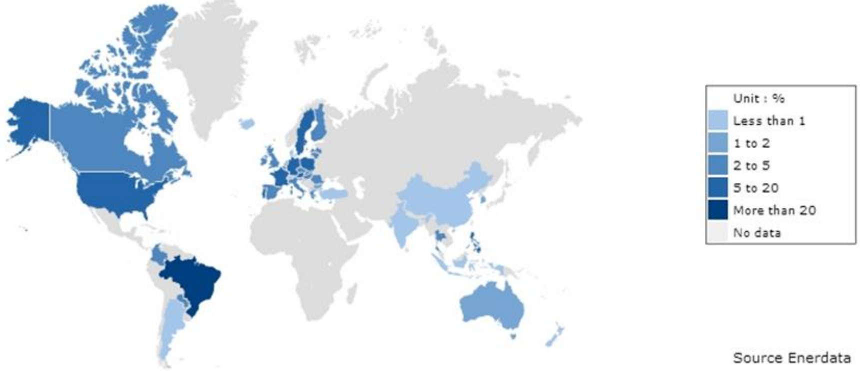

Source Enerdata

Figure 1.4 Share of biofuels in road transport energy consumption (March, 2012 WEC/Enerdata)

1.4.1.1 The EU biofuels policy and regulatory landscape

In a strive to alleviate climate change related environmental degradation as well as the increasing scarcity of conventional energy sources, the European Commission set in 2003 the basis for the promotion of the use of renewable energy in transport. This legislative act was entitled the "Biofuels Directive" as it mainly laid down indicative targets for biofuels use in transport in the European Union from 2005 up to 2010. Accordingly, Member States had been given the possibility to create a detaxation system for biofuels. The Council supported this framework and unanimously approved the Energy Taxation Directive.

In 2009, the European Commission released the major legislative act that is defining the evolution of the European biofuels sector in the next ten years. The main provisions of the Renewable Energy Directive are the following: renewable energy for all sectors and especially for the transport sector will have to follow binding targets for 2020; sustainability criteria are imposed for the first time upon a series of products, namely for biofuels; a certification scheme for sustainable biofuels will be put in place; a promotion scheme for advanced biofuels pathways has been developed. Binding targets for renewable energy in transport (10% in all Member States) and for renewable energy in final energy consumption (20% in all Member States) have been set. The Commission proposal confirmed the conclusion of the March 2007 Energy Council defining a 20% target for all renewable energies and a target of at least 10% for biofuels (meaning that the renewables mix used to attain the overall 20% target shall contain at least 10% of renewable energy in transport in all Member States).

1.4.1.2 Energy independence through increased production of biofuels

Only a few countries currently enjoy energy independence. Every single country throughout the world, however, has the inherent ability to achieve complete and lasting energy independence on a renewable and therefore sustainable basis. The Arab Spring, Libyan uprising and Iran's nuclear issue illustrated the continuing possibility of major disruptions in oil supply and the security risks involved in maintaining access to foreign oil. Biofuels is a way to reduce dependence on foreign oil and increase the nation's overall sustainability. This may be accomplished by adopting the simple agricultural approach of growing vegetable oil crops for the purpose of refining biodiesel fuels. Demand for these biofuels can also give a boost to rural economies, providing support for the economy overall.

1.4.2 Future trend

The IEA's Energy Technology Perspectives (ETP) 2010 BLUE Map Scenario sets a target of 50% reduction in energy-related CO_2 emissions by 2050 from 2005 levels. To achieve the projected emission savings in the transport sector, ETP 2010 projects that sustainably produced biofuels will eventually provide 27% of total transport fuel (Figure 1.5). Based on the BLUE Map Scenario, by 2050 biofuel demand will reach 32 EJ, or 760 million tons of oil equivalent (Mtoe).

Reductions in transport emissions contribute considerably to achieving overall BLUE Map targets, accounting for 23% of total energy-related emissions reduction by 2050 (IEA, 2010c). The highest reductions are achieved in OECD countries, while some non-OECD countries, including India and China, show significant increases because of rapidly growing vehicle fleets. Vehicle efficiency improvements account for one-third of emissions reduction in the transport sector; the use of biofuels is the second-largest contributor, together with electrification of the fleet, accounting for 20% emissions saving (Figure 1.6).

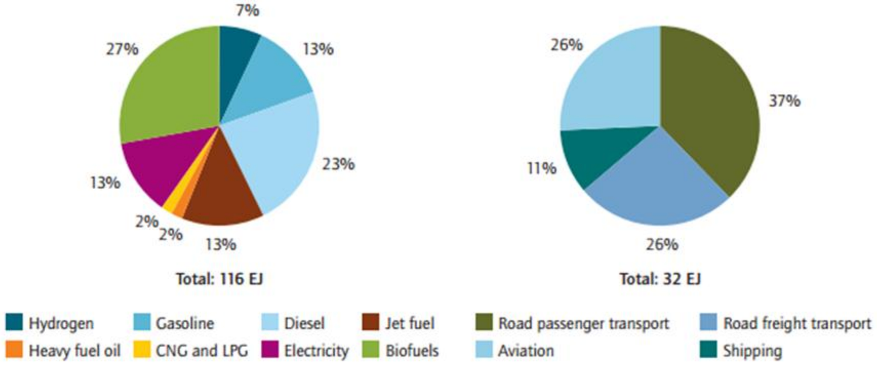

Note: CNG= compressed natural gas; LPG= liquefied petroleum gas.
Source: IEA, 2010c.

Figure 1.5 Global energy use in the transport sector (left) and use of biofuels in different transport modes (right) in 2050 (BLUE Map Scenario)

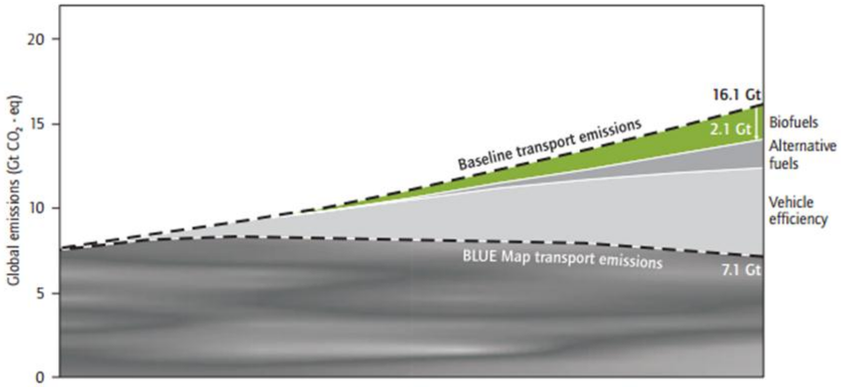

Note: Modal shifts (not included) could contribute an additional 1.8 Gt CO_2-eq. of emission reductions.
Source: IEA, 2010c.

Figure 1.6 Contribution of biofuels to GHG emissions reduction in the transport sector

In this roadmap, biofuel demand over the next decade is expected to be highest in OECD countries, but non-OECD countries will account for 60% of global biofuel demand by 2030 and roughly 70% by 2050, with strongest demand projected in China, India and Latin America (Figure 1.7). The first commercial advanced biofuel projects will be set up in the United States and Europe, as well as in Brazil and China, where several pilot and demonstration plants are already operating.

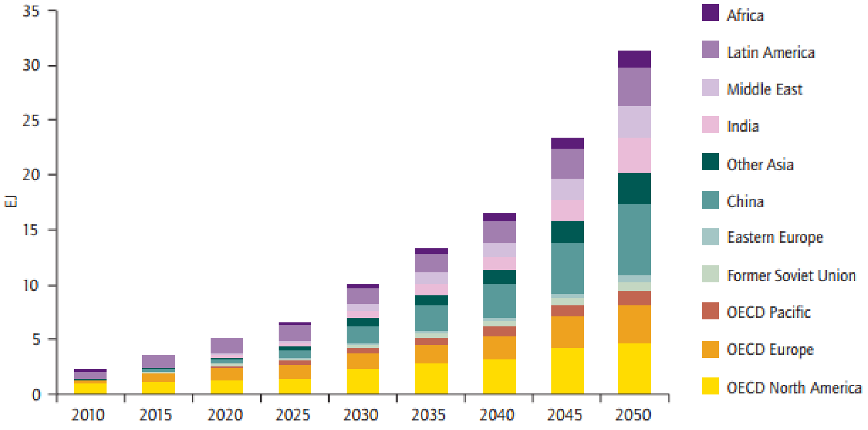

Note: FSU= Former Soviet Union.
Source: IEA, 2010c.

Figure 1.7 Biofuel demand by region 2010-50

1.5 Renewable diesel fuel

The term “biodiesel” in legislation is, till now, a general designation, which can be divided into different specific renewable diesel products: traditional biodiesel (fatty acid methyl ester (FAME)), Hydrotreated vegetable oil (HVO) which is sourced by feedstock like FAME while the end-product is like synthetic diesel, synthetic diesel (paraffinic hydrocarbons) produced from any carbon-based combustable matter by means of Fischer-Tropsch (FT) synthesis process and Dimethyl ether (DME) sourced from methanol or synthesis gas. The following sections will be focused on FAME (mainly RME) and HVO which were used in the experimental tests.

1.5.1 Traditional biodiesel (FAME)

The major components of vegetable oils and animal fats are triacylglycerols (TAG); often also called triglycerides). Chemically, TAG are esters of fatty acids (FA) with glycerol. The TAG of vegetable oils and animal fats typically contain several different FA. Thus, different FA can be attached to one glycerol backbone.

The different FA that are contained in the TAG comprise the FA profile (or FA composition) of the vegetable oil or animal fat. Because different FA have different physical and chemical properties, the FA profile is probably the most important parameter influencing the corresponding properties of a vegetable oil or animal fat.

To obtain traditional biodiesel, the vegetable oil or animal fat is subjected to a chemical reaction termed transesterification. In that reaction, the vegetable oil or animal fat is reacted in the presence of a catalyst (usually a base) with an alcohol (usually methanol) to give the corresponding alkyl esters (or for methanol, the methyl esters) of the FA mixture that is found in the parent vegetable oil or animal fat. Figure 1.8 depicts the transesterification reaction.

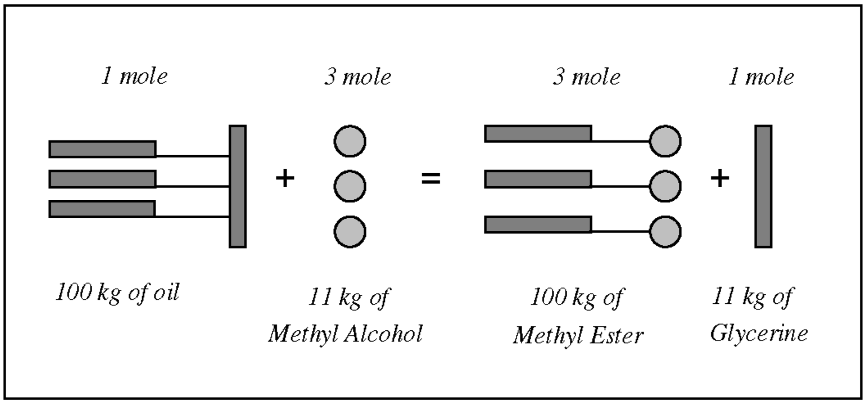

Figure 1.8 The transesterification reaction

Biodiesel can be produced from a great variety of feedstocks. These feedstocks include most common vegetable oils (e.g., soybean, cottonseed, palm, peanut, rapeseed/canola, sunflower, safflower, coconut, jatropha) and animal fats (usually tallow) as well as waste oils (e.g., used frying oils). The choice of feedstock depends largely on geography. Depending on the origin and quality of the feed-stock, changes to the production process may be necessary.

1.5.2 Hydrotreated vegetable oil (HVO)

Hydrotreating of vegetable oils (HVO) and animal fats is a process which is based on oil refining know-how and is used for the production of biofuels for diesel engines. In the process (Figure 1.9), hydrogen is used to remove oxygen from the triglyceride vegetable oil molecules and to split the triglyceride into three separate chains thus creating hydrocarbons which are similar to existing diesel fuel components. This allows the blending in any desired ratio without any concerns regarding quality (Mikkonen s.d.). The end product is clean paraffinic diesel fuel.

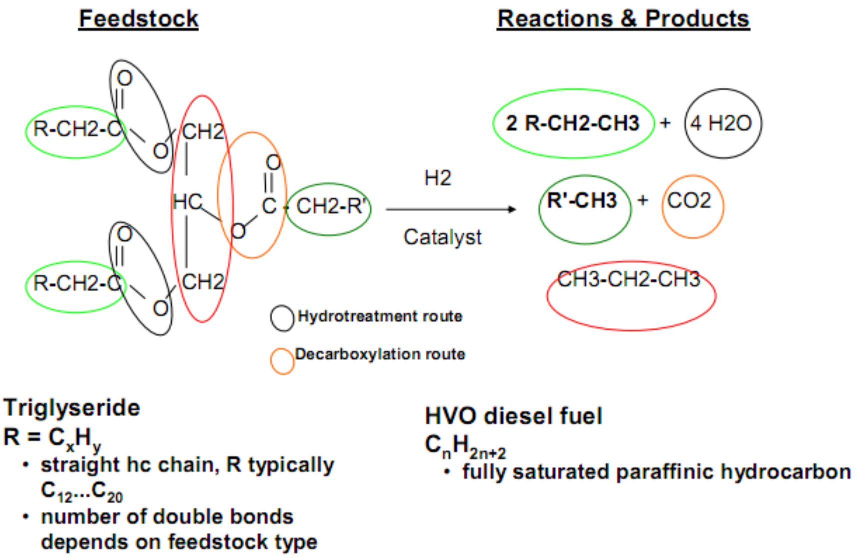
Feedstock
Reactions & Products
R-CH2-C
O
O
CH2
HC
CH2
C
CH2-R'
R-CH2-C
O
O
H2
Catalyst
2 R-CH2-CH3
+
4 H2O
R'-CH3
+
CO2
CH3-CH2-CH3
Hydrotreatment route
Decarboxylation route
Triglyseride
R = CxHy
• straight hc chain, R typically C12...C20
• number of double bonds depends on feedstock type
HVO diesel fuel
CnH2n+2
• fully saturated paraffinic hydrocarbon

Figure 1.9 HVO production process

HVO is a mixture of straight chain and branched paraffins – the simplest type of hydrocarbon molecules from the point of view of clean and complete combustion. Typical carbon numbers are C15 ... C18. Paraffins exist also in fossil diesel fuels which also contain significant amounts of aromatics and naphthenics. Aromatics are not favorable for clean combustion. HVO is practically free of aromatics and its composition is quite similar to GTL (Gas To Liquid) and BTL (Biomass To Liquid) diesel fuels made by Fischer Tropsch synthesis from natural gas and gasified biomass.

Chapter 2 – Experimental Apparatus & Test Procedures

2.1 Introduction

The experimental activity carried out within this thesis, as previously described in the *Introduction Chapter*, is focused on the evaluation of different biofuels on full load performance and part load emissions and on the characterization of soot particle number distributions from diesel engines; the experimental setup and the test procedure adopted for each of the abovementioned activities varies significantly depending on the target of the single activity, due to the specificity of the covered topics. As an example, the experimental characterization of particle number distributions required the usage of a specific instrumentation for the sampling, conditioning and measuring of the exhaust gas flow.

Moreover, as it is well known from literature and as it has been observed during tests, the operating parameters of some of the used measuring devices (*i.e.* the dilution ratio of a dilution system for particle number distribution analysis) may have a significant effect on the raw result obtained through experiments; consequently it was important to take into consideration those effects and try to modify, wherever possible, the experimental setup in order to avoid undesirable results. For these reasons it has been necessary to define, prior to the execution of tests, the right experimental setup and the right test procedure to be adopted in correlation with the final target of each research activity.

This chapter presents the experimental apparatus (*i.e.* type of engine, type of measuring devices, etc.) which was setup; for each of the referred above activities the choice of the experimental setup and a description of the operating principle of sampling and measuring devices will be given, as well as a discussion on the main operating parameters. Finally, each test procedure adopted will be presented.

2.2 Evaluated Fuels

2.2.1 Biodiesel feedstock comparison

In order to evaluate the effects that different feedstocks may have on engines, in terms of both full load performance and engine out emissions, two different first generation biodiesels sourced from rapeseed and Jatropha Curcas oils were investigated during the first part of the study. Therefore experimental tests were initially performed using the five following fuels:

- Diesel: standard Ultra Low Sulphur Diesel (ULSD) fuel compliant with EN590 (sulphur < 10 mg/kg);
- RME (B30): 30% vol. blend of Rapeseed Methyl Ester (RME) biodiesel with 70% diesel;
- JME (B30): 30% vol. blend of Jatropha Methyl Ester (JME) biodiesel with 70% diesel;
- RME (B100): neat RME biodiesel;
- JME (B100): neat JME biodiesel.

The properties of pure diesel and biodiesel fuels used are listed in Table 2.1, while the composition of neat biodiesel fuels, as well as the cetane numbers of each component as reported in (Dieselnet, "Appendix: Biodiesel Composition and Properties of Components" 2009), are listed in Table 2.2. It should be noticed that, as far as neat JME is concerned, the higher content of high cetane saturated fatty acids components, such as palmitic and stearic acids overcomes the effect of medium-low cetane unsaturated fatty acids compounds, such as oleic and linoleic acids, thus leading to a considerably higher cetane number for neat JME respect to neat RME.

As it is well known from literature, see for instance (Postrioti 2004), the higher density and viscosity of neat biodiesel may lead to a significant increase of spray penetration, which determines higher risks of fuel spray impingement on liner and oil dilution. In addition, the boiling curve of biodiesel, which usually shows a very narrow distillation temperature range (generally in the range between 330 and 360°C, see Table 2.1 and Figure 2.1), also affects the residence time of fuel in the oil, with negative consequences in terms of oil dilution behavior. The higher density and viscosity of biodiesel may have a negative impact on injection flow rate, causing a noticeable decrease of injected quantities, especially for short injector actuations (i.e. for pilot injections) (Millo 2013), thus leading to a significant increase of the premixed portion of the main combustion, with negative effects in terms of CO and HC emissions.

Although not all fuel characteristics can be scaled on the basis of the blending percentage, the neat fuels analysis was preferred during this first part of the research project, in order to gather more accurate information concerning biofuel characteristics and to allow at least rough estimates also for different blending ratios. Even if the oxygen content of the biodiesel reduces both its stoichiometric ratio A/F_{st} (13 instead of 14.5 of diesel, with a 11% reduction) and its Lower Heating Value (LHV) (37.4 MJ/kg instead of 43 MJ/kg of diesel, with a 13% reduction), the $LHV/A/F_{st}$ ratio is more closely comparable for biodiesel and diesel (with differences lower than 4%), thus highlighting the potential for recovering engine performance at full load by means of a proper ECU recalibration, since the maximum brake mean effective pressure (BMEP) which can be achieved at a given relative air/fuel ratio λ is proportional to the $LHV/A/F_{st}$ ratio.

Table 2.1 Properties of neat fuels

Properties	Diesel	RME (B100)	JME (B100)
Carbon content C [w%]	86.5	79.6	79.7
Hydrogen content H [w%]	13.5	12.1	12.2
Oxygen content O [w%]	-	8.3	8.1
Distillation Temperatures			
Initial Boiling Point [°C]	171.2	154.5	152.4
10% [°C]	204.0	346.7	343.0
50% [°C]	274.8	349.8	348.0
90% [°C]	342.3	354.6	352.9
Final Boiling Point [°C]	366.9	360.0	353.4
Sulphur content S [ppm] (EN ISO 14596-98)	< 10	< 10	<10
Stoichiometric ratio $(A/F)_{st}$	14.4	13.0	13.0
Net heating value, LHV [kJ/kg] (ASTM D 240-00)	42960	37365	37455
Cetane Number	51.8	51.5	56.6

(ISO 5165-98)			
Density at 15 °C [kg/m^3]	840	883	880
Viscosity at 20 °C [mm^2/s]	3.14	7.09	7
$LHV/(A/F)_{st}$ [MJ/kg]	2.99	2.88	2.88

Table 2.2 Composition of neat fuels

Fatty Acid	Formula	Cetane Number	RME (B100) [%]	JME (B100) [%]
Methyl Oleate	$C_{19}H_{36}O_2$	54	56.4	41.2
Methyl Linoleate	$C_{19}H_{34}O_2$	43	23.5	33.7
Methyl Palmitate	$C_{17}H_{34}O_2$	74	9.0	15.6
Methyl Linolenate	$C_{19}H_{32}O_2$	23	3.5	n.d.
Methyl Elaidate	$C_{19}H_{36}O_2$	-	2.9	1.3
Methyl Stearate	$C_{19}H_{38}O_2$	81	2.4	6.8
Others		-	2.3	1.4

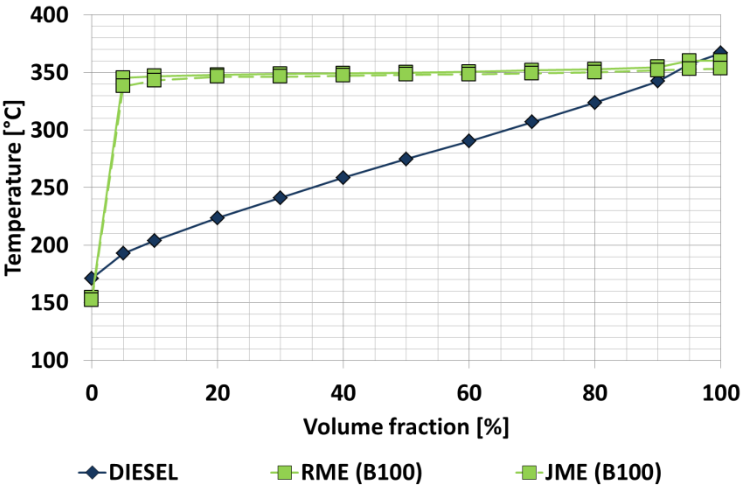

Figure 2.1 Distillation curves of tested fuels

2.2.2 Fatty Acid Methyl Esters and Hydrotreated Vegetable Oil comparison

Two different types of biodiesels were used during the second portion of the study: a first generation biodiesel and a hydrotreated vegetable oil, both sourced from rapeseed. The analysis was focused, in first place, on the characterization of the effects of high percentage biodiesel blends on full load performance and engine out emissions. A special care was given on the evaluation of the impact that different fuel characteristics may have on combustion process as well. Tests were performed using the three following fuels:

- Diesel: standard Ultra Low Sulphur Diesel (ULSD) fuel compliant with EN590 (sulphur < 10 mg/kg);
- RME (B30): 30% vol. blend of Rapeseed Methyl Ester (RME) biodiesel with 70% diesel;
- HVO (B30): 30% vol. blend of Hydrotreated Vegetable Oil (HVO) with 70% diesel.

The main properties of reference diesel and of the two biofuels blends are listed in Table 2.3, while distillation curves and viscosity vs. temperature trends are shown in Figure 2.2 and Figure 2.3, respectively.

It can immediately be noted that the HVO blend shows distillation and viscosity characteristics closer to those of the diesel fuel in comparison with the RME blend, which on the contrary shows a significant shift towards fractions with higher boiling temperatures and towards higher viscosity levels. HVO blend properties, which are closer to those of diesel, ensure that the main fuel spray characteristics are almost the same of diesel fuel sprays, as also shown by (Hulkkonen 2011) and (Sugiyama 2011).

As far as the energy content of the fuels is concerned, the oxygen content of the RME blend reduces its Lower Heating Value to 41.2 MJ/kg instead of 42.8 MJ/kg of diesel, with a 4% loss. Moreover, since the RME blend density is about 2% higher than diesel density and because, if the viscosity and bulk modulus effects on the injection rate could be neglected on first approximation, the amount of fuel injected should scale as the square root of the pressure drop across the injector nozzle multiplied by the fuel density, the injected quantities with the RME blend should be about 1% higher than diesel, for the same injection pressure and duration. This leads to an energy content introduced into the cylinder that should be expected to be about 3% lower with the RME blend in comparison with diesel. Nevertheless results reported in (Millo 2013) suggested that the hypothesis of a change of fuel injected fuel mass proportional to the square root of fuel density, cannot be acceptable for RME B30, especially under low injection pressures and short energizing times operations.

For the HVO blend, the LHV is on the contrary slightly higher than that of diesel fuel (43.3 MJ/kg instead of 42.8 MJ/kg of diesel, with a 1% difference), but the density is about 3% lower, thus leading to an energy content introduced into the cylinder roughly 2.5% lower, assuming again on first approximation that, for the same injection pressure and duration, the injected quantity depend on fuel density only. However, (Sugiyama 2011) reported a significant increase of the injected quantity (up to 5%) when operating the engine with neat HVO, attributing this effect to the lower bulk modulus of HVO. Moreover, if the LHV/$(A/F)_{st}$ ratio is considered, all the three fuels show identical values, thus suggesting the potential for recovering engine performance at full load with biofuel blends by means of a proper ECU re-calibration as has been already highlighted in paragraph 2.2.1.

As far as fuel properties impacting on combustion and emissions are concerned, the lower aromatic contents of RME and HVO blends highlight the potential of reducing smoke and PM emissions, with further additional benefits expected for RME, due to the better local oxygen availability during the combustion process which is assured by the oxygen content of the fuel blend.

The significantly higher cetane number of the HVO blend should lead to a decrease of unburned hydrocarbons (HC) and carbon monoxide (CO) emissions, although the closed loop combustion control implemented in the ECU is expected to minimize combustion phasing shifts due to different fuel ignition qualities, and therefore to minimize fuel conversion efficiency changes as well.

Table 2.3 Main fuel properties

Properties	Diesel	RME (B30)	HVO (B30)
Carbon content C [w%]	86.5	83.4	85.4
Hydrogen content H [w%]	13.5	13.2	14.1
Oxygen content O [w%]	-	3.4	-
Total Aromatics [w%]	25.7	19.2	16.1
Distillation Temperatures			
Initial Boiling Point [°C]	171.5	185	164.5
10% [°C]	202.4	223	204.3
50% [°C]	265.6	302.2	273.2
90% [°C]	335.8	340.2	317.2
Final Boiling Point [°C]	364.6	358.4	349.2

Sulphur content S [ppm] (EN ISO 14596-98)	< 10	< 10	<10
Stoichiometric ratio $(A/F)_{st}$	14.5	13.98	14.66
Net heating value, LHV [kJ/kg] (ASTM D 240-00)	42840	41240	43290
Cetane Number (ISO 5165-98)	51.8	51.5	56.6
Density at 15 °C [kg/m^3]	8837.5	853	812.2
Viscosity at 40 °C [mm^2/s]	2.681	3.183	2.545
LHV/$(A/F)_{st}$ [MJ/kg]	2.95	2.95	2.95
Oxidation Stability [hours] (EN 15751:2009)	-	9.9	27.4
Surface Tension at 20 °C, [mN/m]	30.4	33.1	28

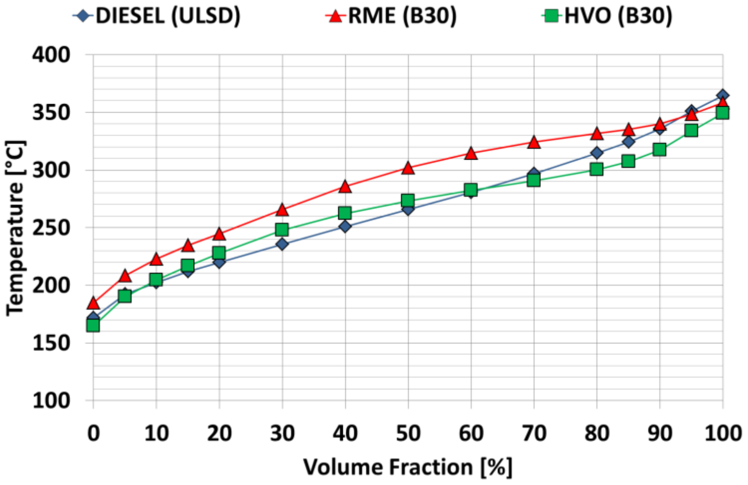

Figure 2.2 Distillation curves for the diesel reference fuel and for the RME and HVO B30 blends

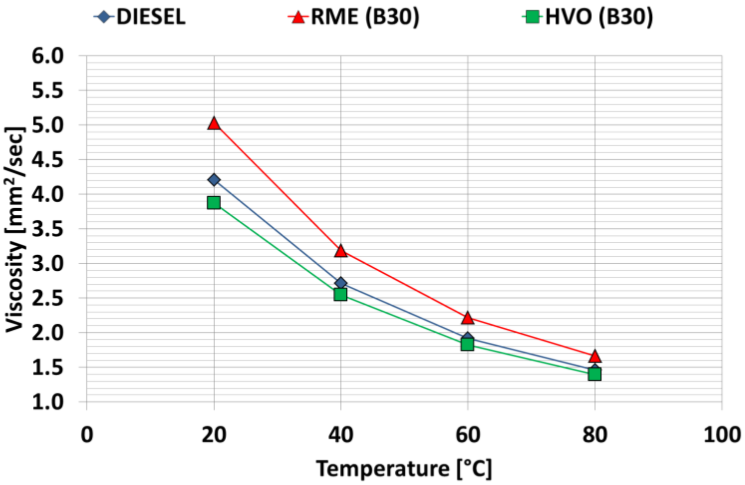

Figure 2.3 Viscosity vs. temperature for the diesel reference fuel and for the RME and HVO B30 blends

2.3 Engine and test rig description

Since the biodiesel usage appears to be particularly challenging in small displacement engines, due to the high risks of lube dilution caused by cylinder liner fuel jet impingement occurring during post-injections used for Diesel Particulate Filter (DPF) regeneration and due to the increased risk of injector nozzle coking in small diameter nozzle holes, the analysis has been carried out on two passenger cars Diesel engines, the main characteristics of which are listed in Table 2.4. The engines had similar hardware solutions: both engines are modern Euro 5 small displacement turbocharged common-rail DI diesel engines and are of the smallest engines on the European market if considering the unit displacements. As far as the Original Equipment Manufacturer (OEM) after-treatment is concerned, the engines are equipped with a close-coupled after-treatment system, featuring a DOC and a catalyzed DPF integrated in a single canning, the main characteristics of which are shown in Table 2.5.

Investigation conducted with both engines was carried out on the same test rig; a scheme of the chosen test bench is shown in Figure 2.4. As the figure depicts, the engine was connected to an eddy current dynamometer, while engine fuel consumption was measured by means of an AVL 733S gravimetric fuel meter; exhaust gases were sampled at the engine outlet and measured through a Fisher-Rosemount NGA-2000 gas analyzer, while an AVL 415S smoke meter was used for the measurement of filter smoke number (FSN) for repeatability checks. Due to the target of the experimental investigation, there was no need for running tests over transient operating conditions (i.e. simulating driving cycles such as NEDC); for this reason, an eddy current dynamometer has been chosen, which enabled the operation of the engines under steady-state conditions.

During tests, all the engine control parameters were controlled by a PC that was directly connected to the engine ECU: the test engines were also equipped with a closed-loop combustion control capable of maintaining the 50% of mass fraction burned (MFB50) crank angle at its optimal position under part load operating conditions. Moreover, the piezoresistive pressure transducers integrated in the glow plugs used for the closed loop combustion control were also used for the measurement of the in-cylinder pressure. The output from these transducers was first filtered by a low-pass filter to reduce high frequency noise and to prevent aliasing errors and signal distortion and then finally sampled by means of a 12 bit high-speed multichannel data acquisition board (National Instruments DAQCard-Al-16E4), coupled to a high resolution (0.4°) crank-angle encoder to ensure proper timing of the sampled data. At each operating condition 100 consecutive engine cycles were recorded to obtain a wide statistical sample. Data acquisition and post-processing were performed by means of ICE Analyzer a suitable developed program for internal combustion engine indicating analysis (Badami 2001).

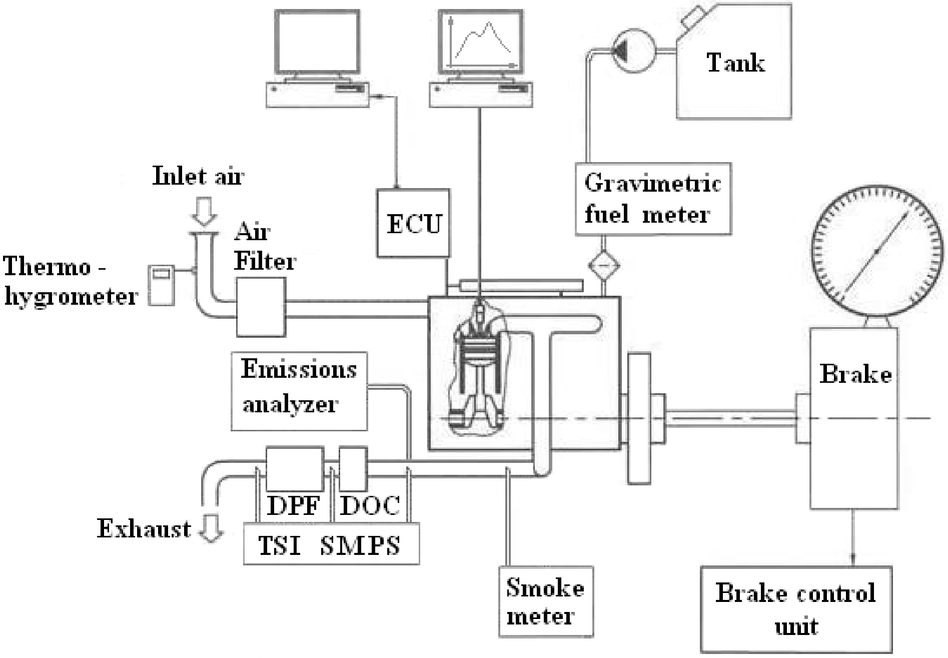

Figure 2.4 Scheme of the experimental test rig

Table 2.4 Main characteristics of the engines under test

	Biodiesel feedstock comparison	FAME and HVO comparison
Engine Type	Diesel, 4 stroke, EU5	Diesel, 4 stroke, EU5
Displacement	1248 cm^3	1248 cm^3
Cylinders arrangement	4 in line	4 in line
Bore x Stroke	69.6 mm x 82 mm	69.6 mm x 82 mm
Compression ratio	16.8:1	16.8:1
Air Management System	Turbocharger with WG; Cooled High Pressure EGR	Turbocharger with VGT; Cooled High Pressure EGR
Fuel injection system	Common Rail	Common Rail
Maximum Power	55 kW @ 4000 rpm	72 kW @ 3500 rpm
Maximum Torque	200 Nm @ 2000 rpm	230 Nm @ 2250 rpm

Table 2.5 Main characteristics of the after-treatment system

	DOC	DPF
Substrate volume [dm^3]	1.1	2.6
Substrate length [mm]	76.2	177.8
Wall Thickness [mil]	4.5	10

2.4 Full load performance and part load emissions characterization

2.4.1 Test procedure

Experiments were initially carried out evaluating the effects of biodiesel blends on engine performance at full load: it is well known from (Millo 2011, Millo 2010) that when running the engine with biodiesel without any modification in ECU calibration, the torque output is reduced due to the lower LHV of the fuel blend (approximately -13% for neat biofuels and -4% for B30 blends on average).

Due to this performance gap, tests were subsequently performed running the engine with a specifically adjusted ECU calibration (which will be hereafter referred to as "Specific Calibration"), obtained by changing properly the injected quantity up to reach the same torque or the same smoke level measured under diesel operation (whichever occurring first), so to more completely evaluate the performance potential of biodiesel blends.

Moreover, the effects on engine emissions and fuel consumption of biodiesel feedstock first and biodiesel typology afterwards, were also evaluated at different part load operating points, listed in Table 2.6, selected after a preliminary numerical simulation as representative of the New European Driving Cycle. It should be noticed that the chosen engines were adopted on different vehicles with different road loads and equipped with different gearboxes aimed to comply different mission profiles, thus explaining the differences among the operating points which were tested with each engine as it is shown in Table 2.6.

Since the change in fuel from diesel to biofuel blends may lead to a reduction in the torque output due to the lower energy content of the injected fuel blend, the same BMEP target was obtained by means of an adjustment of the energizing time of the main injection while keeping unchanged the pedal position, and thus the operating point position on the engine calibration map. It should be pointed out that in this way all the main engine control parameters (e.g. injection pressure and timing, EGR rate, etc.) are not changed from the standard calibration, and therefore the biofuel potentialities in terms of emissions reductions may not be fully exploited.

Finally, further experimental investigations were carried out to fully exploit the benefits that could be obtained for instance by adjusting the EGR rates in order to take into account the different biofuel blends Soot-BSNO$_x$ and BSCO-BSNO$_x$ trade-offs: these effects were therefore evaluated for each operating point by varying the EGR rate from 0% to the maximum achievable value corresponding to the fully open EGR valve position.

Table 2.6 Part load operating points

	Biodiesel feedstock comparison		FAME and HVO comparison	
Operating Point	Speed [rpm]	BMEP [bar]	Speed [rpm]	BMEP [bar]
1	1500	2	1000	4
2	1500	5	1500	2
3	2000	2	1500	5
4	2000	5	1500	8
5	2500	5	2000	5

6	2500	8	2000	8
7	-	-	2500	8

2.5 Analysis of the sensitivity of the different fuels to engine calibration

This type of analysis was carried out only when fuelling the engine with RME and HVO blends. Objective of this activity was to evaluate that the sensitivity of the different fuels to different calibration settings, such as for instance injection timing.

2.5.1 Test procedure

Tests were carried out at low load, low speed operating point (1500 [rpm] @ 2 [bar] BMEP) running the engine with a specifically adjusted injection pattern featuring a single injection event (main injection) with and without EGR.

The accelerator pedal position, which was used with diesel fuel, was used even when the engine was ran with biofuels. This approach was chosen in order to maintain unchanged the injection duration, when different fuels were used, thus focusing the attention on the effects of the timing only, and of the sensitivity to the timing of the different fuels. A range of start of injections from 3 [deg BTDC] up to 10 [deg BTDC], with a step of 1 [deg], was explored (see Table 2.7). Figure 2.5 depicts the injection pattern used for this kind of analysis.

Table 2.7 Test matrix of start of injection (SOI) sweep tests

Operating Point	Start of Injection (SoI) [deg BTDC]
1500 [rpm] @ 2 [bar] BMEP (with and without EGR)	2.7
	3.7
	4.7
	5.7 (cal.point)
	6.7
	7.7
	8.7
	9.7

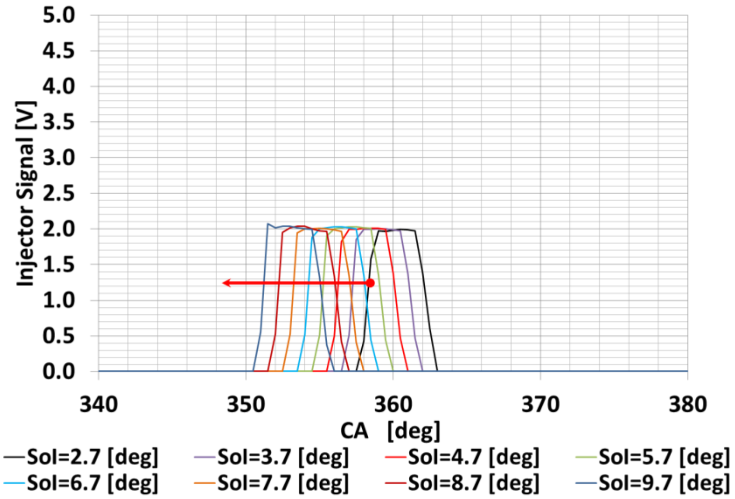

Figure 2.5 Sweep of the start of the main injection

2.6 PM gravimetric analysis

Gravimetric as well as thermogravimetric analysis of PM, (section 2.7) and mutagenic investigation (section 2.9) of PM were carried out only with RME and HVO blends. Objective of this activity was to evaluate the effects that different fuel characteristics may have on PM emitted from the engine.

2.6.1 Experimental setup

An AVL SPC-472 partial flow smart sampler was used to collect PM on filters under different engine operating conditions. This instrument is composed of:

- a control cabinet;
- a dilution tunnel and a filter rack.

A scheme of a partial flow dilution tunnel is shown in Figure 2.6. The sampled exhaust gases are diluted with compressed air provided by the test cell supply system after undergoing a complete conditioning in the control cabinet. The dilution starts at the mixer at the tunnel entrance and continues throughout the tunnel under turbulent flow conditions. The dilution tunnel has a diameter of about 30 mm and it is about 635 mm long. After the tunnel, the diluted exhaust gas stream is led through the analysis filter. The flows of both exhaust gases and dilution air are taken under control by the control cabinet.

As far as the smart sampler operating parameters are concerned, the dilution tunnel was kept at about 190°C during the whole test campaign in order to obtain a temperature upstream the analysis filter of about 50°C. Two different dilution ratios were used depending on the tested operating conditions.

PM sampled at engine exhaust was collected on PALLFLEX Membrane TISSUQUARTZ 2500QAT-UP filters of 70mm of diameter suitable for exposure in aggressive environments characterized by high temperatures (up to 1093°C). Therefore, there was no detectable weight loss to be attributed to filters when thermogravimetric tests were performed. PM mass collected on analysis filters was measured by means of a Mettler Toledo UMX2 microbalance with 0.1 micrograms of resolution and a maximum load of 210 mg.

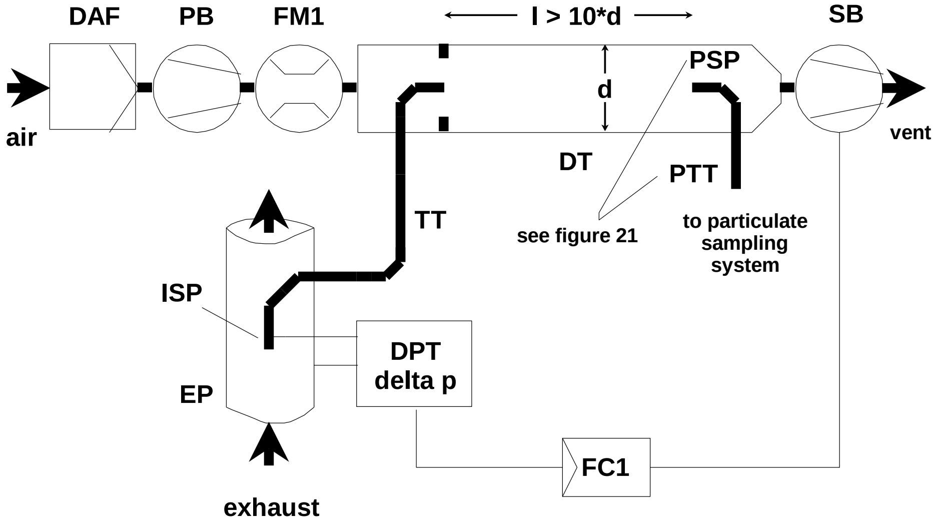

Figure 2.6 Partial flow dilution tunnel scheme

2.6.2 Test procedure

In order to highlight the effects of engine load on PM in terms of both mass and chemical composition (see next paragraph 2.7) a sweep of engine loads was performed. Three different levels of load were chosen (Table 2.8) while the engine was running at 1500 rpm. When biofuels were used, tests were carried out adopting the same specifically adjusted calibration used during part load emission characterization (see paragraph 2.4.1).

The main operating parameters adopted during tests, such as dilution ratio and diluted exhaust gases temperature upstream the filter are listed in Table 2.9. During tests, exhaust gases were sampled downstream of the turbine at engine out position. At each operating point at least three filters were loaded for repeatability check. In more detail, a dilution ratio of 9 was adopted at medium and high loads while a volume of 0.1 Nm^3 of diluted exhaust gases was flowed through the filter. When the low load operating point was tested, a dilution ratio of 5 was adopted, instead, in order to avoid a prolonged exposure of the analysis filter at the exhaust stream. At low load operating point only, filters were fed with about 0.2 Nm^3 of diluted exhaust gases, thus allowing to load a noticeable PM mass on the filters even though the engine was running at conditions characterized by low PM emissions.

In order to increase tests reproducibility, filters were weighted after being exposed at controlled atmosphere (environment temperature 20 ±1°C and 50±5% of relative humidity) for 48 h according to (EN 14907:2005 s.d.) standard.

Table 2.8: Gravimetric analysis operating points

FAME and HVO assessment		
Operating Point	Speed [rpm]	BMEP [bar]
2	1500	2
3	1500	5
4	1500	8

Table 2.9 Test conditions and parameters used during gravimetric tests

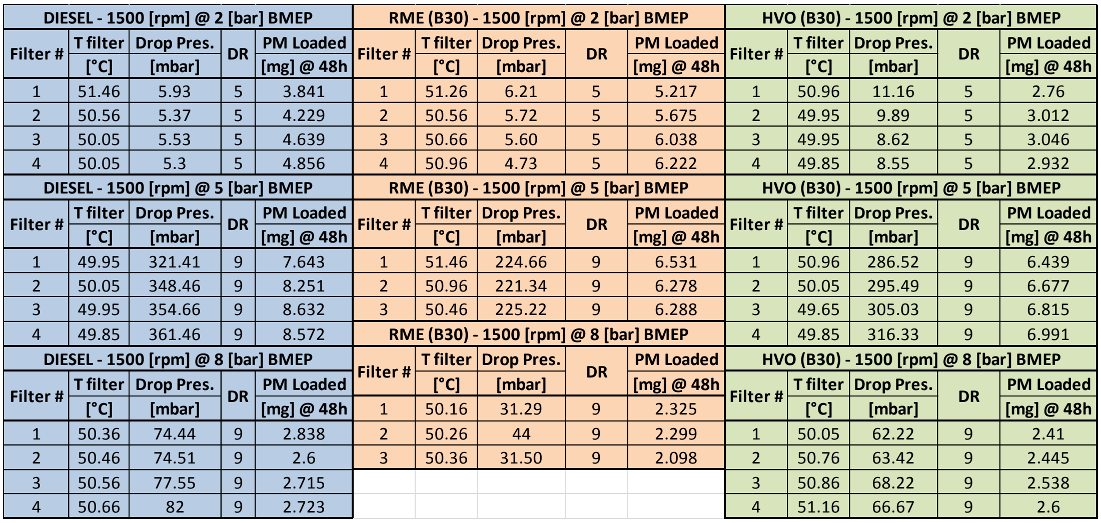

DIESEL - 1500 [rpm] @ 2 [bar] BMEP

Filter #	T filter [°C]	Drop Pres. [mbar]	DR	PM Loaded [mg] @ 48h
1	51.46	5.93	5	3.841
2	50.56	5.37	5	4.229
3	50.05	5.53	5	4.639
4	50.05	5.3	5	4.856

RME (B30) - 1500 [rpm] @ 2 [bar] BMEP

Filter #	T filter [°C]	Drop Pres. [mbar]	DR	PM Loaded [mg] @ 48h
1	51.26	6.21	5	5.217
2	50.56	5.72	5	5.675
3	50.66	5.60	5	6.038
4	50.96	4.73	5	6.222

HVO (B30) - 1500 [rpm] @ 2 [bar] BMEP

Filter #	T filter [°C]	Drop Pres. [mbar]	DR	PM Loaded [mg] @ 48h
1	50.96	11.16	5	2.76
2	49.95	9.89	5	3.012
3	49.95	8.62	5	3.046
4	49.85	8.55	5	2.932

DIESEL - 1500 [rpm] @ 5 [bar] BMEP

Filter #	T filter [°C]	Drop Pres. [mbar]	DR	PM Loaded [mg] @ 48h
1	49.95	321.41	9	7.643
2	50.05	348.46	9	8.251
3	49.95	354.66	9	8.632
4	49.85	361.46	9	8.572

RME (B30) - 1500 [rpm] @ 5 [bar] BMEP

Filter #	T filter [°C]	Drop Pres. [mbar]	DR	PM Loaded [mg] @ 48h
1	51.46	224.66	9	6.531
2	50.96	221.34	9	6.278
3	50.46	225.22	9	6.288

HVO (B30) - 1500 [rpm] @ 5 [bar] BMEP

Filter #	T filter [°C]	Drop Pres. [mbar]	DR	PM Loaded [mg] @ 48h
1	50.96	286.52	9	6.439
2	50.05	295.49	9	6.677
3	49.65	305.03	9	6.815
4	49.85	316.33	9	6.991

DIESEL - 1500 [rpm] @ 8 [bar] BMEP

Filter #	T filter [°C]	Drop Pres. [mbar]	DR	PM Loaded [mg] @ 48h
1	50.36	74.44	9	2.838
2	50.46	74.51	9	2.6
3	50.56	77.55	9	2.715
4	50.66	82	9	2.723

RME (B30) - 1500 [rpm] @ 8 [bar] BMEP

Filter #	T filter [°C]	Drop Pres. [mbar]	DR	PM Loaded [mg] @ 48h
1	50.16	31.29	9	2.325
2	50.26	44	9	2.299
3	50.36	31.50	9	2.098

HVO (B30) - 1500 [rpm] @ 8 [bar] BMEP

Filter #	T filter [°C]	Drop Pres. [mbar]	DR	PM Loaded [mg] @ 48h
1	50.05	62.22	9	2.41
2	50.76	63.42	9	2.445
3	50.86	68.22	9	2.538
4	51.16	66.67	9	2.6

2.7 PM chemical composition (TGA) analysis

The analysis on the chemical composition of PM was executed on the same filters which were loaded during analysis discussed in section 2.6.

2.7.1 Experimental setup

TGA was carried out by means of a TA Q50 thermogravimetric analyzer provided by TA Instruments at Bureau Veritas Laboratories. The thermogravimetric analyzer measures the amount and rate of weight change in the sample as a function of increasing temperature in a controlled atmosphere (for more details about test procedure see 2.7.2 section). Data collected by sample weight changes provide precious information concerning the chemical composition of PM.

As far as the operating parameters are concerned, the analyzer was calibrated in terms of both mass and temperature before test execution. In more detail, since precise transition temperatures are essential during TGA, during temperature calibration the Curie temperature of nickel element was checked. Moreover a sample pan of alumina was chosen for tests.

2.7.2 TGA test procedure

At least one filter for each operating point listed in paragraph 2.6 was analyzed. Samples after being mounted on TGA analyzer, were exposed at an inert atmosphere composed of nitrogen and left to stabilize at room temperature (25°C); then were heated up to 225°C. The mass loss which was detected during this phase could be linked to water and volatile organic compounds vaporization (see Figure 2.7). Subsequently, samples temperature was risen up to 800°C and stabilized at this conditions for 5min in order to desorb most of the volatile fraction of PM. In this case the mass depletion gave information about vaporization and thermolysis of medium and high molecular weight organic compounds (see Figure 2.7) In both cases filters were exposed to a nitrogen flow of 90ml/min and a temperature rate of 10°C/min was used. Afterwards, the inert atmosphere was replaced by an oxidant one (air) and temperature was risen up to 1000°C. In more detail an air flow of 90ml/min and a temperature rate of 10°C/min were used. In this phase due to the presence of air, soot was oxidized to form gaseous carbon oxides while only mineral compounds remained on the pan at the end of the test (Figure 2.7). Samples weight was continuously monitored throughout the test. Table 2.10 TGA test procedure summarizes the above described procedure.

Table 2.10 TGA test procedure

Test phases	Atmosphere	Mass loss linked to:
Room temperature 25°C	Nitrogen	no mass loss was detected
Temperature increase: 25°C to 225°C (@ 10°C/min)	Nitrogen (@ 90mL/min)	vaporization of water and low boiling compounds
Temperature increase: 225°C to 800°C (@ 10°C/min)	Nitrogen (@ 90mL/min)	vaporization of high boiling compounds
Temperature increase: 800°C to 1000°C (@ 10°C/min)	Air (@ 90mL/min)	oxidation of PM soot fraction

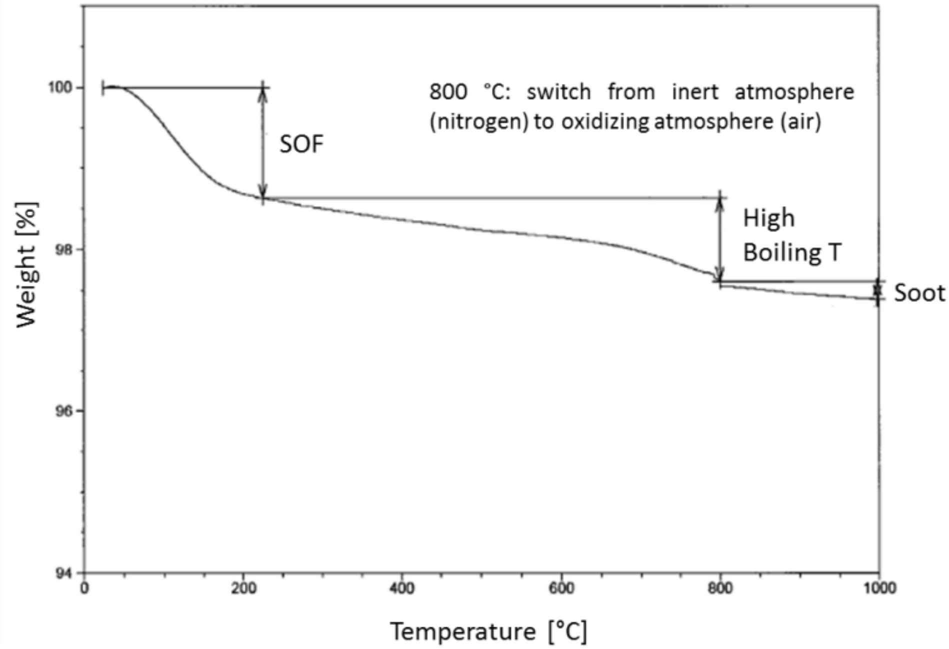

Figure 2.7 Sample mass loss as a function of sample temperature

2.8 PM particles number and size distribution analysis

2.8.1 Experimental setup

2.8.1.1 Measuring system

A TSI model 3080 scanning mobility particle sizer (SMPS) was used to record particle size distributions for exhaust soot particles under different engine operating conditions. This instrument is composed of:

- an electrostatic classifier TSI 3080 with a Kr-85 Bipolar Charger using Kripton as ion source;
- an inlet impactor;
- a differential mobility analyzer TSI 3081;
- a condensation particle counter TSI 3025A.

A detailed description of the operating principle of a measuring device similar to the one here adopted is given by (De Filippo 2009).

As far as the SMPS operating parameters are concerned, the polydisperse aerosol flow was set to 1.5 lpm, with a sheath flow at 15 lpm; with a 0.071 cm impactor nozzle, it was possible to cover a broad range of particle diameters from 6 to 225 nm, namely those within the *Fine Particles* classification (EPA 2004). These classes of nano-particles are the most significant because they include both the *Ultrafine Particles* and the smaller range of the *Accumulation Mode* which represent the typical classes of nano-particles emitted from automotive diesel engines (Kittelson 1998). The size distributions were corrected for multiple-charged particles produced in the neutralizer within the SMPS.

2.8.1.2 Sampling system

Exhaust gas was sampled from engine outlet (i.e. downstream of the turbine). The sampling system consists of two dilution stages and a sampling line, named Line A in Figure 2.8. This line (1m long, 4 mm inner diameter) consists of an heated and insulated stainless steel pipe which connects the sampling point to the first dilution stage (first dilutor of a DEKATI DI-1000 package) heated at 250°C to reduce nucleation (I. S. Abdul-Khalek 1998).

Exhaust gas was sampled into the primary ejector pump at approximately 5 lpm leading to ~ 0.15s residence time which is sufficiently short to minimize diffusion losses and produce a minimum increase in mean particle diameter from coagulation, according to (Maricq 2010). In the first dilution stage filtered compressed air heated to 150 °C flows through an orifice placed on the sample flow axis as shown in Figure 2.8. In order to obtain a higher dilution ratio (DR), a second dilution stage was used (second dilutor of a DEKATI DI-1000 package); the second stage is not heated and it is directly connected to the TSI 3080 SMPS by means of a flexible pipe (7.5 m long), which length could not be reduced due to safety reasons and room constraints. Each dilution stage nominally provides a DR of 8, which leads to a total DR of 64, which should likely reduce particle agglomeration according to (Abdul Khalek 1998) and (Abdul Khalek 1999), (Lüders 1998).

The significant length of the flexible pipe upstream to the SMPS could undoubtedly affect the measured number distributions, especially in the range of the smallest nanoparticles, typically referred to as the “*Nucleation Mode*”. Two sets of data were recorded in order to evaluate the effect of the transfer line length on the measured size distributions. The engine operating conditions were kept equal for both sets of data, namely with the engine running at 2000 rpm @ 5 bar BMEP.

For both sets of data, the SMPS 3080 was equipped with a 0.457 mm impactor which allowed the coverage of the size range of particle diameters from 15 to 660 nm. The only difference between the two sets of the data was the length of the pipe that connected the second stage diluter with the inlet of the SMPS: a longer (about 7.5 m long) and a shorter (about 1 m long) transfer line.

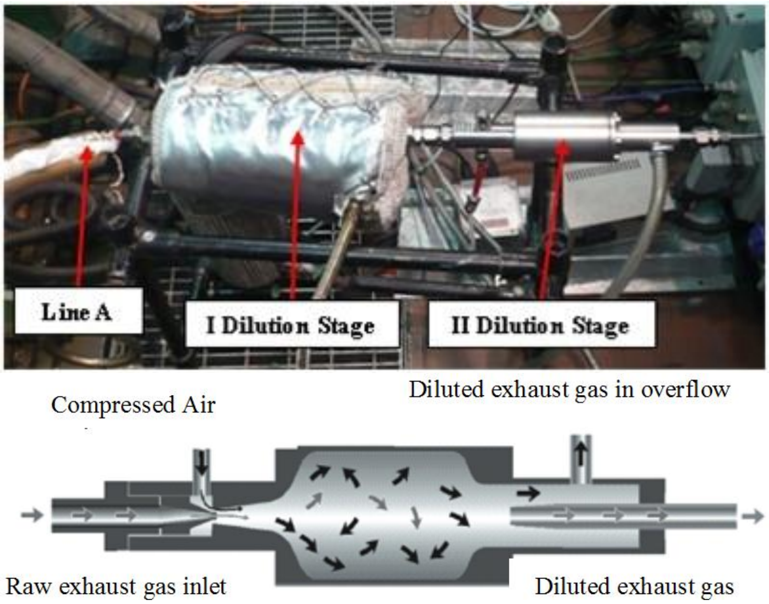

Figure 2.8 Two stage dilution system (top); scheme of the first stage dilutor (bottom)

Figure 2.9 displays the comparison between number and mass size distributions measured with the longer (yellow symbols) and the shorter transfer line (black symbols). In general, the two number distributions do not differ qualitatively (peak diameter at about 50 nm) and quantitatively (max peak number is ~ $6*10^7$ particle/cm^3). However, it is possible to observe a slight decrease in PN concentration for particles smaller than 40 nm. Specifically this reduction is significant at sizes with d<20nm (>60%) but it reduces below 15% at sizes d=40 nm. Since for safety reasons and room constraints the shorter transfer line could not be used for the whole experimental activity, the long transfer line had to be selected, even though it affects particle concentration below 40 nm, as shown in Figure 2.9.

However, it is worth noticing that the results presented in this work, which basically are comparisons between different engine operating conditions or fuels, were obtained with the same experimental set-up and are therefore comparable relatively to each other; however, the comparison of the presented results with other studies reported in literature should be carried out carefully, due to differences that may be caused by the different sampling systems.

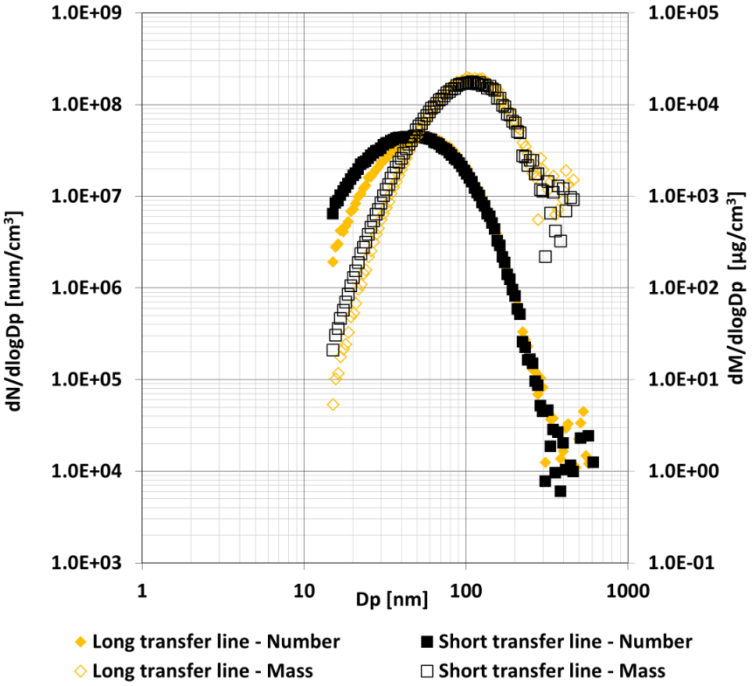

Figure 2.9 Particle number and size distribution comparison for long and short transfer line, 2000 rpm and 5 bar BMEP engine operating point

2.8.2 Test procedure

Particle number and size distribution were evaluated at different engine operating conditions, typically under part load under normal mode fuelling the engine with diesel and different biofuels blends, in order to highlight the impact of the different fuels on PM characteristics.

In Table 2.11 is listed the test matrix, in more detail, during the second portion of this study PM number distributions were explored by sweeping engine load from 2 bar BMEP up to 8 bar while keeping constant the engine speed (1500 rpm). Due to the fact that the adoption of biofuel blends may lead to a reduction in the torque output of the engine because of the lower energy content of the injected fuel blend, the same BMEP target among fuels was obtained by means of a specifically adjusted ECU calibration as it has been already highlighted in paragraph 2.4.1.

Table 2.11 Particle size and number distribution test matrix

	Biodiesel feedstock comparison		FAME and HVO assessment	
Operating Point	Speed [rpm]	BMEP [bar]	Speed [rpm]	BMEP [bar]
1	1500	2	1500	2
2	2000	5	1500	5
3	2500	8	1500	8

2.9 Mutagenicity analysis of PM emissions

2.9.1 Test procedure

Mutagenicity tests were carried out on PM samples collected during tests discussed in section 2.6 when the engine was ran at low load and low speed operating conditions (1500 rpm @ 2 bar BMEP) and fuelled with conventional diesel, RME B30 and HVO B30. Table 2.12 lists the PM mass collected on filters as well as the volume of diluted exhaust gases with was flowed through each filter.

Table 2.12 Samples specifications

Fuel	PM mass [mg]	Diluted exhaust gases volume [l]
ULSD	4.69	216.77
RME	6.13	214.03
HVO	3.05	213.51

Samples were extracted firstly by means of sonication in dichloromethane and subsequently in a Soxhlet apparatus. The solvents once unified were dried and then redissolved in DMSO (dimethylsulfoxide), immediately before Ames tests execution.

Mutagenicity analysis was performed employing the standard test protocol (Standard Methods 2005). In more detail TA98 and TA100 Salmonella typhimurium strains were chosen since these strains were shown to be most sensitive to mutagens of organic extracts of diesel engine particles. Depending on the tester strain different types of mutations can be detected:

- TA98 detects mutagens that cause frameshift mutation and so module shift;
- TA100 detects mutagens that cause base-pair substitutions and therefore mutagens that induce to a wrongly reading of DNA.

Moreover tests were performed with and without metabolic activation by microsomal mixed-function oxidase systems (S9 fraction). Preparation of the liver S9 fraction from rats was carried out as described in (Standard Methods 2005).

Tests were performed using petri capsules containing a plate on which was applied an agar containing a limited amount of histidine and biotin, a suspension of Salmonella typhimurium, the sample to be tested at different dilution ratio with DMSO and, in the case of metabolic activation a 10% of S9 mix. Plates were incubated at 37°C for 48 h. and subsequently, the histidine revertant colonies were counted.

When tests were performed without metabolic activation the following two mutagens were used as positive controls:

- the sodium azide mutagen that causes base-pair substitutions mutations and thus able to detect TA100 strain;
- the 2-nitrofluorene mutagen that causes frameshift mutations in TA98 strain.

When S9 fraction was used, the 2-aminofluorene mutagen was chosen for detecting both TA98 and TA100 strains.

Every sample, was tested thrice. According to the criteria given by (Standard Methods 2005) results were considered positive if the number of revertants on the plates containing the test concentration was more than double the number of spontaneous revertants and a reproducible dose-response relationship was observed.

The mutagenicity ratio, was used in order to represent outcomes obtained from this tests campaign. Mutagenicity ratio (MR) was calculated as follows:

$$MR = \frac{RN}{Revertants_{Spontaneous}}$$

Where RN is referred to the number of net revertants:

$$RN = Revertants_{Sample} - Revertants_{Spontaneous}$$

The number of revertants which grow in these conditions is directly linked to the mutagenic potential of the used mutagen. In order to compare results obtained by different fuels, RN and MR referred to 1mg of sample and 1 Nm^3 of air were calculated as well.

Chapter 3 – Full Load Performance And Part Load Emissions Assessment

3.1 Introduction

In this chapter results from the experimental activity described in section 2.4 will be presented and discussed. The analysis will start with the assessment of the engine performance when running the unit under tests at full load with different fuels. In more detail, results obtain with both standard and specific engine calibrations will be analyzed within two different sections: the first one related to the biodiesel feedstock comparison (section 3.2.1.1) the second one focused on the comparison between FAME and HVO fuels (section 3.2.1.2).

Afterwards a discussion related to the outcomes provided by operating the engine at part load with conventional and renewable diesel fuels will follow. The comparison between results obtained when fuelling the engine with biodiesel sourced by different feedstock will be presented in section 3.2.2.1. As far as HVO assessment is concerned, results will be discussed in section 3.2.2.2.

Finally the sensitivity of the different fuels to different engine calibrations will be analyzed in in paragraph 3.2.3.

3.2 Results analysis and discussion

3.2.1 Full load performance

3.2.1.1 Biodiesel feedstock comparison

Results concerning the comparison of full load engine performance for the different fuel blends with the standard ECU calibration are shown in Figure 3.1 on the left. As expected when biofuels were used a loss of engine performance was observed due to the lower LHV of the blends and to the lower injected volume that cannot be fully compensated by the small increase in fuel density of biodiesel blends (see Table 2.3 for fuel properties) (Millo 2013). In more detail in the range of revolution speeds which goes from 1500 rpm up to the maximum explored revolution speed (3250 rpm) a decrease, on average, of 1.5% for 30%v/v blends was observed independently of the used feedstock. The performance gap was increased up to 8% in the case of neat JME (B100) and 6.7% in the case of neat RME (B100). Similar outcomes were observed by (Beatrice 2009). In that case, differences in the engine performance between different feedstocks were attributed to the actual fuel properties (e.g. viscosity or compressibility) that biofuels had at full load engine working conditions with respect to the ones measured at more moderate reference conditions.

Moreover, some issues in the low end torque are quite evident, in particular at 1250 rpm, with a considerable decrease (6% for 30%v/v blends and 13.3% for neat biodiesel) of the engine torque output, far beyond the expected engine derating due to the lower energy content of the injected biofuel.

Figure 3.2 reports the measured cylinder pressure, mass fraction burned and injector signal traces for all the tested fuels when the engine was running at 1250 rpm and at full load with standard calibration. All injection parameters were kept constant for all fuels and also the injected volume estimated by the ECU was constant for all tests. It is evident that the lower IMEP value of biofuels with respect to diesel is to the consequence of the lower pressure traces which were achieved throughout the combustion process, even if similar boost pressure levels were achieved with all fuels (Figure 3.3 on the left).

Notwithstanding the detected torque penalty with biodiesels, they tend to increase the fuel conversion efficiency, as demonstrated by the Figure 3.4 (graph on the left). An increase of about 1.8% and 4% for B30 blends and neat biofuels with respect to diesel fuel was observed.

Finally, as far as the smoke emissions are concerned, an overall decrease of filter smoke number of almost 0.5 and 0.9 FSN for 30%v/v blends and neat biofuels were observed respectively. This reduction could be attributed to the presence of oxygen inside the biofuel molecule (see Figure 3.5 graph on the left) as well as to the lack of aromatics compounds in the fuel molecule.

Figure 3.1 (graph on the right) shows the comparison of full load engine performance for the different fuel blends with the specific ECU calibration. The calibration adjustment allowed RME and JME B30 and B100 blends to fully recover the performance gap related to the lower energy content of the biofuel, with even some performance benefit in the medium-low speed range. Moreover, it should also be pointed out that, even after the calibration adjustment, smoke emissions (which were significantly lower with the standard ECU calibration) were still appreciably lower in comparison with diesel values, as reported in Figure 3.5 (graph on the right).

The increase in torque output in the medium-low speed range cannot be only explained on the basis of the calibration adjustment. As matter of fact, due to the slightly lower LHV/$(A/F)_{st}$ ratio of neat biodiesels (roughly 4% lower), the torque output measured under biodiesel operation should never exceed diesel values even when running the engine at the same relative air-fuel ratio (unless one makes the hypothesis of large fuel conversion efficiency variations). Figure 3.4 (on the right) depicts the fuel conversion efficiency during full load tests for all fuels when ECU recalibration was carried out; with specific calibration all fuels exhibited similar efficiencies. However, the relaxation of the maximum injected quantity limits mapped in the ECU determined an increase in the injected fuel quantities higher than the expected, which leaded to a decrease in the relative air-fuel ratio for neat biodiesel; this resulted in an increase of the introduced energy content into the combustion chamber and also in an increase of the energy available for the turbocharging system which finally leaded to higher boost levels (see Figure 3.4 on the left); this behavior can explain the higher torque level measured in the medium-low speed range under biodiesel operation, although it is worth to be noticed that a significant FSN reduction can still be achieved in comparison with diesel (see Figure 3.5).

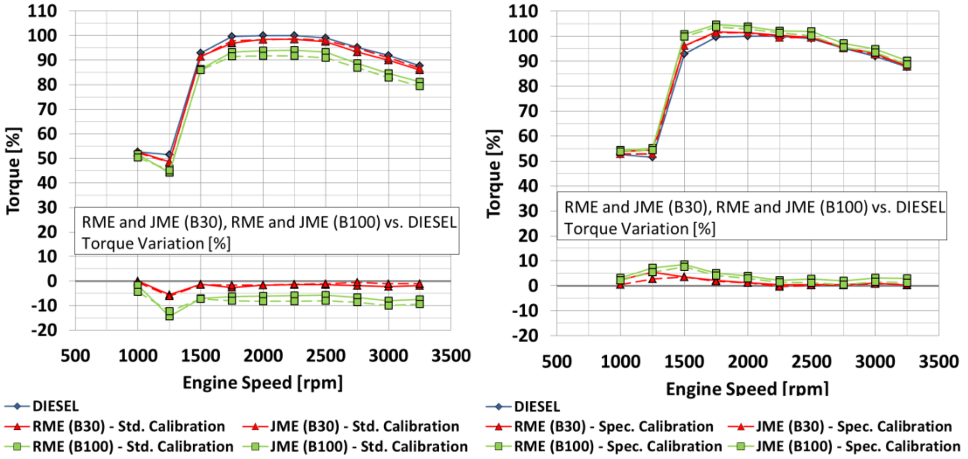

Figure 3.1 Full load engine performance with standard ECU calibration (left) and specific calibration (right) with all the tested fuels

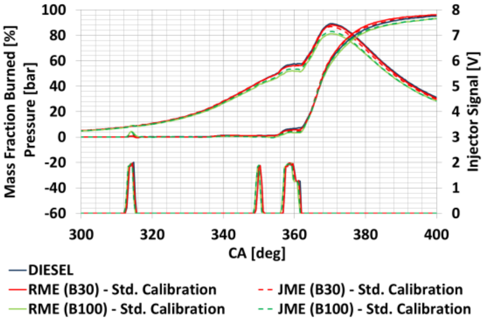

Figure 3.2 Cylinder pressure trace and injector signal for all fuels at 1250 rpm and full load (standard calibration).

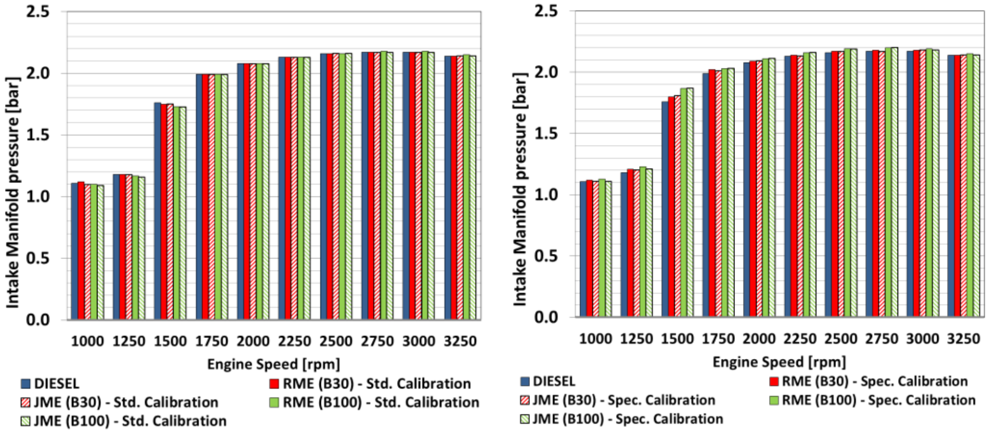

Figure 3.3 Intake manifold pressure during full load tests with standard (left) and specific (right) calibration and all fuels

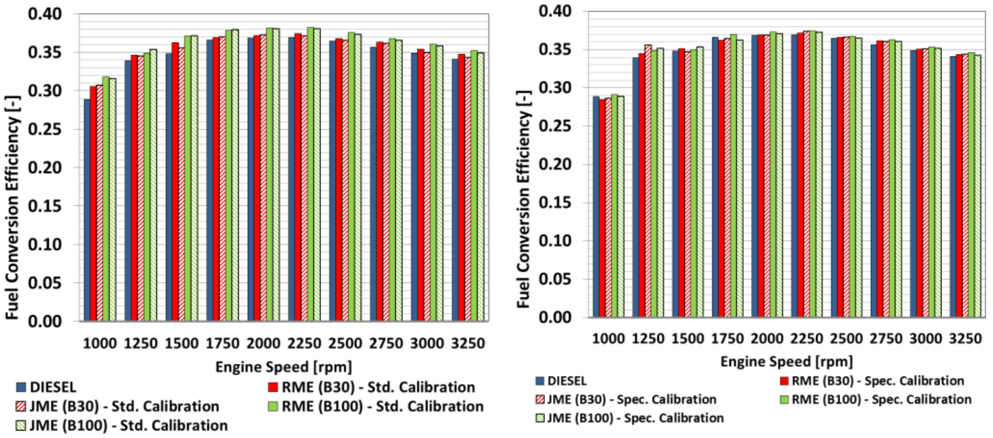

Figure 3.4 Fuel conversion efficiency at full load for all fuels: standard calibration (left), specific calibration (right)

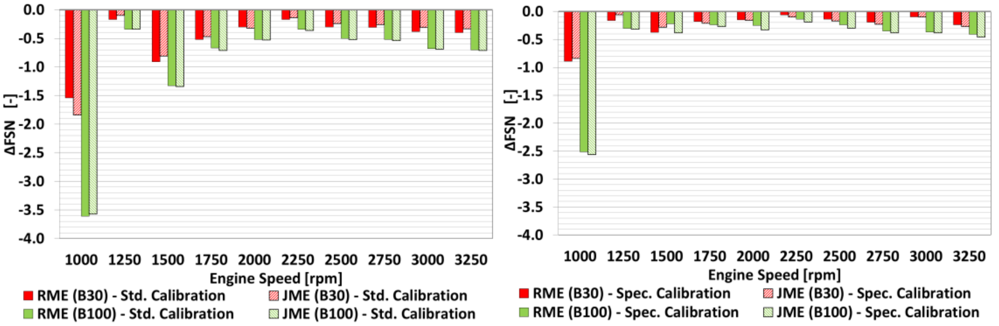

Figure 3.5 FSN reduction at full load for biodiesel blends compared to diesel: standard calibration (left), specific calibration (right)

3.2.1.2 *FAME vs HVO characterization*

The comparison of full load engine performance for diesel, RME and HVO B30 blends, without any modification in ECU calibration, is shown in Figure 3.6 (on the left). It is worth to be mentioned that the engine on which the tests were carried out is equipped with a different turbocharging system (featuring a VGT instead of a waste gate (WG)) from the engine which was used for the previous analysis: as a results, the torque versus speed output of the two engines are not directly comparable to each other. When fuelling the engine with the RME B30 blend a noticeable decrease of about 4 to 5 % on average in the torque output can be observed over almost the entire speed range. Moreover, as far as the HVO B30 blend is concerned, comparable levels of torque output with respect to the reference diesel (with differences lower than 1% on average) could be observed over almost the entire speed range, since a slightly higher LHV mitigates the negative effect of the lower fuel density. Similar levels of fuel conversion efficiency were registered for HVO B30 and diesel, while an overall increase in the fuel conversion efficiency of about 2% was observed when RME B30 was used (Figure 3.7).

Smoke levels measured under RME B30 blend operations with standard calibration were significantly lower in comparison with diesel operation, showing impressive FSN reductions as reported in Figure 3.8. HVO B30 smoke emissions were generally still appreciably lower in comparison with diesel values. In more detail, when the engine was running in a range between 1500 rpm and 4250 rpm a decrease of filter smoke number of about 0.6 and 0.2 for RME B30 and HVO B30 with respect to diesel was observed respectively. This decrease could be attributed mainly to the presence of oxygen in the RME molecule and at the absence of aromatic hydrocarbons in HVO molecule. A maximum decrease of about 2 filter smoke number for RME B30 if compared to diesel was observed at the lowest revolution speed (1250 rpm).

Further performance improvements were obtained by modifying the engine calibration in order to obtain the same smoke levels measured under diesel operation. The outcomes of the full load performance tests using the specific calibration and fuelling the engine with diesel RME and HVO are showed in Figure 3.6 (graph on the right). RME B30 fully recovered the performance gap highlighted before, with even an improvement in terms of torque output at low engine revolution speeds. (1250 rpm).

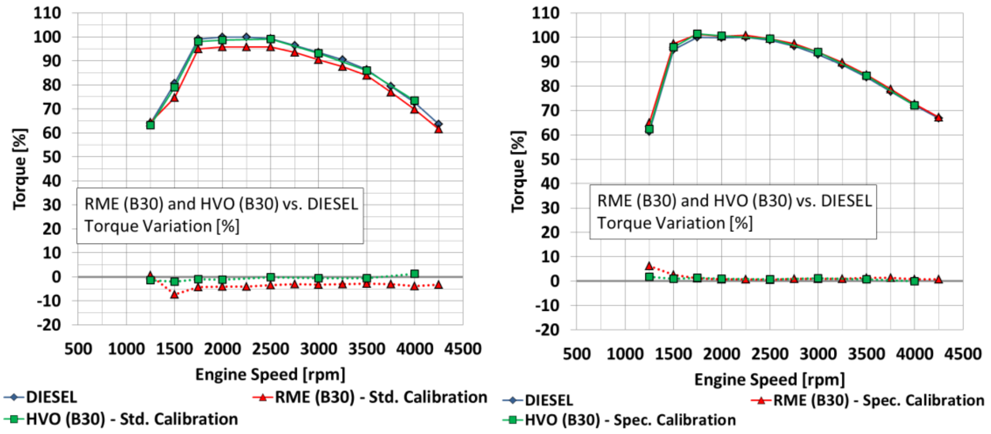

Figure 3.6 Full load engine performance with diesel, RME B30 and HVO B30: standard calibration (left), specific calibration (right)

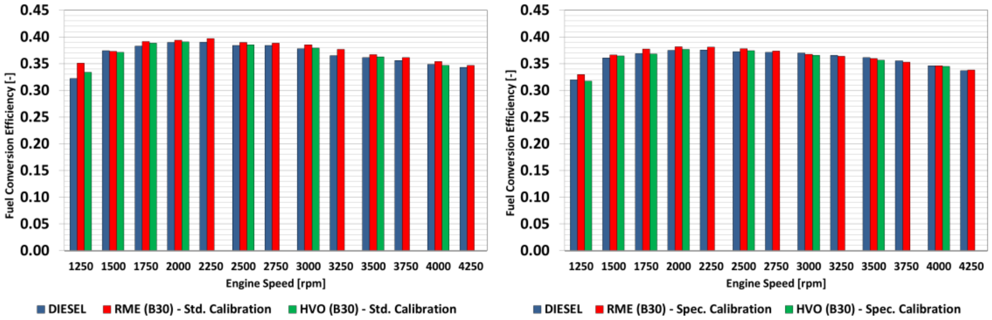

Figure 3.7 Fuel conversion efficiency at full load for all fuels: standard calibration (left), specific calibration (right)

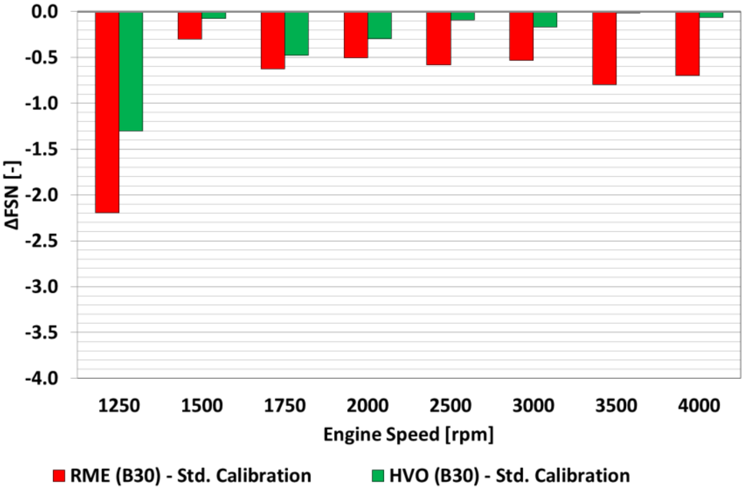

Figure 3.8 Filter Smoke Numbers reduction for biofuels respect to diesel at full load with standard calibration

3.2.2 Part load emission characterization

3.2.2.1 Biodiesel feedstock comparison

Engine parameters analysis for the selected k-points

Graphs depicted starting from Figure 3.9 up to Figure 3.14. report the main engine working parameters in terms of accelerator pedal position, main injection energizing time, engine intake air mass, boost pressure, EGR Rate, relative air to fuel ratio (λ), start of main injection (SoI main), 50% of mass fraction burned position and rail pressure for all fuels at the tested operating points. For each figure, left column refers to standard calibration, while right column to specific calibration. In all the diagrams the standard deviation bars measured on three repetition tests with all fuels and calibrations are also displayed, in order to decouple the engine repeatability from the net fuel effects.

With standard calibration, for biodiesel fuelling, it was necessary to increase the accelerator pedal position to obtain the same torque of the correspondent test with diesel fuel (Figure 3.9). This increase was necessary due to the decrease in the available energy content when biodiesel blends were used. The shift of the accelerator pedal position was "interpreted", from ECU point of view, as a change of engine operating point. This, in turn, caused a variation of engine control input parameters, as it is possible to observe in the following figures. Generally, at low load (@2 bar BMEP), the effect of the accelerator pedal position variation is not relevant in terms of change of operating input parameters, as should be noted in Figure 3.10 and Figure 3.11 as far as the energizing time of the main injection and the total air mass at the engine intake is concerned. Moreover, similar boost levels were achieved with all fuels (Figure 3.12) due to the poor turbocharger boosting capability typical of low speed/low load operating point. In fact, in the operating region around low load points, the boost pressure keeps just above the atmospheric pressure, therefore for little variations of the pedal position no significant increment of pressure was recorded for all biodiesel blends. Moreover, similar levels of EGR rate (Figure 3.13) and of λ (Figure 3.14) were observed for all fuels. At high load operating points (@ 8 [bar] BMEP), the accelerator pedal position drift in the case of neat biodiesels fuelling causes a larger variation in the engine parameters than at lower load operating points. Therefore a significant increase of engine intake air mass, boost pressure and relative air to fuel ratio as well as a significant decrease of EGR rate were observed especially for neat biofuels with respect to diesel and 30%v/v biodiesel blends. This drift had a significant impact on emissions as will be discussed in the following paragraph. As far as 30%v/v blends is concerned similar to diesel fuel levels were observed for all operating parameters. While most of the comments noted during the analysis of the high load tested points are still valid, the tests performed at medium load operating points (1500 rpm@ 5 bar BMEP and 2000 rpm @ 5 bar BMEP) highlighted a significant drift in the start of main injection for all biofuels (Figure 3.15). This drift should be explained taking into account the fact that these operating points are crucial as far as the combustion noise, BSFC and emissions are concerned. The correspondent SOI main values are generally targeted to have a delayed combustion timing so to keep both NO_x and combustion noise under control; as a consequence, any rise in accelerator pedal value to the ECU triggers a delayed MFB50 setpoint with respect to diesel fuel (Figure 3.16).

When the specific calibration was used, tests were carried out maintaining the accelerator pedal position fixed for all the fuels (Figure 3.9 graph on the right) and thus the MFB50 position (Figure 3.16). Therefore, in order to achieve the same

BMEP level obtained with diesel a variation of energizing time (ET) and SOI of the main injection only were observed (Figure 3.10 and Figure 3.15). Finally, similar operating parameters, i.e. EGR rate, λ etc. were observed for all fuels in contrast with standard calibration where the main operating parameters changed accordingly to the drift of the accelerator pedal position.

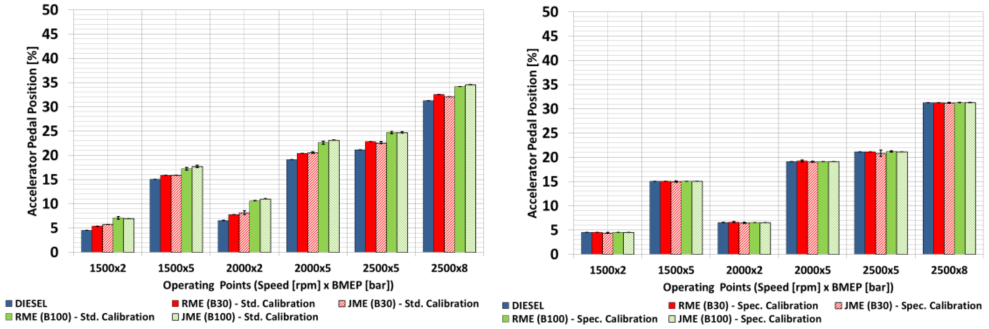

Figure 3.9 Accelerator pedal position for all fuels; standard calibration on the left and specific calibration on the right

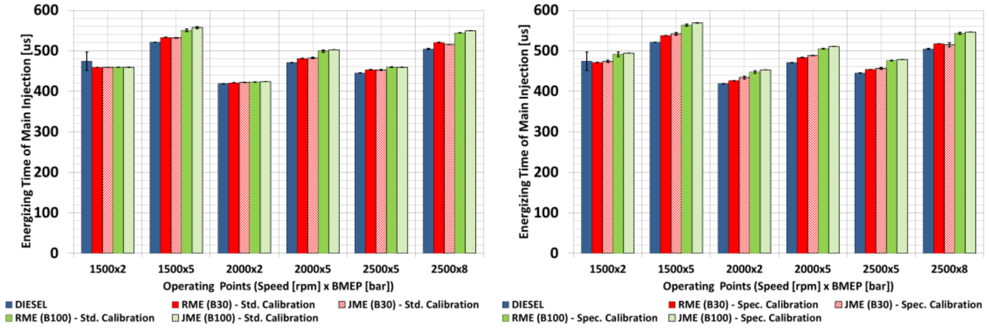

Figure 3.10 Main injection energizing time for all fuels; standard calibration on the left and specific calibration on the right

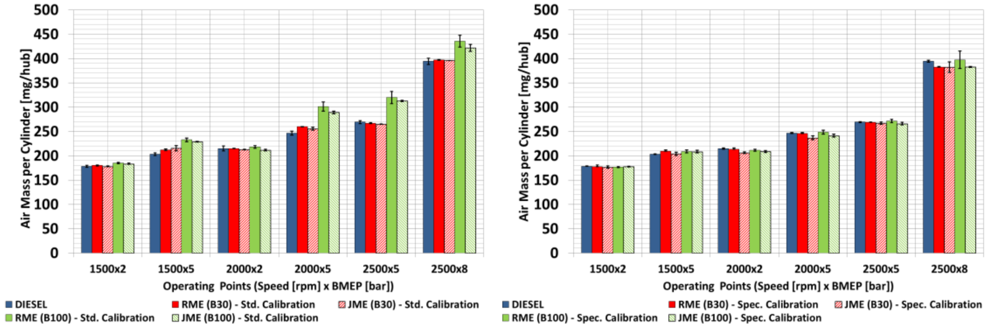

Figure 3.11 Trapped air mass per cylinder for all fuels; standard calibration on the left and specific calibration on the right

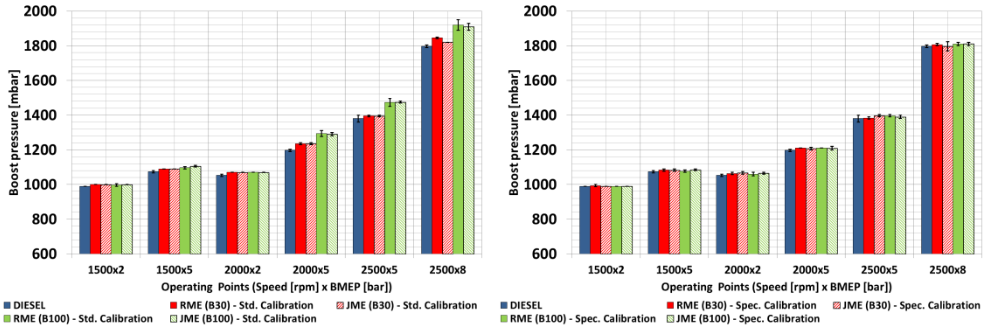

Figure 3.12 Boost pressure for all fuels; standard calibration on the left and specific calibration on the right

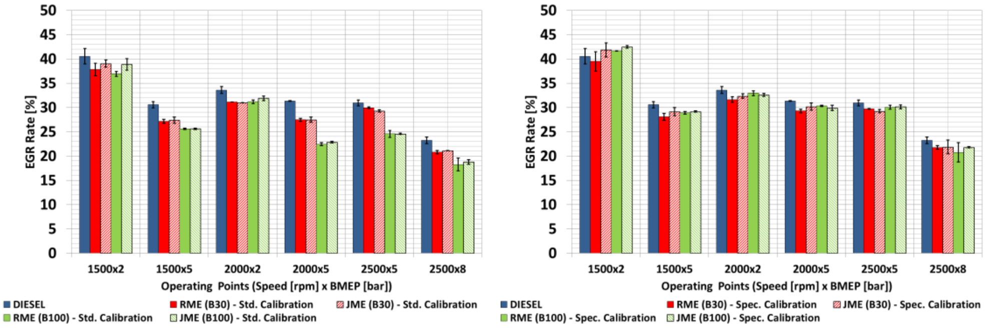

Figure 3.13 EGR rate for all fuels; standard calibration on the left and specific calibration on the right

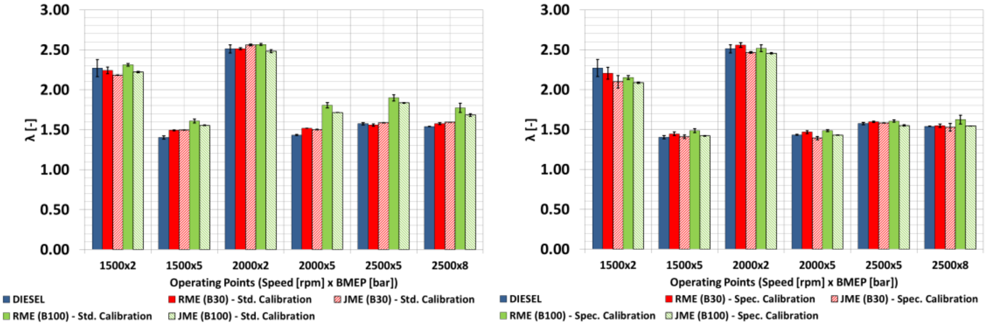

Figure 3.14 Relative air to fuel ratio (λ) for all fuels; standard calibration on the left and specific calibration on the right

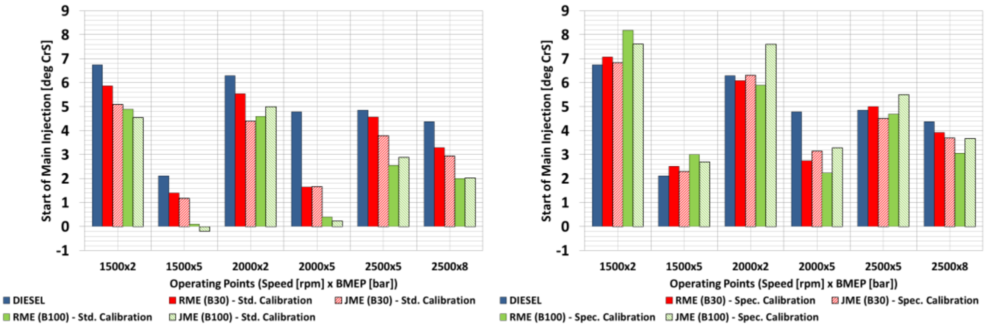

Figure 3.15 Start of main injection for all fuels; standard calibration on the left and specific calibration on the right

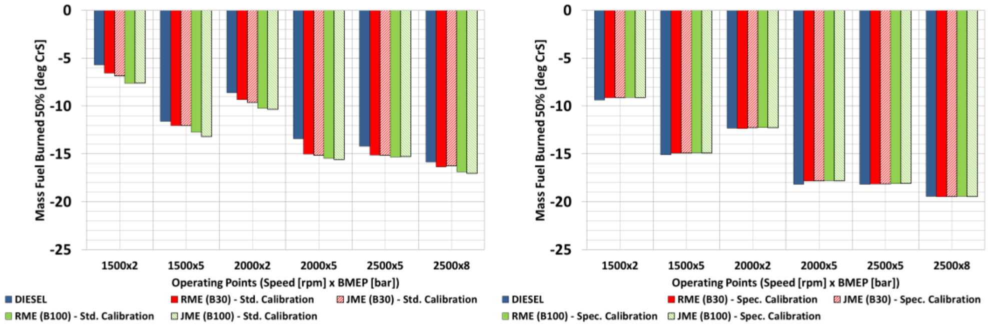

Figure 3.16 50% of fuel mass burned for all fuels; standard calibration on the left and specific calibration on the right

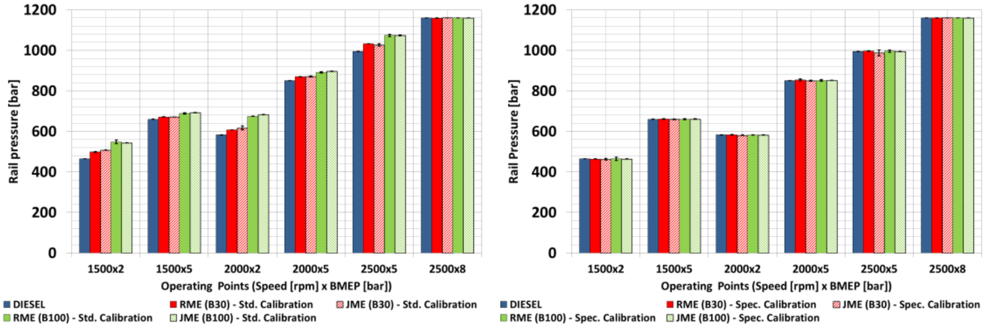

Figure 3.17 Rail pressure for all fuels; standard calibration on the left and specific calibration on the right

Combustion analysis for the selected k-points

Figures 3.18 – 3.20 report, for three operating conditions representative of low, medium and high load operation, respectively, the related indicating data, i.e. the cylinder pressure traces, injector signal, heat release rate (HRR) and cumulative mass fraction burned measured for cylinder 1. In order to maintain a good readability of the figures a comparison between diesel, JME B30 and JME B100 fuels only is shown, since both RME and JME biodiesel blends exhibited similar traces independently of the feedstock which was adopted for their production. All four engine cylinders were fitted with pressure transducers the signals of which are rooted to both ECU and ICE Analyzer software. The indicating diagrams highlight primarily the beneficial effect of the specific calibration in re-centering the pressure cycles for biodiesel fuelling.

At 1500 rpm @ 2 bar BMEP, JME B30 and JME B100 showed trends in terms of combustion pattern that are influenced both by the change of the engine calibration parameters with respect to diesel fuel and by their physical - chemical properties (Figure 3.18). With standard calibration, biofuels showed a delayed combustion timing with respect to the diesel. The change in the SOI of the main injection was directly connected to the accelerator pedal position. Furthermore the augment in accelerator pedal position (Figure 3.9) led to a not negligible increase in rail pressure (Figure 3.17) which could enhance fuel atomization and thus the combustion process of the fuel injected during pilot injection. Therefore, as far as the pilot injection combustion is concerned, all fuels exhibited similar behavior, although an appreciable delay can be noticed for the biofuels: the different ignitability properties of biofuels in conjunction with the more favorable conditions established in the combustion chamber when the biofuel was injected led to similar HRR traces, although again with noticeable delays for the biofuels. Notwithstanding the change in pedal position, the engine operated in conditions characterized by high EGR rates (of almost 40%) and similar relative air to fuel ratios (Figure 3.13 and Figure 3.14), thus similar HRR peak values for all fuels were registered during the combustion of the main injection. The combustion with biofuels was however slower; as a matter of fact an increase in the MFB10-90 was observed for biofuels if compared to diesel fuels (from 13 deg registered with diesel, the MFB10-90 angular interval was increased up to 15 deg and 19 deg for JME B30 and B100 respectively).

The in-cylinder analysis for the specific calibration at 1500 rpm, 2 bar BMEP operating point is shown on Figure 3.18 as well (graphs on the right). It can be clearly noticed that running the engine with biodiesel, the closed-loop combustion control progressively advances the start of injection in order to keep the MFB50 at the optimal mapped value. While for JME B30 no significant variations in the heat release of pilot and main injections can be observed, B100 blend shows a reduced heat release of the pilot injection, with a consequent increase of the premixed portion of the combustion. This change in the combustion process may be the main reason for the increased CO and HC emissions at low loads operating points as it will be discussed in the following paragraph. The increase in CO emissions at low loads (which is accompanied by a corresponding increase in HC emissions as shown in Figure 3.25 on the right) could be attributed to a change in the combustion process, since the higher viscosity and the higher distillation temperatures of the biodiesel can lead to a substantial deterioration of the fuel atomization and vaporization (Postrioti 2004), especially at low injection pressures and low in cylinder temperatures and pressures as for the 2 bar BMEP operating points (Figure 3.18). Moreover, the lower energy content of the biodiesel blends could also significantly affect the energy released by the pilot injection, thus causing an increase of the premixed portion of the combustion, while at higher loads this effect is usually not noticeable.

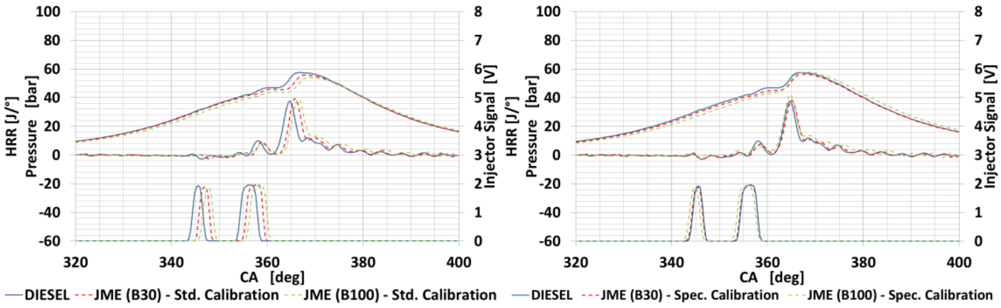

Standard Calibration (a) Specific Calibration (b)

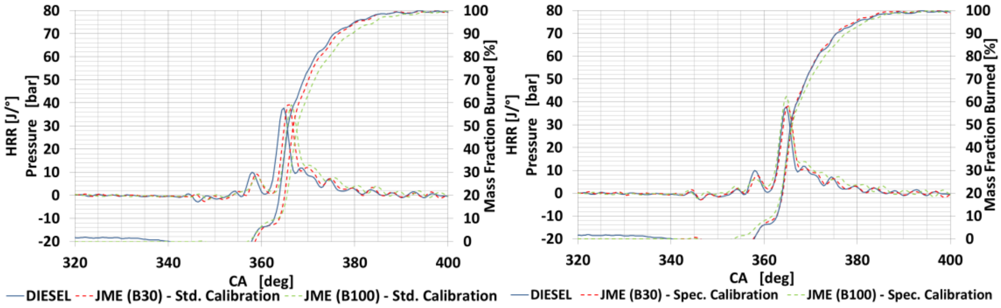

Standard Calibration (c) Specific Calibration (d)

Figure 3.18 Indicating analysis for the 1500 [rpm] @ 2 [bar] BMEP engine op. point for diesel, JME (B30) and JME (B100): in-cylinder pressure, heat release rate and injection pattern (top, figures a and b), heat release rate and mass fraction burned (bottom, figures c and d).

Increasing the engine load (@ 5 bar BMEP) (Figure 3.19) with standard calibration the increase in accelerator pedal position led to a delayed injection and to a delayed combustion process for biofuels. In more detail, biodiesel exhibited a similar behavior to diesel during combustion process, although showing some noticeable delay in the HRR process.

On the contrary, the specific calibration re-centered the combustion process in order to keep the MFB50 at its optimal mapped value, as shown in Figure 3.19 right.

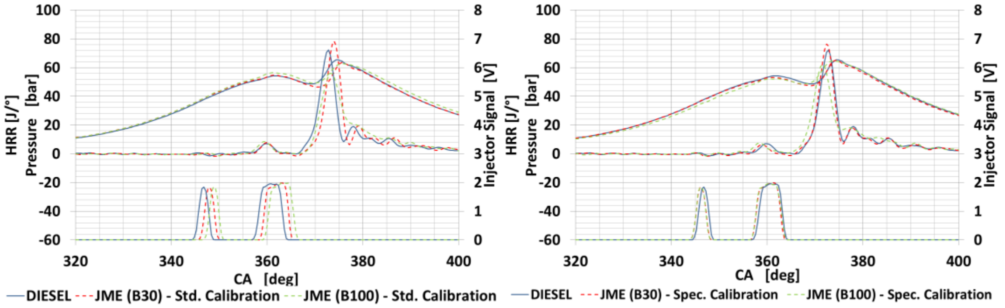

Standard Calibration (a) Specific Calibration (b)

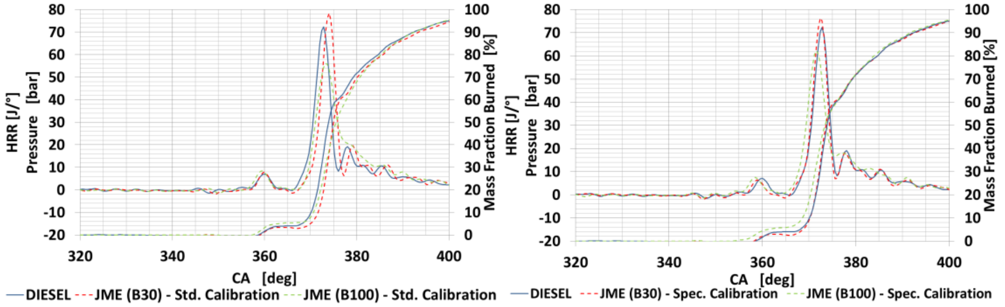

Standard Calibration (c) Specific Calibration (d)

Figure 3.19 Indicating analysis for the 2000 [rpm] @ 5 [bar] BMEP engine op. point for diesel, JME (B30) and JME (B100): in-cylinder pressure, heat release rate and injection pattern (top portion, figures a and b), heat release rate and mass fraction burned (bottom, figures c and d).

A further increase of the load with standard calibration led to a significant shift of the accelerator pedal position in the case of neat biodiesel fuelling; this increase causes a larger variation in the engine parameters, i.e. rail pressure, trapped air mass, boost pressure and their effects on NO_x and PM emissions, as it will be observed later. At high engine speed and load, the diffusive combustion phase is dominant and mitigates the effect of fuel properties. Then the critical effects of biodiesel blends on HRR pattern linked with the low pilot combustion efficiency and a different air/fuel mixing are reduced thanks to the high cylinder temperature reached at the TDC. When the engine was operated at same calibration input parameters as for the specific calibration, the HHR patterns for all fuels almost completely overlapped.

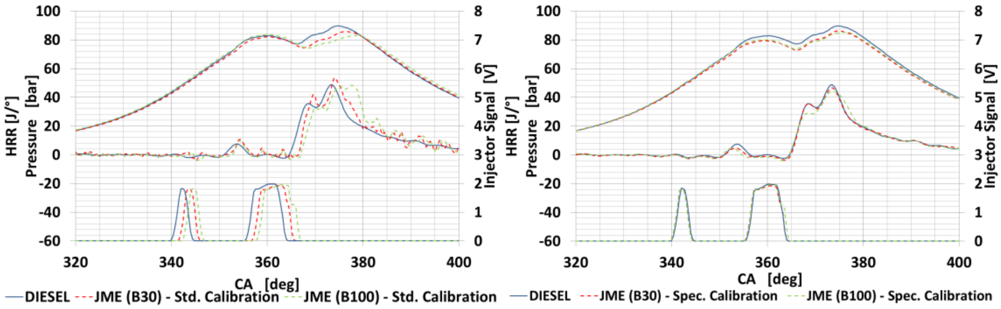

Standard Calibration (a) Specific Calibration (b)

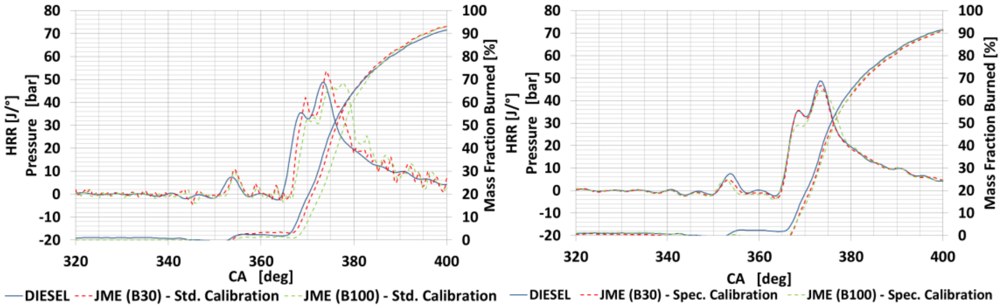

Standard Calibration (c) Specific Calibration (d)

Figure 3.20 Indicating analysis for the 2500 [rpm] @ 8 [bar] BMEP engine op. point for diesel, JME (B30) and JME (B100): in-cylinder pressure, heat release rate and injection pattern (top, figures a and b), heat release rate and mass fraction burned (bottom, figures c and d).

FC, BSFC and pollutant emission analysis for the selected k-points

The experimental results obtained under part load operating conditions with both engine calibrations (standard and specific) are shown in Figures 3.21 - 3.27, reporting respectively brake specific fuel consumption, engine fuel conversion efficiency, brake specific CO_2 , CO, HC and NO_x emissions and smoke emissions. For each figure, left column refers to standard calibration, while right column to specific calibration. In the following section the outcomes obtained with the specific calibration will be discussed first.

Brake specific fuel consumption (Figure 3.21) shows a 4% on average increase for both RME and JME B30 blends, which grows up to a 12% on average for B100, in good agreement with the lower LHV values for neat and blended biodiesel. Taking into account fuel densities, the volumetric fuel consumption increase – which is the performance parameter perceived by the final user – would be reduced to a more acceptable value of 2.5% and 7% respectively with RME and JME B30 and B100. Moreover, no significant differences could be observed based on the biodiesel feedstock (i.e. between JME and RME).

As far as fuel conversion efficiency is concerned (Figure 3.22), no appreciable differences can be seen between diesel and biofuels, with the only exception for the low speed – low load operating point (1500 rpm @ 2 bar BMEP), where a slight worsening of efficiency can be observed for biofuels. As a matter of fact, under part load operating conditions the closed-loop combustion control is capable of maintaining MFB50 at its optimum position, compensating for different fuel characteristics, as it has been reported (Millo 2011).

Thanks to the lower carbon content of neat RME and JME, the increase in CO_2 emissions that could be expected from BSFC data measured under biodiesel operation was partially compensated, as reported in Figure 3.23; as a result, from a pure Tank-To-Wheel approach, a modest increase in CO_2 emissions should be expected only in case of neat biodiesel usage.

BSCO emissions (Figure 3.24) measured under biodiesel blends operations were found to be comparable with diesel emissions at medium-high loads operating conditions, without appreciable differences depending on the biofuel feedstock; an appreciable increase was instead measured at low loads (2 bar BMEP) operating points. This increase in CO emissions could be attributed to a variation in the combustion process as highlighted in the previous paragraph.

As for CO emissions, an appreciable increase in BSHC (Figure 3.25) could be observed at low loads for both RME and JME blends (for both B30 and B100), while at medium-high loads HC emissions for biofuels were found to be comparable or only slightly higher to diesel levels.

Figure 3.26 shows $BSNO_x$ emissions. The modified ECU calibration allows to obtain comparable engine-out NO_x emissions when fuelling the engine with biofuels at medium-high loads, for both B30 and B100 blends, without significant differences between feedstocks; as far as low loads engine operating points are concerned, the high EGR rate used is likely to produce an highly premixed low temperature combustion, with an even more marked shift towards this kind of combustion regime when the engine is operated with biofuels, due to the lower energy released by the pilot combustion, thus resulting in significant NO_x emissions reductions (as already highlighted in Figure 3.18).

As far as engine-out smoke emissions are concerned (Figure 3.27), a noteworthy reduction can be observed for medium and high load operating conditions, especially for B100 biodiesel blends; at low loads, smoke reduction is modest, although even under diesel operation quite low FSN levels were measured. These significant smoke reductions could be expected due to the absence of soot promoters as aromatic hydrocarbons in the biofuel molecule and to the increased local oxygen availability during the combustion process, thanks to the oxygen content of the biofuel molecules (about 8% on a weight basis). Finally, JME B30 blend showed a higher sensitivity to re-calibration, especially at medium loads where a small change in the EGR rate (see trade-off in Figure 3.28) can produce a large increase in soot emissions with only a modest change in NO_x.

The outcomes of tests carried out under part load operation with the standard calibration are shown in Figures 3.21 - 3.27 (graphs on the left). Both calibrations showed similar trends for BSFC , fuel conversion efficiency and all the pollutants with the only exception of $BSNO_x$. For the latter the change in the operating point due to the increase of the accelerator pedal position and thus a significant reduction of EGR rate (Figure 3.13) led to an increase in emissions especially for medium and high loads.

Soot-NO_x trade-off results obtained for the three operating points, representative of low, medium and high loads respectively, are shown in Figures 3.28 - 3.30, while Table 3.1 reports the tested EGR rates; it should be pointed out that, for each operating point the same EGR rate values were tested for diesel, and RME and JME blends, in order to better compare the trade-off curves obtained with the different fuels.

At low engine speed and load (1500 rpm, 2 bar BMEP Figure 3.28) an unusual soot-NO_x trade-off trend for all the tested fuels can be noticed since increasing the EGR rate produces a shift towards an highly premixed, low temperature combustion, causing a simultaneous reduction of NO_x and soot emissions; at this operating point the ECU calibration point can therefore be set at the maximum EGR rate even under diesel operation, because the highly premixed combustion allows to obtain a simultaneous reduction of both NO_x and soot emissions. Although soot levels are indeed already extremely low with diesel fuel, appreciable reductions of soot emissions at constant NO_x levels could be obtained thanks to biodiesel usage, without any need of change of the EGR level calibration point. The results for the medium load operating conditions are shown in Figure 3.29; in this case the RME and JME B30 blends trade-offs are quite similar in shape to the diesel trade-off, and do not show significant margins for further improvements, because any additional increase of the EGR rate from the calibration point would cause a dramatic increase in soot emissions also for the two biofuel blends. On the contrary, significant reductions of soot emissions at constant NO_x levels could by obtained thanks to neat biodiesel usage, again without the need of change of the EGR level calibration point.

Similar remarks could also be done for the soot-NO_x trade-off at high load which is shown in Figure 3.30.

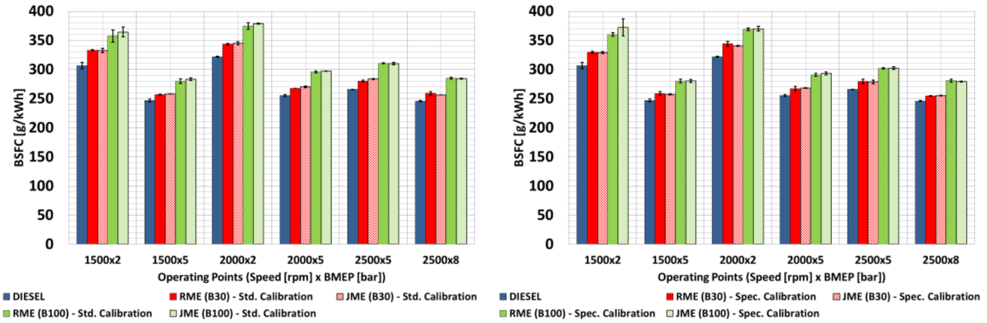

Figure 3.21 Brake Specific Fuel Consumption (BSFC): standard calibration (left), specific calibration (right)

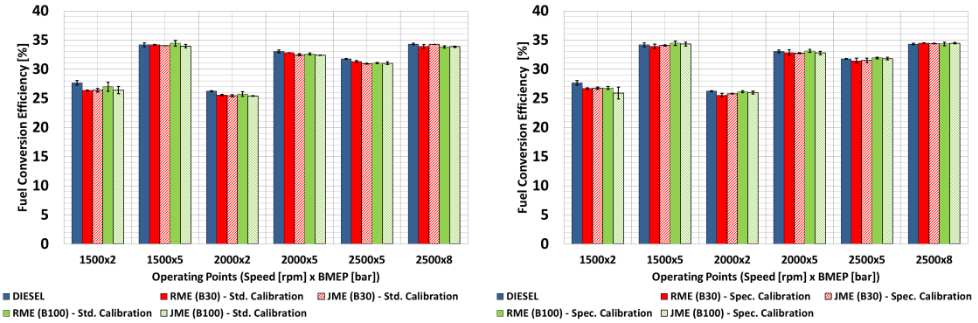

Figure 3.22 Fuel conversion efficiency: standard calibration (left), specific calibration (right)

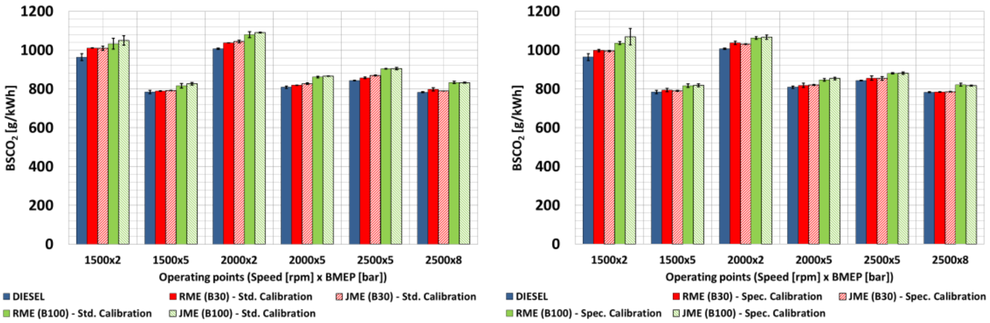

Figure 3.23 Brake Specific CO_2 emissions (engine outlet): standard calibration (left), specific calibration (right)

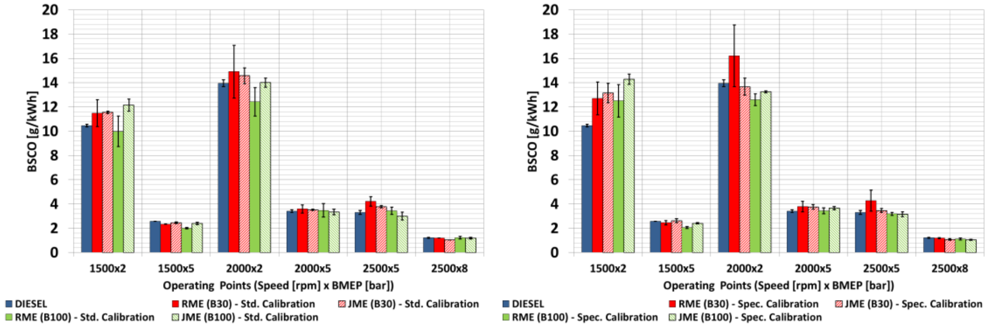

Figure 3.24 Brake Specific CO emissions (engine outlet): standard calibration (left), specific calibration (right)

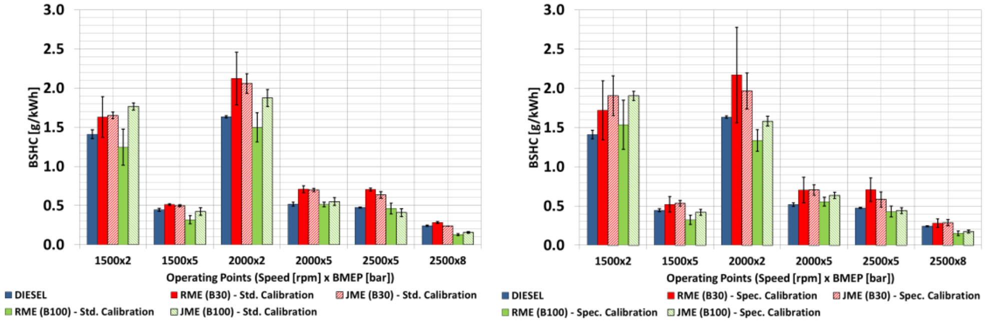

Figure 3.25 Brake Specific HC emissions (engine outlet): standard calibration (left), specific calibration (right)

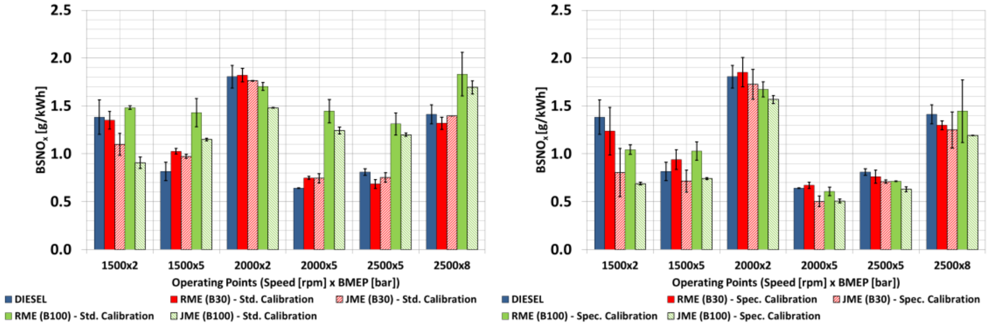

Figure 3.26 Brake Specific NO$_x$ emissions (engine outlet): standard calibration (left), specific calibration (right)

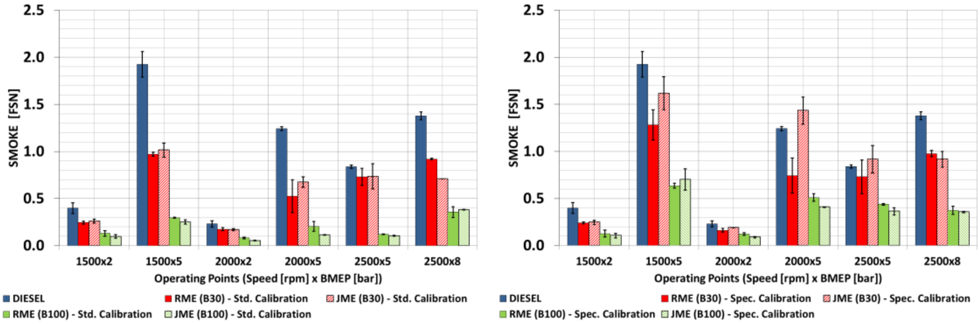

Figure 3.27 FSN (engine outlet): standard calibration (left), specific calibration (right)

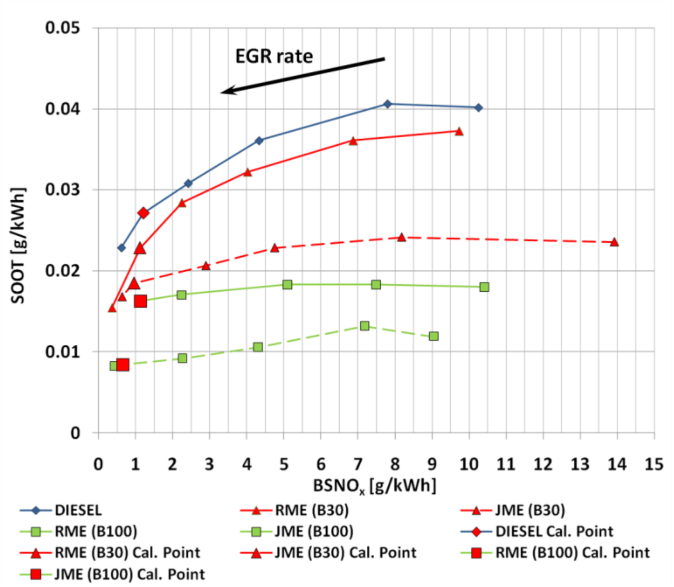

Figure 3.28 Soot–BSNO$_x$ trade-off comparison at 1500 [rpm], 2 [bar] BMEP

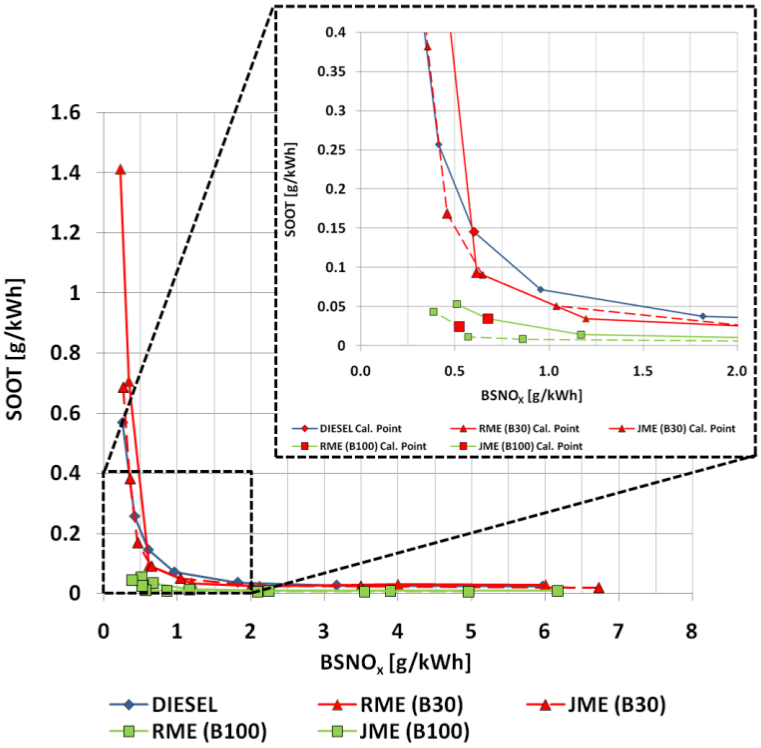

Figure 3.29 Soot–BSNO$_x$ trade-off comparison at 2000 [rpm], 5 [bar] BMEP.

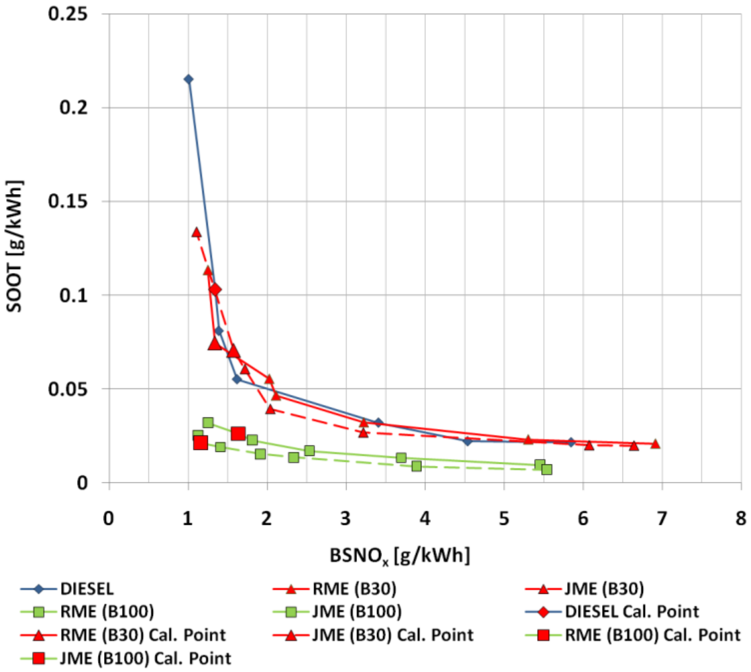

Figure 3.30 Soot–BSNO$_x$ trade-off comparison at 2500 [rpm], 8 [bar] BMEP.

Table 3.1 Trade-off tests EGR rates [%].

	Operating points (Speed [rpm] x BMEP [bar]		
	1500x2	2000x5	2500x8
EGR Rates]%]	0	0	0
	10	8	4
	20	15	8
	29	22	13
	37	26	16
	40	28	20

3.2.2.2 HVO characterization

During HVO characterization campaign, tests were carried out adopting a standard and a specifically adjusted ECU calibration. As highlighted in the previous section, as far as B30 blends are concerned, both calibrations led to similar outcomes in terms of engine parameters, indicating analysis and emissions. Therefore only the results obtained with the specific calibration will be discussed hereafter. The main experimental results obtained under part load operating conditions are shown in Figures 3.31 – 3.37, reporting respectively brake specific fuel consumption, engine fuel conversion efficiency, brake specific CO_2, CO, HC and NO_x emissions and smoke emissions.

No appreciable variations of BSFC were found with the HVO B30 blend, again in good agreement with the LHV data, and differently from what is reported in literature (see for instance (Sugiyama 2011)). As far as RME B30 is concerned results were in good agreement with outcomes discussed in 3.2.2.1. As a matter of fact, brake specific fuel consumption shows a 4% average increase for the RME B30 blend (Figure 3.31), in good agreement with the 4% lower LHV of the fuel blend. As expected from the BSFC analysis, fuel conversion efficiency (Figure 3.32) does not show appreciable variations when switching from diesel fuel to RME and HVO B30 blends.

As far as CO_2 emissions are concerned, the lower carbon content of the RME blend allows to compensate for its higher fuel consumption, thus significantly reducing the increase in CO_2 emissions levels that could be expected from BSFC data, as shown in Figure 3.33. Differences between the HVO B30 blend and the reference diesel fuel in terms of CO_2 emissions are almost negligible, being the

BSFC of the HVO blend almost identical to the diesel one, as well as its carbon content.

CO and HC specific emissions (Figure 3.34 and Figure 3.35) appear to be significantly reduced with both RME and HVO B30 blends at low and medium loads, while only modest or even insignificant variations were registered at higher loads: The more relevant differences were found at the lower load level (2 bar BMEP), in particular for the HVO blend, and are therefore likely to be attributed to the better ignition quality of the HVO. This behavior could therefore be emphasized when considering engine cold conditions (i.e. the conditions at the start of the relevant homologation testing procedures).

NO_x specific emissions are reported in Figure 3.36: NO_x emissions with the two biofuel blends were generally comparable with those of the reference diesel fuel, with the only significant exception of the low load point (2 bar BMEP), for which a relevant increase of NO_x emissions was measured for the HVO blend, and are therefore likely because of the better ignition quality of the biofuel.

The modest effect of fuel composition on NO_x at medium loads could be expected since the engine will be operated with closely comparable relative air/fuel ratios λ (and so with roughly the same oxygen availability and combustion temperatures).

As far as smoke emissions are concerned (Figure 3.37), a noteworthy reduction can generally be observed for medium and high load operating conditions (5 and 8 bar BMEP), with only modest reductions at low loads (2 bar BMEP) for the RME blend, and even a slight increase with the HVO blend. These significant smoke reductions could be expected, due to the absence of soot promoters as aromatic hydrocarbons in the biofuel molecule and, for the RME blend only, to the increased local oxygen availability during the combustion process, thanks to the oxygen content of the biofuel molecules (about 3% on a weight basis). Smoke reductions are therefore more significant for the RME blend, and more moderate for the HVO blend. However, it should be pointed out that FSN measurements are basically determined by the soot fraction only, while, especially at low loads, significant increases in the SOF fraction with biodiesel usage - which cannot be detected by FSN measurements - have been found by several researchers, since the unburned hydrocarbons produced by the biodiesel combustion process are more likely to condense and to absorb over the soot particles, due to their higher distillation temperatures. Further investigation complementing soot emission evaluations based on FSN with gravimetric PM measurements will be proposed in the following Chapter 4).

Finally, combustion noise values, computed according to (Herbert 1982), (Badami 2001) are shown in Figure 3.38: while the RME B30 shows values which are always quite close to the Diesel ones, the HVO B30 values appear to be appreciably lower (about 1.5 dB on average) than Diesel ones, likely because of the better ignition quality of the fuel and of the lower variations of the injected energy quantities during the pilot injections. Further confirmations of these effects can also be found by means of the in-cylinder pressure and of the heat release rate analysis, as shown, by way of example, in Figure 3.39 for the 1500 rpm, 2 bar BMEP operating point: a higher heat release peak during pilot combustion, followed by a lower heat release peak during the main combustion can be clearly seen for the HVO B30 in comparison with Diesel, thus resulting in a smoother in-cylinder pressure increase and therefore in a slightly lower combustion noise.

Further experimental investigations were carried out to fully exploit the benefits that could be obtained for instance by adjusting the EGR rates in order to take into account the different biofuel blends Soot-BSNO$_x$ and BSCO-BSNO$_x$ trade-offs. Although the analysis was carried out for all the 7 selected part load operating points, only the results obtained for the 2000 rpm, 5 bar BMEP conditions will be shown in Figure 3.40 and Figure 3.41 for sake of brevity, as representative of the biofuel blends behavior.

As far as the Soot-BSNO$_x$ trade-off is concerned (Figure 3.40), while the RME B30 shows a good potential for achieving significant smoke reduction at fixed NO$_x$ levels the HVO B30 does not shows significant advantages in comparison with the reference diesel fuel, thus suggesting that, for this operating condition, the better local oxygen availability during the combustion process which is assured by the oxygen content of the RME blend plays a fundamental role for smoke reduction.

A quite different situation was found instead for the BSCO-BSNO$_x$ trade-off, which is shown in Figure 3.41: in this case, while the RME B30 follows quite closely the reference diesel trend, significantly lower CO emissions were found for the HVO B30, thanks to its better ignition quality.

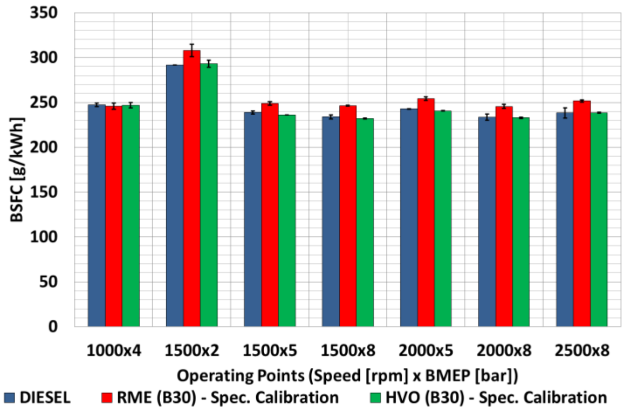

Figure 3.31 BSFC at part load

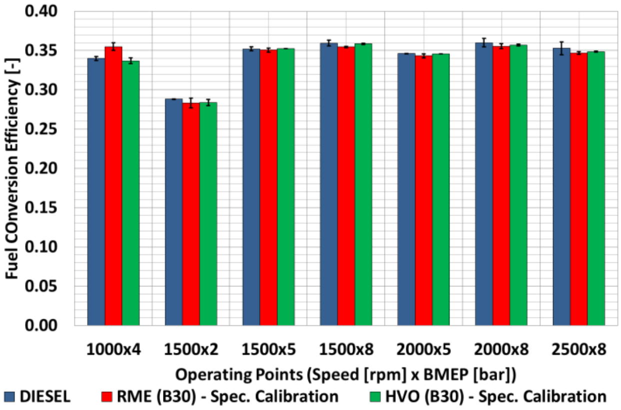

Figure 3.32 Fuel conversion efficiency at part load

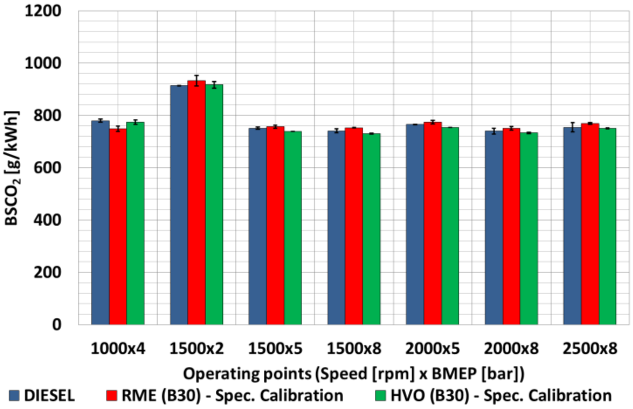

Figure 3.33 BSCO$_2$ emissions at part load

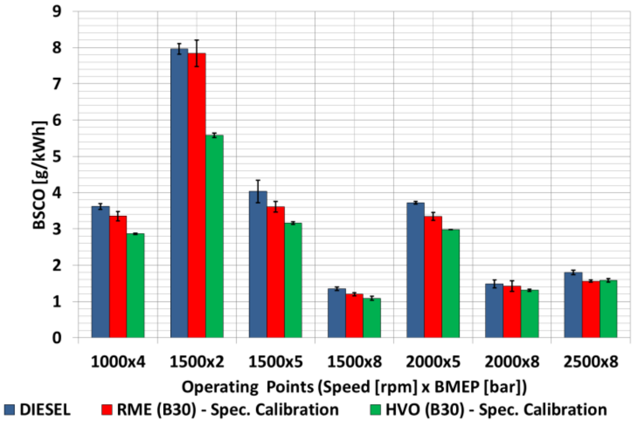

Figure 3.34 BSCO emissions at part load

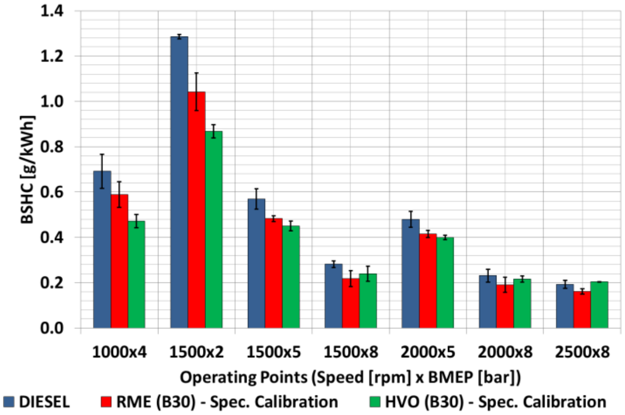

Figure 3.35 BSHC emissions at part load

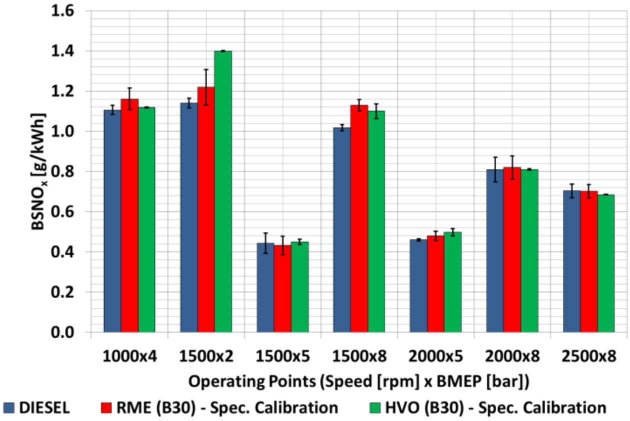

Figure 3.36 BSNO$_x$ emissions at part load

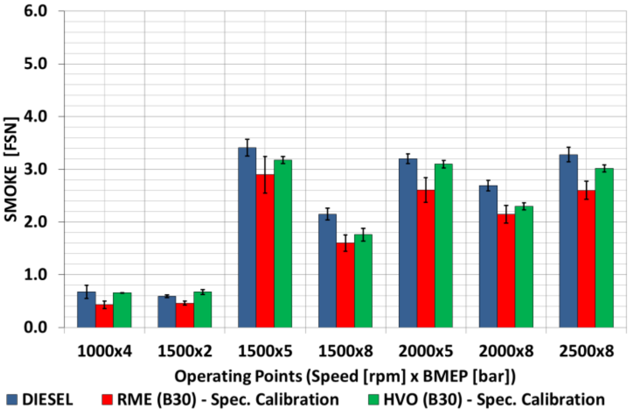

Figure 3.37 Filter Smoke Number at part load

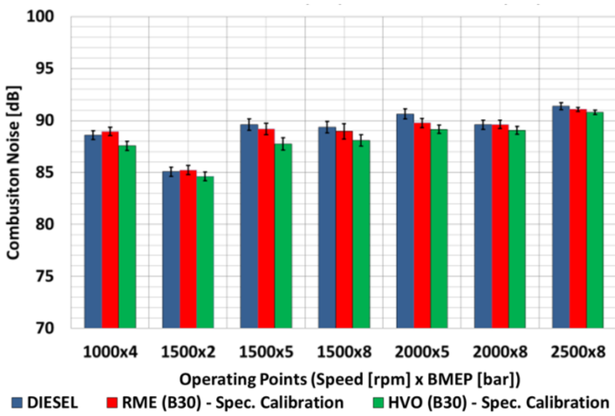

Figure 3.38 Combustion noise at part load

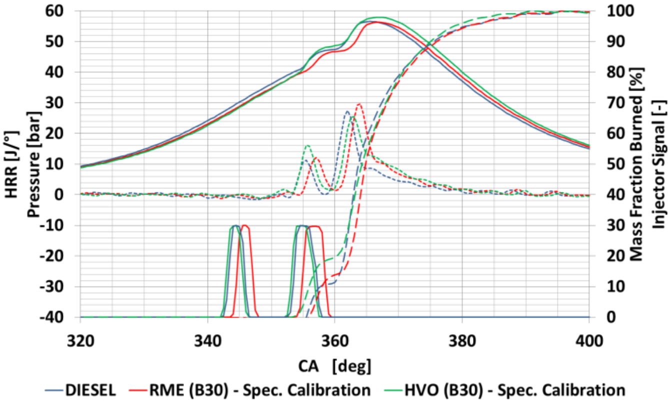

Figure 3.39 In-cylinder pressure, heat release rate, mass fraction burned and injector signal traces at 1500 rpm, 2 bar BMEP

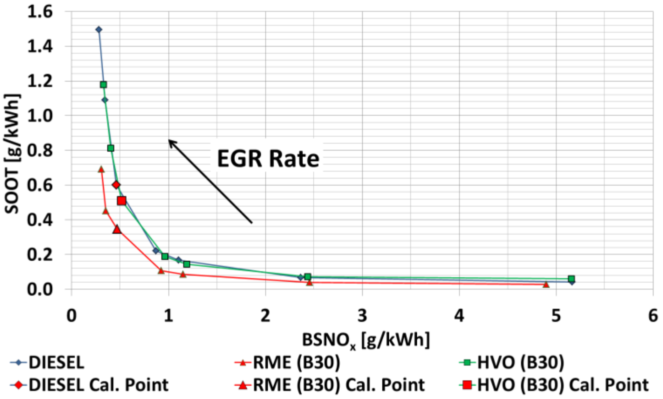

Figure 3.40 Soot-BSNO$_x$ trade-off for at 2000 rpm, 5 bar BMEP for all fuels

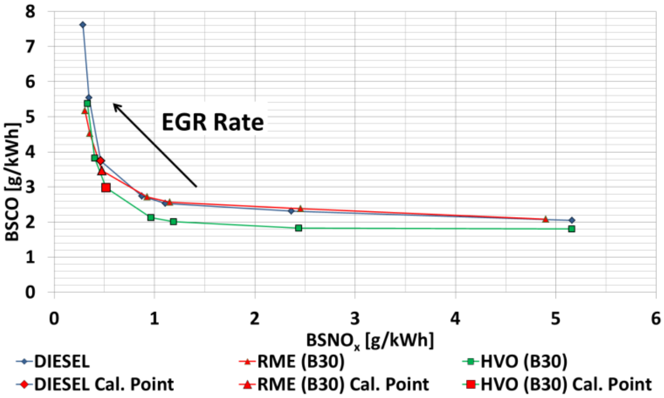

Figure 3.41 BSCO-BSNO$_x$ trade-off at 2000 rpm, 5 bar BMEP *for all fuels*

3.2.3 Analysis of the sensitivity of the different fuels to engine calibration

In this section results from the experimental activity, carried out according to methodology described in chapter 2.5 and concerning the influence of pilot and main injections timing on soot, NO$_x$, BSHC, BSCO and BSFC when the engine was fuelled with diesel, RME B30 and HVO B30 under part load operation will be discussed. During investigation only one single injection event was analyzed performing a sweep of the start of the injection (see section 2.5 for more details), and running the engine with and without EGR.

During tests, with and without EGR, all the operating parameters i.e. energizing time of the main injection, rail pressure, trapped air mass, boost pressure, EGR Rate and relative air/fuel ratio were the same among fuels due to the fact that during tests the accelerator pedal position was kept fixed independently of the type of fuel which was used. The effects of start of injection timing on combustion process and on emissions are well known especially when a single injection event occurs per cycle. Therefore in the present section the comparison among diesel, RME B30 and HVO B30 will be discussed only. Figures 3.42 – 3.44 report indicating analysis data obtained with all fuels at three different values of start of injection with and without EGR. For sake of brevity the discussion will be focused on only three out of seven tested values of SoI, i.e. 5.7 deg BTDC, 2.7 deg BTDC and 7.7 deg BTDC which represents the original calibrated value on the diesel oriented calibration, the minimum explored SoI and the SoI where the combustion has the maximum efficiency respectively

Figure 3.42 depicts the indicating data for all fuels at calibration point. During the tests carried out without EGR HVO B30 exhibited a lower ignition delay due to its higher cetane number, thus leading to a more advanced combustion respect to other fuels as could be confirmed by MFB50 position, thus leading to lower CO and HC emissions respect to other fuels as will be showed in the following section. On the contrary, diesel and RME B30 exhibited similar HRR traces while comparable HRR peak values for all fuels were observed. While most of the comments noted previously are still valid, in the case of EGR different ignition properties among fuels are further stressed. In more detail, the more advanced combustion pattern of HVO suggests lower CO emissions among fuels, while as far as RME is concerned, the steepest mass fraction burned trace suggests a major production of NO_x if compared to other fuels.

Figure 3.43 depicts indicating data obtained when SoI was 2.7 deg before TDC with and without EGR. A significant variation of in-cylinder pressure, HRR and mass fraction burned traces for HVO respect to diesel and RME was observed in both cases and especially when EGR was activated. Lower viscosity and a more favorable distillation curve with respect to other fuels enhance air/fuel mixture forming and ignition even when the injection event is close to TDC. These data confirm the better ignition properties of HVO if compared to both conventional diesel and RME B30 highlighting the importance of fuel quality and properties during engine calibration development.

When the start of injection was increased up to 7.7 deg BTDC (Figure 3.44), all fuels showed similar combustion processes in both cases with EGR activated and deactivated. In more detail in the case with EGR HVO still showed a MFB50 position closer to TDC, while RME B30 exhibited the fastest combustion.

The experimental results in terms of brake specific fuel consumption, engine fuel conversion efficiency, brake specific CO, HC and NO_x emissions obtained with the sweep of SoI are shown in Figures 3.45 – 3.49. For each figure, left column refers to the case without EGR, while right column to the case with activated EGR system. In the following, outcomes regarding smoke emissions will be omitted because of the low levels of smoke emissions reached at this operating point which are very close to the detection limit of the instrument (measures in a range of 0-0.08 FSN were detected during all test campaign).

Figure 3.45 depicts the BSFC during the sweep of SoI in the cases with and without EGR.. In the case without EGR a decrease of BSFC of almost 7% and 12 % for diesel and RME was observed respectively when SoI was increased from 2.7 deg BTDC up to 7.7 deg before BTDC. On the contrary HVO exhibited an almost constant BSFC level during all test campaign. In the case with EGR the variation in BSFC was greater, in more detail a decrease of 35% and 30% for diesel and RME was observed respectively passing from SoI of 2.7 deg up to 7.7 deg before TDC.

Fuel conversion efficiency for all fuels and SoI values is depicted in Figure 3.46. In the case without EGR, HVO exhibited the maximum efficiency if compared to other fuels. In the case without exhaust gases recirculation the impact of fuels on combustion efficiency is not so evident as it is in the case with EGR. As a matter of fact when EGR is activated a significant increase of fuel conversion efficiency was observed for diesel and RME when SoI was increased from 2.7 up to 7.7 deg BTDC. Tests with a SoI 7.7 deg BTDC showed the maximum fuel conversion efficiency, as was highlighted by indicating analysis data. A further increase in SoI leads to a slight decrease of fuel conversion efficiency.

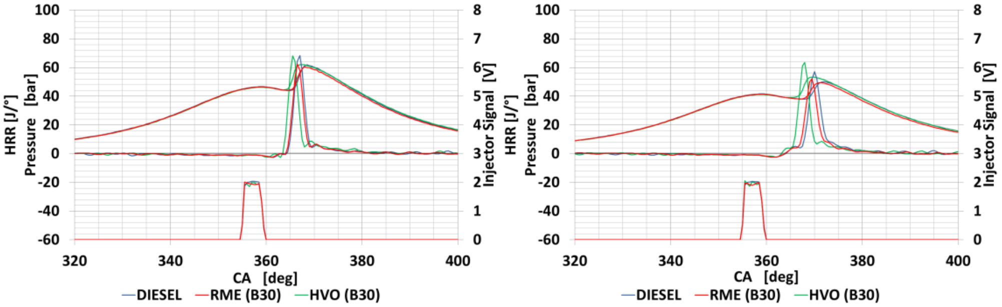

without EGR

with EGR

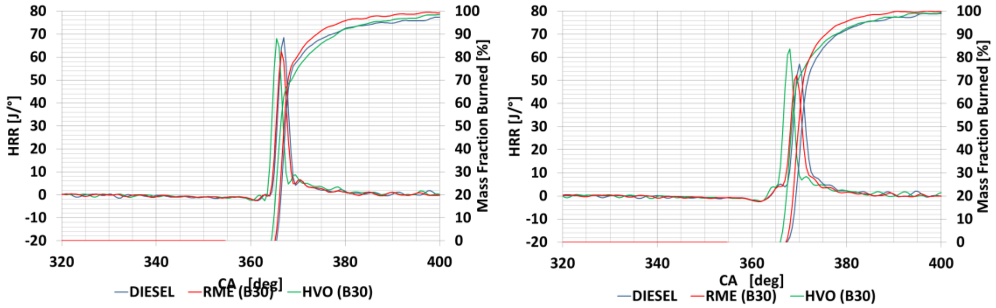

Figure 3.42 Indicating analysis for the 1500 [rpm] @ 2 [bar] BMEP engine op. point for diesel, RME (B30) and HVO (B30) at SoI=5.7 deg BTDC (calibration point) without EGR (left column) and with EGR (right column): in-cylinder pressure, heat release rate and injection pattern (top), heat release rate and mass fraction burned (bottom).

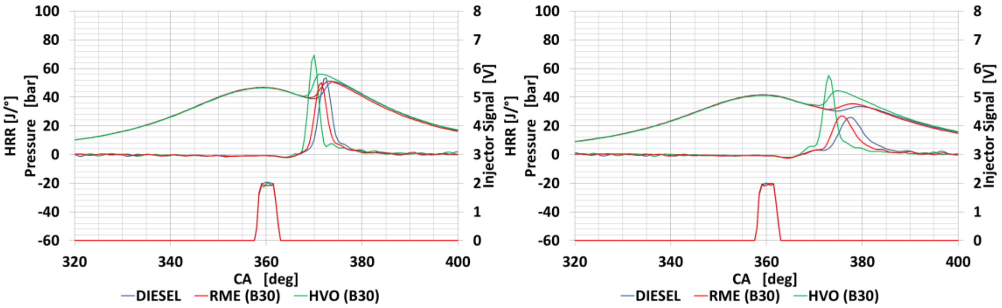

without EGR
with EGR

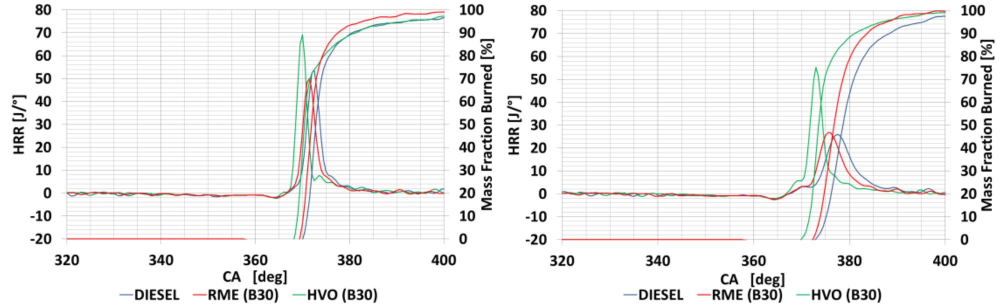

Figure 3.43 Indicating analysis for the 1500 [rpm] @ 2 [bar] BMEP engine op. point for diesel, RME (B30) and HVO (B30) at SoI=2.7 deg BTDC without EGR (left column) and with EGR (right column): in-cylinder pressure, heat release rate and injection pattern (top), heat release rate and mass fraction burned (bottom).

Figures 3.47 and 3.48 show BSCO and BSHC emissions respectively at different SoI. As highlighted by indicating analysis data, when the start of injection is postponed at 2.7 deg before TDC combustion efficiency is very low for diesel and RME, therefore an increase of BSCO and BSHC is expected. As a matter of fact a decrease on average of BSCO and BSHC of 68% and 82% for diesel and RME was observed when SoI was increased from the minimum angle up to 7.7 deg before TDC. Finally NO_x emissions are showed in Figure 3.49.

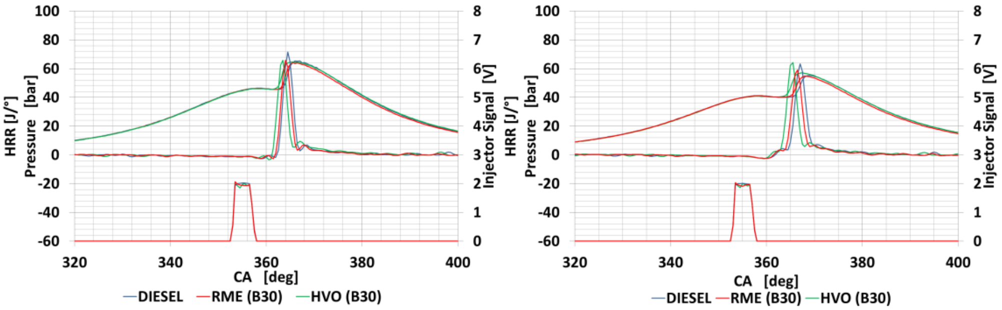

without EGR with EGR

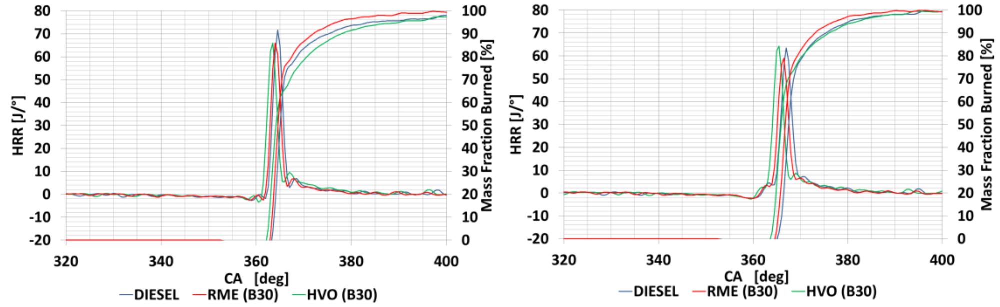

Figure 3.44 Indicating analysis for the 1500 [rpm] @ 2 [bar] BMEP engine op. point for diesel, RME (B30) and HVO (B30) at SoI=7.7 deg BTDC without EGR (left column) and with EGR (right column): in-cylinder pressure, heat release rate and injection pattern (top), heat release rate and mass fraction burned (bottom).

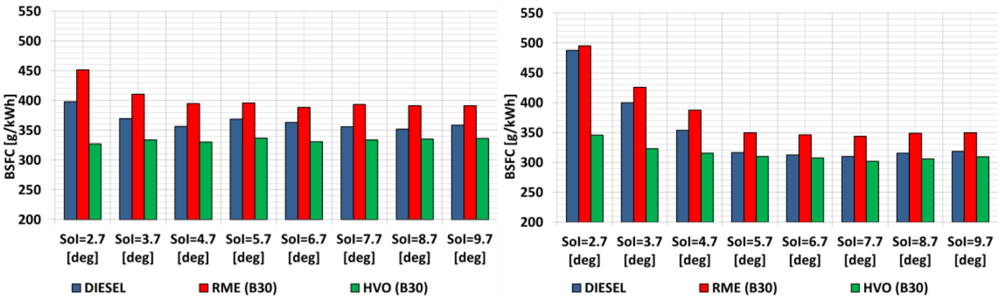

Figure 3.45 BSFC with all fuels and SoI at 1500 rpm @ 2 bar BMEP: without EGR (left), with EGR (right)

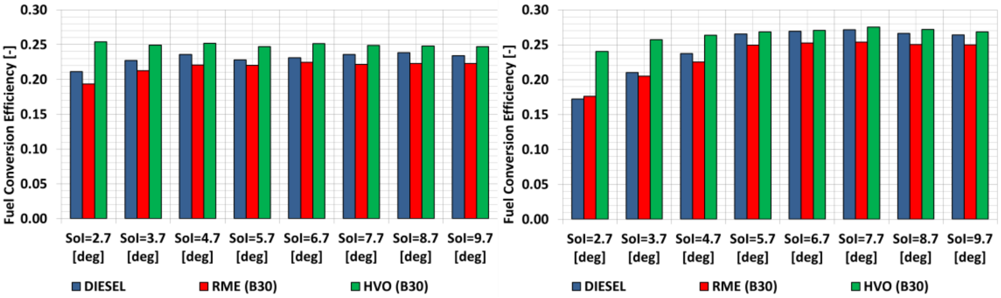

Figure 3.46 Fuel conversion efficiency with all fuels and SoI at 1500 rpm @ 2 bar BMEP: without EGR (left), with EGR (right)

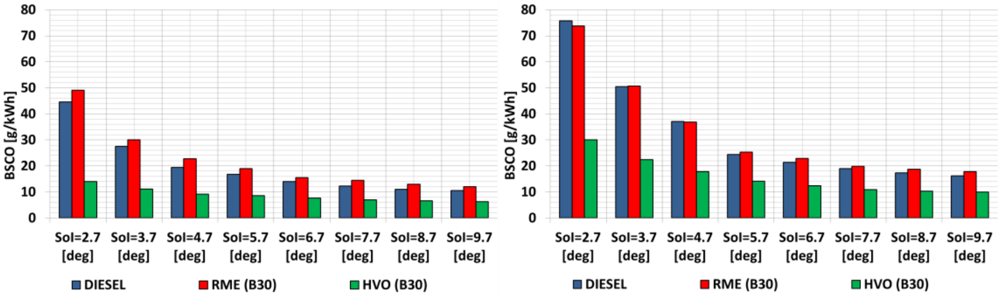

Figure 3.47 BSCO with all fuels and SoI at 1500 rpm @ 2 bar BMEP: without EGR (left), with EGR (right)

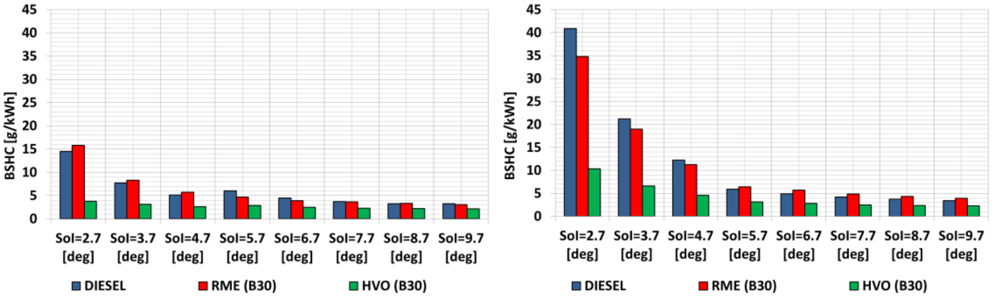

Figure 3.48 BSHC with all fuels and SoI at 1500 rpm @ 2 bar BMEP: without EGR (left), with EGR (right)

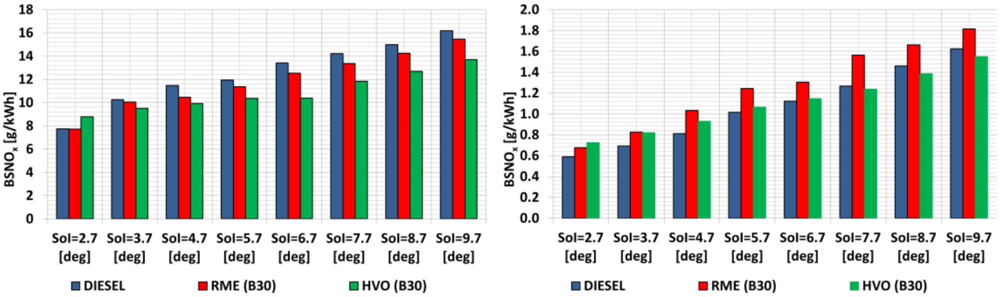

Figure 3.49 BSNO$_x$ with all fuels and SoI at 1500 rpm @ 2 bar BMEP: without EGR (left), with EGR (right)

Chapter 4 – Particulate Matter characterization

4.1 Introduction

In this chapter results from the experimental activity, carried out according to methodology described in chapter 2 and concerning the characterization of PM emitted from diesel engines operated with different fuels will be presented. The discussion will focus, firstly, on PM characterization in terms of both total mass and chemical composition obtained by gravimetric and thermogravimetric tests respectively (see sections 2.6 and 2.7 for more details). Afterwards PN and size distributions will be presented and discussed.

Finally the analysis of the mutagenic potential of PM emissions produced by different types of fuels will be exposed.

4.2 Results analysis and discussion

4.2.1 PM gravimetric and chemical composition analysis

PM gravimetric analysis

As described in paragraph 2.6, PM gravimetric analysis was conducted under part load operation fuelling the engine with both conventional diesel and biofuels. Tests were executed by weighting filters before and after being loaded with PM by means of a high resolution microbalance. Figure 4.1 depicts the main results of the investigation and related to the selected operating points (1500 rpm @ 2 bar BMEP, 1500rpm @ 5 bar BMEP and 1500 rpm @ 8 bar BMEP) when the engine was fueled with diesel, RME B30 and HVO B30.

It is worth to be noticed that RME B30 and HVO B30 showed at medium and high loads a noticeable reduction of specific PM emissions (34% and 14% on average respectively) if compared to diesel fuel. On the contrary at low speed/low load operating point (1500 rpm @ 2 bar BMEP), RME B30 exhibited a 32% of increase respect to diesel fuel whereas HVO B30 still showed a 32% of reduction if compared to diesel.

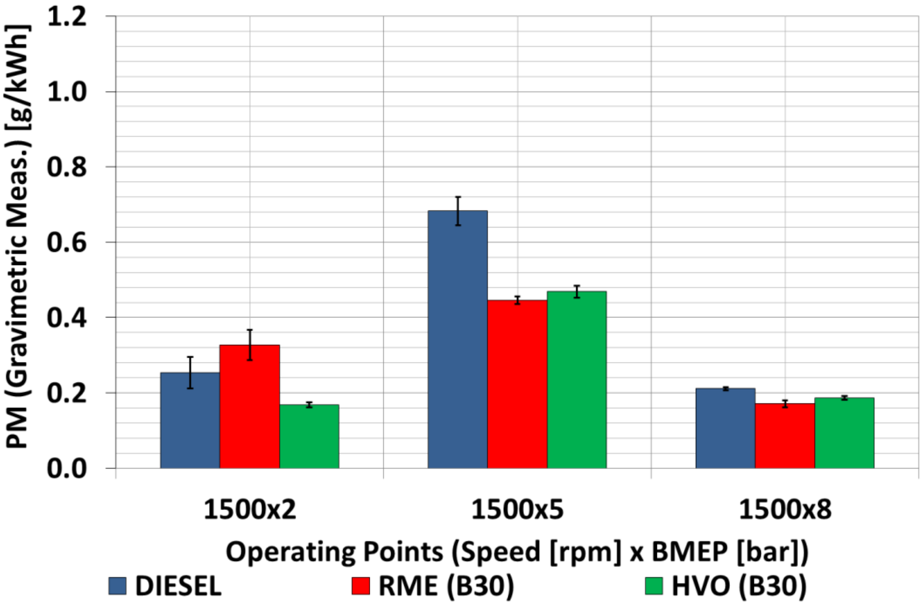

Figure 4.1 PM specific emissions for all op. points and evaluated fuels.

As far as HVO B30 is concerned, the highlighted overall decrease in PM emissions could be attributed to the chemical properties of this biofuel; the higher cetane number enhances ignitability properties of HVO, while the lack of aromatics in HVO molecule leads to a lower soot formation .

It is worth to be mentioned that the increase of PM emissions for RME B30 which was observed at low load is not linked to smoke emissions as shown in Figure 4.2. At low load operating point, all three fuels had similar smoke emissions, thus suggesting that, in the case of FAME, the soluble organic fraction (SOF) of PM may be predominant among other PM fractions, i.e. soot. This bigger portion of SOF could be attributed, in first place, to an increase of HC emissions for RME B30 respect to other fuels during low load operation. However, results discussed in section 3.2.2.2 (Figure 3.35), and replicated in Figure 4.2, concerning the impact of both RME and HVO 30%v/v blends on emissions under part load operation highlighted a decrease in HC emissions for biofuels at 1500 rpm @ 2 bar BMEP. Moreover, the BSHC-A/F relative ratio trade off related to the same operating point and obtained with all fuels (Figure 4.3) confirmed the abovementioned decrease of HC emissions for RME.

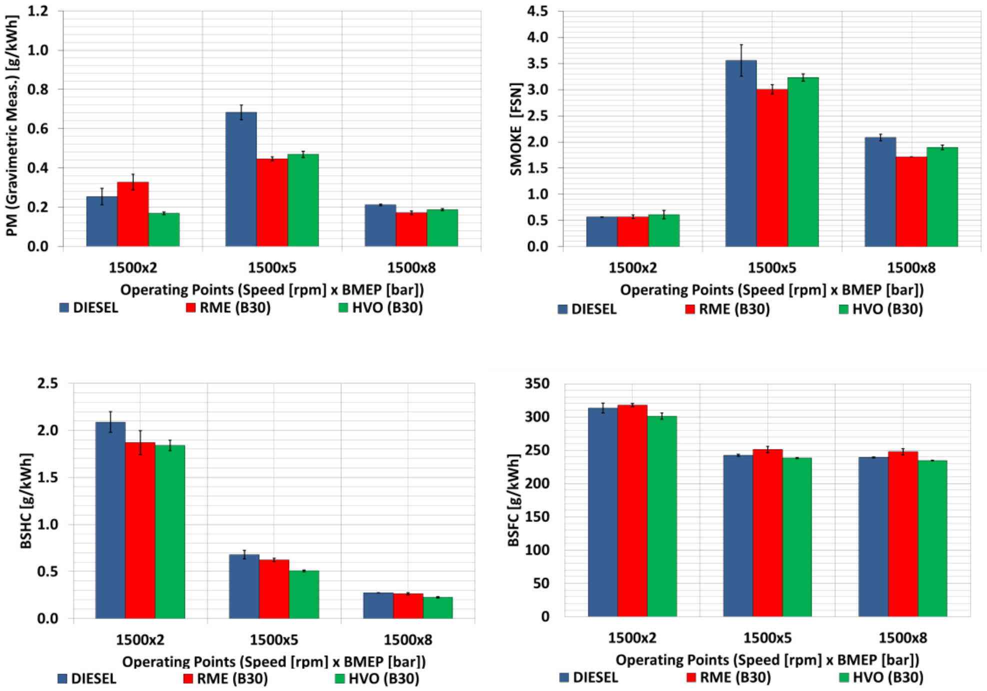

Figure 4.2 Correlation between specific PM emissions and smoke, BSFC, BSHC for all fuels and tested operating points

The discrepancy between gravimetric analysis and HC emissions could be partially explained if the chemical properties of RME B30 are taken into account: RME B30 has a higher boiling point and a lower volatility than diesel fuel, therefore when unburned biodiesel is present in the dilution tunnel, it should be more likely to condense and adsorb on the carbon particle surfaces. This effect in conjunction with the fact that SOF of RME B30 is more sensitive to variations of the dilution ratio during filter loading tests as already highlighted by (Van Gerpen 1998) (see section 2.6.2 for more details on test procedure) could explain the higher condensation of unburned hydrocarbons from biodiesel in the sampling system, even at 190°C (Van Gerpen 1998) and (Sharp 2000)).

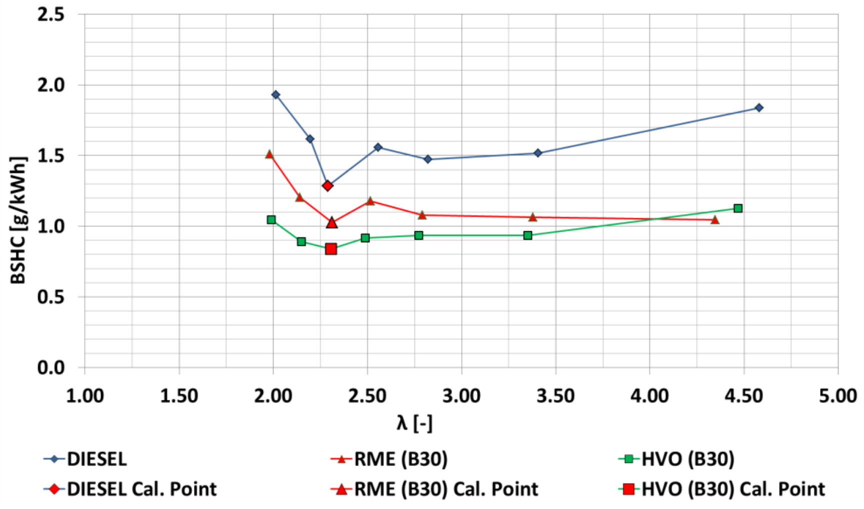

Figure 4.3 BSHC versus relative air fuel ratio at 1500 rpm @ 2 bar BMEP

In order to gather more information on a possible correlation between experimental data and PM emissions which are usually estimated on the basis of smoke measurements by means of AVL and MIRA formulas (see Appendix II) when different fuels are used, the above discussed outcomes were compared with calculated results obtained by using AVL and MIRA relationships (Figure 4.4).

At medium and high load conditions, experimental and calculated results were in good agreement even though both relationships seemed to overestimate experimental data. On the contrary, at low load, variation noticeable difference between measured and calculated PM emissions was observed. This could be mainly due to the fact that both relationships did not take into account the different nature of fuels.

In order to gather more details regarding the abovementioned phenomena breakdown analysis of calculated PM emissions was performed for both AVL and MIRA PM estimates. Figure 4.5 highlights the contribute of each fraction adopted for PM calculation. It should be noticed that the weight of each of these factors is different accordingly to engine load. At medium and high loads PM is consisted, mainly, by soot ("dry" PM), thus explaining the good agreement between experimental and simulated data highlighted before. On the contrary, at low load

SOF is predominant over other PM fractions, while soot fraction was similar for all fuels. Since the noticeable increase in PM emissions encountered during low load operation with RME B30, is not detectable with standard FSN and gaseous emissions measurements, the significance of these standard measurements which are commonly carried out during the engine calibration activity should be carefully considered as far as biofuel blends are concerned.

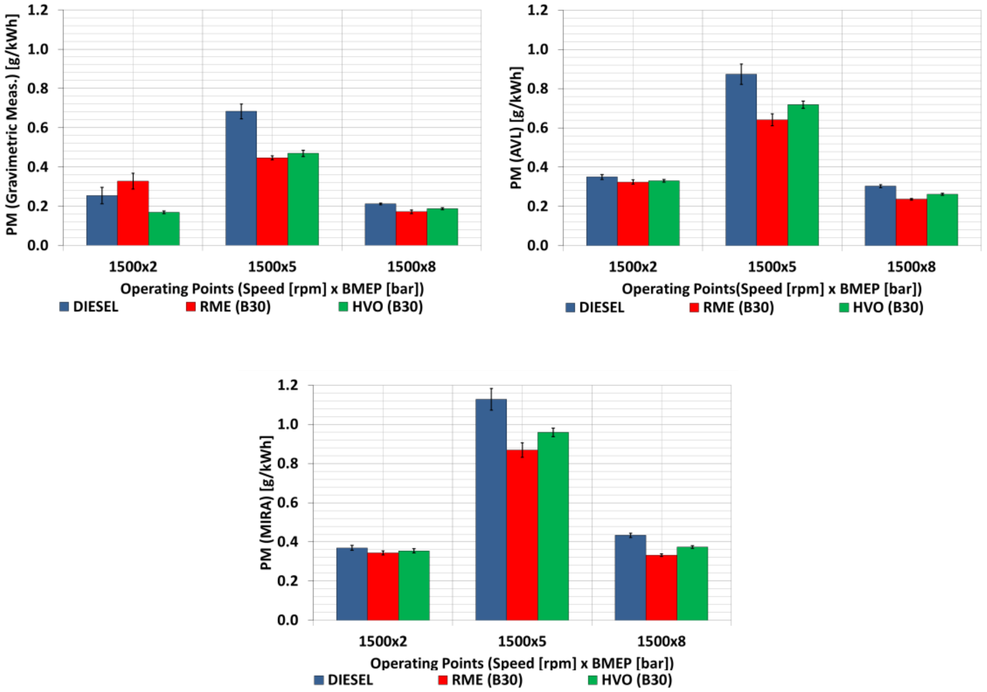

Figure 4.4 Specific PM emissions obtained by using AVL and MIRA models

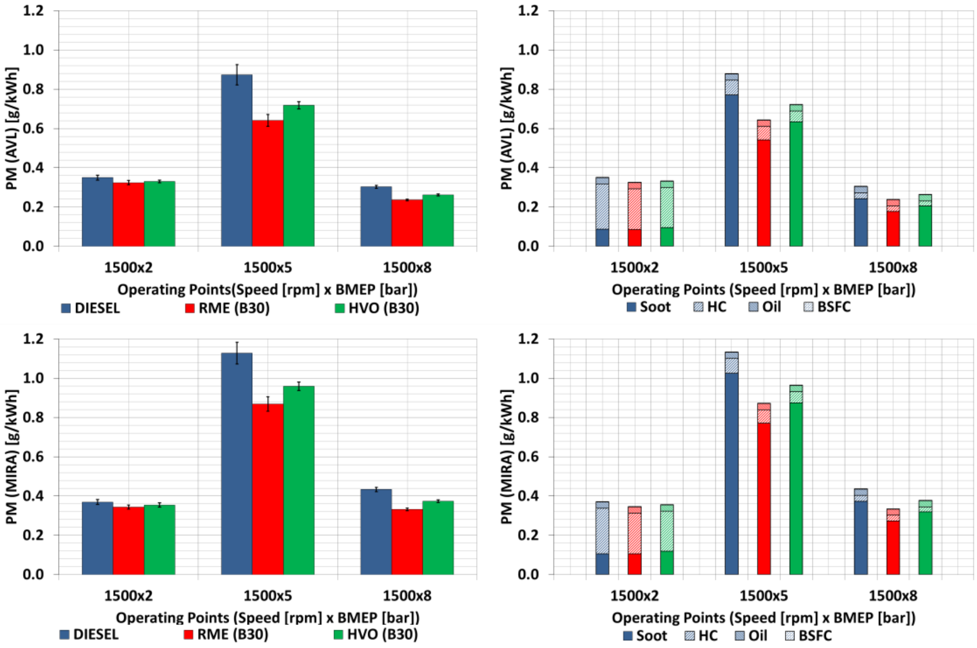

Figure 4.5 Breakdown analysis of PM emissions according to AVL and MIRA model

PM chemical composition analysis

Results of thermogravimetric test executed at Bureau Veritas Laboratoires are presented and discussed in the present section. Figure 4.6 depicts the TGA analysis outcomes for the low speed low load tested operating point (1500 rpm @ 2 bar BMEP). As the figures depicts, VOF takes up majority of overall particulate mass (more than 80%) for all fuels, which proves the expectations from gravimetric analysis. The substantially huge portion of SOF fraction for RME B30 (62% over total PM mass) compared to SOF portion of PM detected with diesel and HVO B30 fuels (51% and 47% over total PM mass, respectively) could be rooted to its physical properties as has been highlighted previously. On the contrary, the almost negligible soot portion of PM for RME respect to the one observed for the remaining fuels (14% and 16% over total PM mass for diesel and HVO B30 respectively) is in contradiction with smoke emissions which were similar for all fuels (see Figure 4.2 and Figure 4.5).

At medium load operating conditions (1500 rpm @ 5 bar BMEP), for each tested fuel, soot covers the largest portion of total PM mass with respect to PM detected under low and high load operations (Figure 4.7). This could explain why the results obtained by means of smokemeters were in good agreement with gravimetric analysis when medium loads were explored. As far as PM emitted with different fuels is concerned, a maximum content of almost 33% of SOF for

RME was detected. At high load condition (Figure 4.8), soot still occupies the largest portion of total PM mass, even if, in absolute terms, is less important than the soot portion of PM detected at medium load, probably due to the lower EGR rate used during 8 bar BMEP operating point respect to medium load (Figure 4.9).

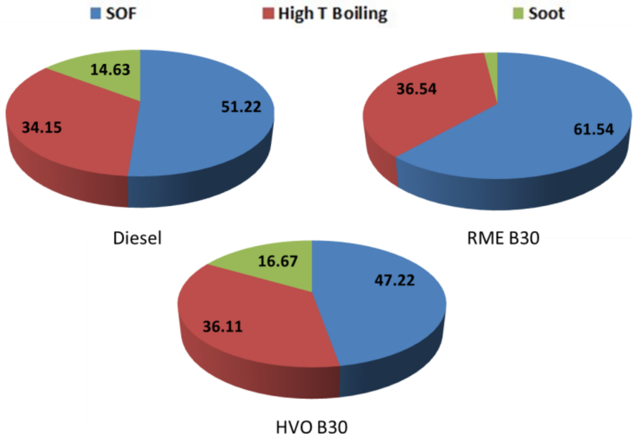

Figure 4.6 Particulate matter chemical composition for three tested fuel at 1500 rpm @ 2 bar BMEP load condition

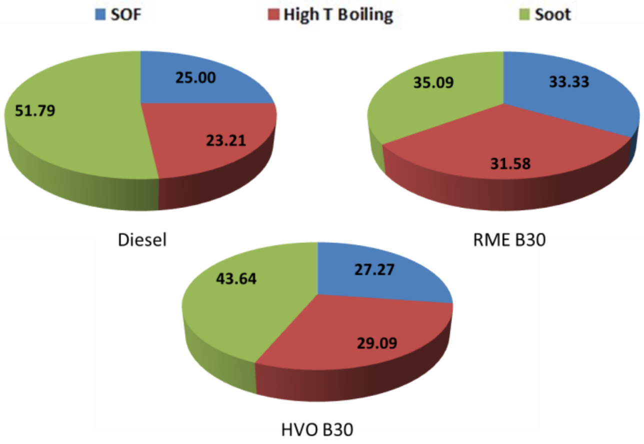

Figure 4.7 Particulate matter chemical composition for three tested fuel at 1500 rpm @ 5 bar BMEP load condition

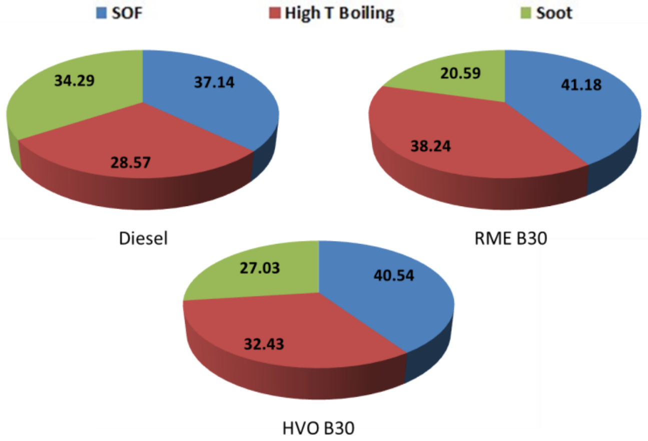

Figure 4.8 Particulate matter chemical composition for three tested fuel at 1500 rpm @ 8 bar BMEP load condition

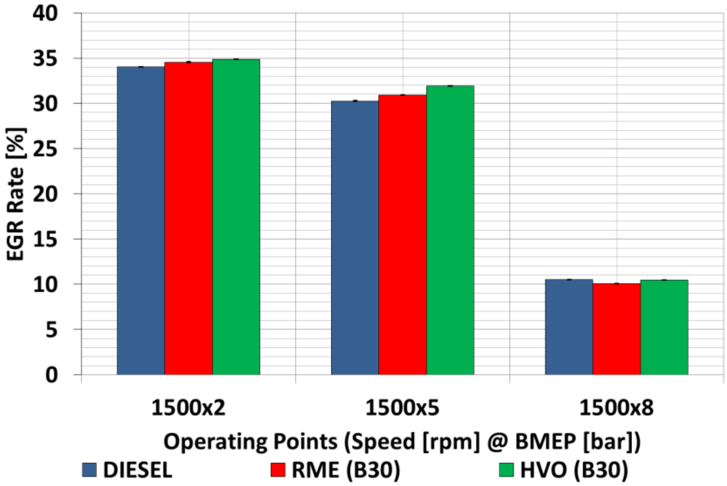

Figure 4.9 EGR rate of three fuels at thermo-gravimetric analysis

4.2.2 Particle size and number distribution

In this section results from the experimental investigation on soot particles number distributions are analyzed and discussed. Prior to starting the discussion on particle number distribution results, an additional clarification about following results measured through the experimental apparatus described in paragraph 2.8 should be given.

Generally, test results concerning particle number and mass size distributions could be reported both in terms of logarithmic or linear y-axis scales; the first is useful for a comparison between data with different orders of magnitude such as, for instance, data measured upstream and downstream of the DPF, while the second better highlights the distribution shape and allows an easier location of its maximum value.

Number and mass size distribution, reported in terms of dN/dlogDp and dM/dlogDp respectively, are normalized to one decade of particle size, which allows particle size distributions to be compared regardless of the size range and distributions are already corrected taking into account the DR realized by the two stages dilution system. Moreover, mass calculation has been carried out automatically by the SMPS control software according to (TSI 2006); in particular, the adopted methodology assumes that all particles are perfect spheres with an assumed constant density of 1.8 g/cm^3, which is a representative value for diesel soot. Since the mass size distribution is calculated on basis of number size distribution, the following discussions are mainly focused on number size distribution.

For statistical reasons, data shown hereafter represent averages of at least four repeatable scans carried out at each engine operating condition or sampling point on the exhaust line; as an example of repeatability, Figure 4.10 shows the comparison of five number distributions obtained from five non-consecutive SMPS scans measured at the engine outlet for the 2000 rpm, 5 bar BMEP engine operating point under normal operating conditions, while Table 4.1 lists the statistic calculation for each of the number distribution performed according to the methodology reported in (TSI 2006). It is possible to observe that number distributions are quite repeatable, with variations between the five scans in mean diameter or geometric mean diameter within 5%.

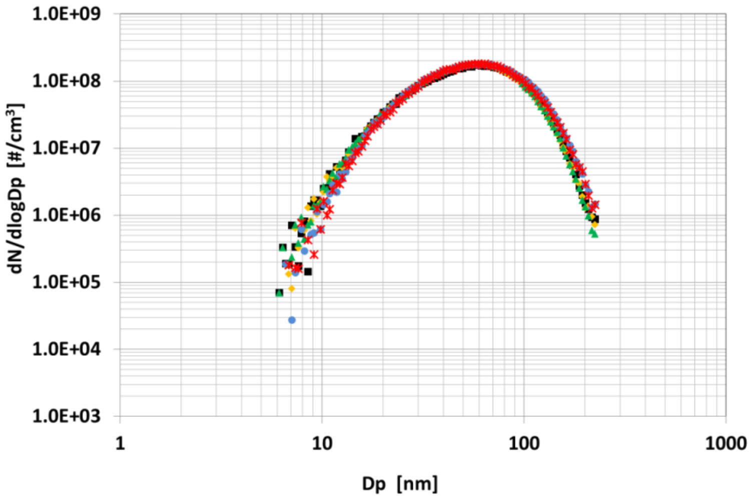

Figure 4.10 Comparison of five SMPS scans measured at the engine outlet for the 2000 rpm @ 5 bar BMEP engine operating point

Table 4.1 Statistic calculations performed by the Aerosol Instrument Manager® Software

	SAMP. #1	SAMP. #2	SAMP. #3	SAMP. #4	SAMP. #5
Median (nm)	54.0	55.2	54.2	56.1	55.7
Mean (nm)	58.8	60.0	58.9	62	61.4
Geo. Mean (nm)	52.2	53.0	52.2	54.7	54.4
Mode (nm)	61.5	57.3	59.4	57.3	59.4
Geo. St. Dev.	1.66	1.68	1.66	1.67	1.65
Total Conc.	1.55e+06 (#/cm³)	1.49e+06 (#/cm³)	1.47e+06 (#/cm³)	1.59e+06 (#/cm³)	1.55e+06 (#/cm³)

4.2.2.1 FAME vs. HVO characterization

Figure 4.11, Figure 4.14 and Figure 4.15 show particles number and size distributions for the 1500 rpm @ 2 bar BMEP, 1500 rpm @ 5 bar BMEP and 1500 rpm @ 8 bar BMEP operating points measured at engine outlet with three different fuels; results are reported with either linear (graphs on the left) and logarithmical (graph on the right) y-axis scales. Since the mass size distribution is calculated on basis of number size distribution, the following discussions are mainly focused on number size distribution.

Low load operating point (1500 rpm @ 2 bar BMEP)

At low load (1500 rpm @ 2 bar BMEP) operating point (Figure 4.11), HVO B30 showed a significant increase of almost 26% of particles number peak value with respect to diesel, while RME B30 exhibited PN distribution similar to diesel. The distributions mean diameters are 62.3nm for diesel, 61.4nm for RME B30 while it increases up to 66.8nm for HVO B30, with a 7% of increase in mean distribution diameter in the case of HVO. These changes in PM number distribution could be explained if the EGR rates and relative air to fuel ratios obtained with different fuels are taken into account during low load operation. As could be observed from Table 4.2, switching fuel from diesel or RME to HVO, the relative air-fuel ratio showed a noticeable decrease of almost 8% passing from 2.4 to 2.2; moreover, it should be noticed that due to the position of the calibration point on the soot-λ trade off curve obtained with HVO (Figure 4.12) a slight variation of EGR and so of λ could be enough to change significantly soot production. On the contrary, RME B30, exhibits an overall smoother trade off curve which lies on lower soot values with respect to other fuels. The increased local oxygen availability seems therefore to significantly reduce the soot formation.

Finally, the extremely important effects on PM emissions that can be attributed to shifts in the engine operating points on the calibration maps highlight the need for a specific adjustment of the engine calibration on the basis of the fuel characteristics (e.g., for the higher LHV of HVO B30 blends) in order to avoid jeopardizing the potential emission benefits of biofuels.

Table 4.2 Relative A/F ratios and EGR rates levels for all fuels at 1500 rpm @ 2 bar BMEP

	DIESEL	RME B30	HVO B30
Relative air/fuel ratio	2.41	2.48	2.29
EGR rate	33	33	35

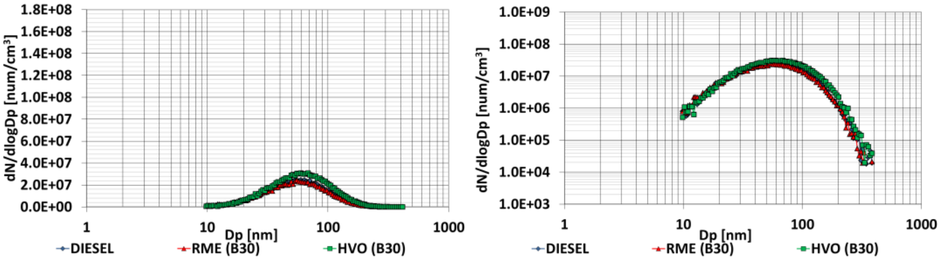

Figure 4.11 PN distribution at 1500 rpm @ 2 bar BMEP: semi-log graph (left), log-log graph (right)

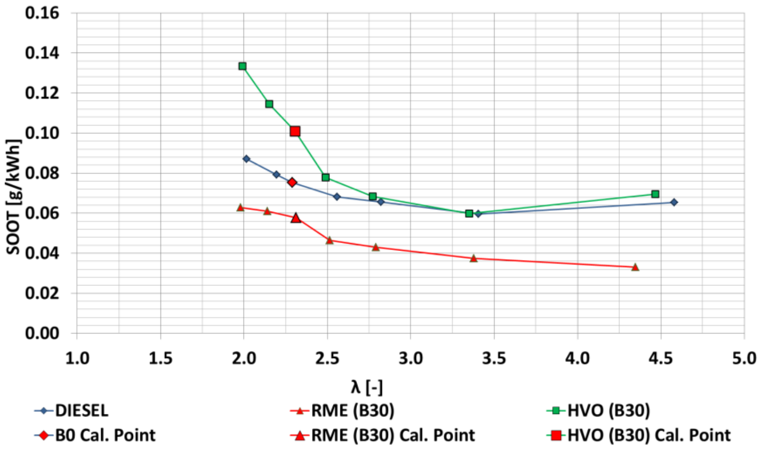

Figure 4.12 Soot-λ tradeoff curve with all fuels at 1500 rpm @ 2 bar BMEP

Medium load operating point (1500 rpm @ 5 bar BMEP)

Even if the calibration points for diesel and HVO B30 are similar (Figure 4.13); HVO B30 still shows an increase of 24% of particles number peak value with respect to diesel (Figure 4.14) whereas, no appreciable difference between RME B30 and diesel were observed.

Moreover, as far as diesel fuel is concerned, a slight shift of PN distribution towards bigger diameters was observed (Figure 4.14). The increase of mean diameter of particle of diesel is mainly to the lower dilution ratio. At 1500 rpm @ 5 bar BMEP operating condition, the dilution ratio with diesel was 71, while a DR of almost 86 was used during tests with both RME B30 and HVO B30. The lower dilution ratio used with diesel could mitigate nanoparticles detection.

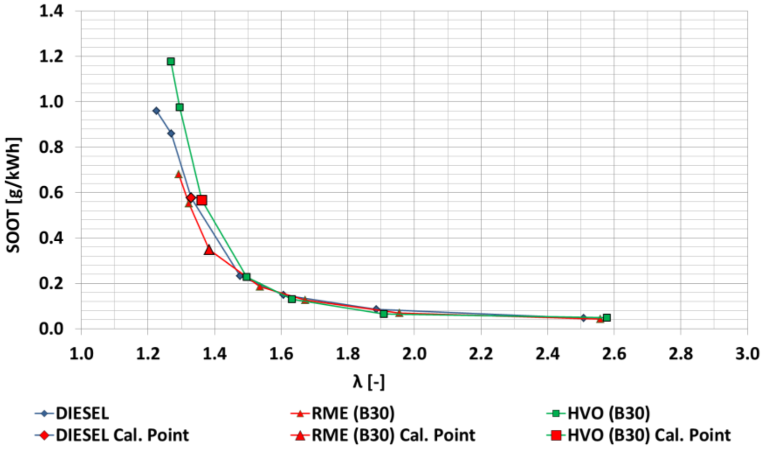

Figure 4.13 Soot-λ tradeoff curve with all fuels at 1500 rpm @ 5 bar BMEP

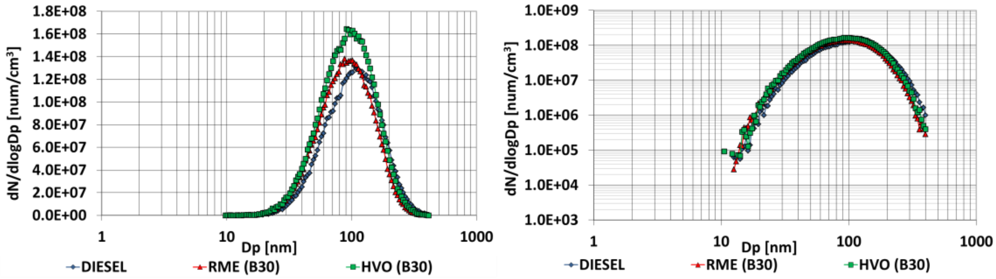

Figure 4.14 PN distribution at 1500 rpm @ 5 bar BMEP: semi-log graph (left), log-log graph (right)

High load operating point (1500 rpm @ 8 bar BMEP)

A further increase in engine load from 5 bar to 8 bar does not lead to any appreciable variations in number distributions for all fuels (Figure 4.15). The peak distribution diameter lied at almost 80 nm for all fuels; it should be noticed that during RME operation an increase of nanoparticles was observed. The reason for high concentration of nanoparticles of RME B30 could be due to the high local oxygen availability which enhanced soot oxidation which led to a decrease of the size of PM.

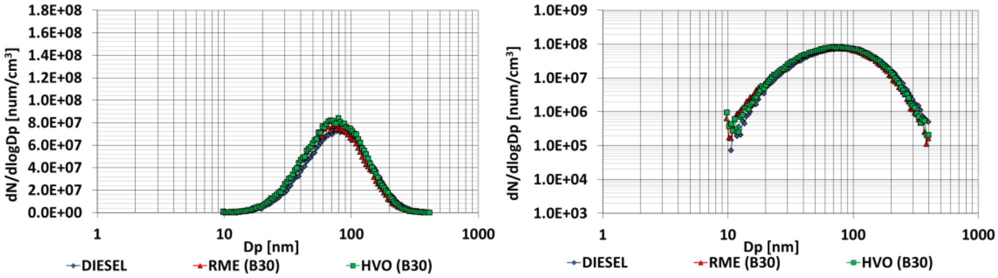

Figure 4.15 PN distribution at 1500 rpm @ 8 bar BMEP: semi-log graph (left), log-log graph (right)

4.2.2.2 Biodiesel feedstock comparison

In order to gather more information on the effect that different biodiesel feedstocks may have on PM emissions, tests were performed under part load conditions and with 5 different fuels i.e. reference diesel, RME and JME B30, RME and JME B100. As an example Figure 4.16 shows results obtained running the engine at 2500 rpm @ 8 bar BMEP with all tested fuels. Results confirmed the outcomes highlighted in the previous section, i.e. with B30 blends negligible differences on PM particles number distributions were observed respect to diesel. On the contrary, when neat biodiesels were adopted, an appreciable reduction on

PM particles number distribution was observed (45% on average) if compared to other fuels. Moreover, when neat biodiesels were used, a slight shift of the PM particles number distribution geometric mean Dp value of almost 15% and 33% was observed with respect to B30 blends and diesel respectively. Finally, different feedstocks led to similar PN distributions, therefore the nature of the source of biodiesel did not affect PM emissions, result which confirmed outcomes discussed previously related to the biodiesel feedstock origin (Chapter 2).

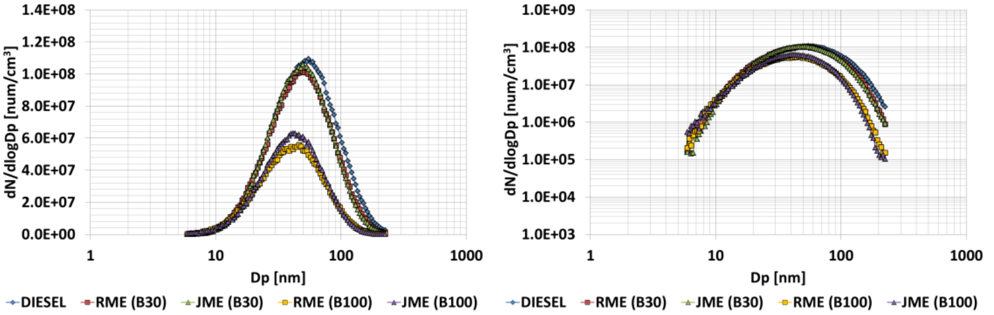

Figure 4.16 PN and size distributions with diesel, RME and JME (B30 and B100) at 2500 rpm @ 8 bar BMEP

4.2.3 PM mutagenic characterization

Results concerning toxicological assessment of PM emitted from engine fuelled with conventional diesel and biofuels are described in the present section. Table 4.3 lists the revertants levels obtained during Ames test as an average of three measurements at different dilution ratios. In more detail Table 4.3 lists the average and the standard deviation of spontaneous revertants, of rerertants which were induced by standard mutagen, and finally of revertants related to PM each sample which was tested.

Analysis results highlighted that samples were more sensible at strain TA98 instead of TA100 one, thus suggesting that the sampled PM was composed mainly of compounds which when reacting with mutagens caused frameshift mutations (see section 2.9 for more details). Moreover, it should be noticed that TA98 caused mutations in both cases: with and without metabolic activation. Therefore, the mutagenic activity could be determined by means of compounds and molecules directly or indirectly, i.e. taking into account metabolic reactions.

In order to wrap up some conclusions, the following remarks could be done: PM produced with all three fuels, was sensible to strain TA98 (with and without metabolic activation); the adoption of strain TA100 gave positive response only in the case without metabolic activation and only when the minimum dilution ratio was tested (see Table 4.3). In addition, as far as diesel fuel is concerned, a toxic activity with strain TA98-S9 was observed only when the sample with the minimum dilution ratio was tested. This activity was null when S9 fraction was used, thus suggesting its detoxifying activity of S9 fraction. Finally, tests performed with TA100-S9 on samples with the minimum dilution ratio (for all fuels) demonstrated, as well, that the toxicity is annulled in presence of metabolic activation.

In order to appreciate better the outcomes of Ames test and to compare results which are referred to different fuels, the levels of mutagenicity ratio and net revertants number calculated per mg of PM and m^3 of sampled air are listed for each of the tested strains in Table 4.4.

It should be taken into account the fact that: results expressed as Rev/m^3 and MG/m^3 were definitely too high, due to the fact that they are referred to samples which were collected directly from the exhaust system of the engine, thus without being diluted first at high dilution ratio representative of real life conditions.

Finally, an increase in biological activity, measured as MR/mg, for samples sourced from HVO (B30) fuel respect to samples derived by other fuels was observed (Table 4.4).

Table 4.3 Number of revertants with different mutagens for all the tested samples (red fonts are referred to toxic activity)

	TA 98 - S9	Colonies number (average ± st. deviation)	TA 100 - S9	Colonies number (average ± st. deviation)
	Spontaneous	21 ± 1	Spontaneous	112 ± 13
	2NF	440 ± 93	SA	1058 ± 201
DIESEL	0.2 mg/plate	toxic	0.2 mg/plate	toxic
	0.1 mg/plate	67 ± 16	0.1 mg/plate	236 ± 26
	0.02 mg/plate	36 ± 2	0.02 mg/plate	155 ± 23
	0.01 mg/plate	30 ± 6	0.01 mg/plate	187 ± 13
	0.002 mg/plate	22 ± 1	0.002 mg/plate	140 ± 20
RME (B30)	0.3 mg/plate	99 ± 14	0.3 mg/plate	toxic
	0.1 mg/plate	58 ± 4	0.1 mg/plate	222 ± 18
	0.03 mg/plate	44 ± 9	0.03 mg/plate	145 ± 17
	0.01 mg/plate	25 ± 7	0.01 mg/plate	180 ± 17
	0.003 mg/plate	26 ± 9	0.003 mg/plate	140 ± 17
HVO (B30)	0.2 mg/plate	124 ± 5	0.2 mg/plate	toxic
	0.1 mg/plate	70 ± 8	0.1 mg/plate	250 ± 54
	0.02 mg/plate	32 ± 5	0.02 mg/plate	177 ± 21
	0.01 mg/plate	24 ± 6	0.01 mg/plate	136 ± 23
	0.002 mg/plate	28 ± 6	0.002 mg/plate	138 ± 9
	TA 98 + S9	Colonies number (average ± st. deviation)	TA 100 + S9	Colonies number (average ± st. deviation)
	Spontaneous	30 ± 13	Spontaneous	137 ± 16
	2AF	2757 ± 157	2AF	1160 ± 308
DIESEL	0.2 mg/plate	43 ± 14	0.2 mg/plate	154 ± 16
	0.1 mg/plate	42 ± 5	0.1 mg/plate	134 ± 18
	0.02 mg/plate	27 ± 1	0.02 mg/plate	128 ± 11
	0.01 mg/plate	28 ± 1	0.01 mg/plate	118 ± 19
	0.002 mg/plate	24 ± 11	0.002 mg/plate	126 ± 18
RME (B30)	0.3 mg/plate	35 ± 11	0.3 mg/plate	191 ± 72
	0.1 mg/plate	35 ± 13	0.1 mg/plate	201 ± 5
	0.03 mg/plate	23 ± 2	0.03 mg/plate	162 ± 14
	0.01 mg/plate	21 ± 6	0.01 mg/plate	135 ± 30
	0.003 mg/plate	20 ± 3	0.003 mg/plate	144 ± 28
HVO (B30)	0.2 mg/plate	60 ± 18	0.2 mg/plate	139 ± 19
	0.1 mg/plate	49 ± 9	0.1 mg/plate	142 ± 12
	0.02 mg/plate	19 ± 7	0.02 mg/plate	134 ± 10
	0.01 mg/plate	22 ± 6	0.01 mg/plate	143 ± 14
	0.002 mg/plate	14 ± 4	0.002 mg/plate	110 ± 8

Table 4.4 Mutagenicity ratio and net revertants number for all fuels

DIESEL				
Strain	MR/mg	MR/m^3	Rev/mg	Rev/m^3
TA 98 -	21	412	429	8504
TA 98 +	0	0	0	0
TA 100 -	9	176	1014	19816
TA 100 +	0	0	0	0
RME (B30)				
Strain	MR/mg	MR/m^3	Rev/mg	Rev/m^3
TA 98 -	12	317	250	6587
TA 98 +	0	0	0	0
TA 100 -	8	213	903	23933
TA 100 +	0	0		0
HVO (B30)				
Strain	MR/mg	MR/m^3	Rev/mg	Rev/m^3
TA 98 -	18.5	264	504	7239
TA 98 +	5	79	163	2365
TA 100 -	10	145	1157	16433
TA 100 +	0	0	0	0

Conclusions

The effects of using high percentage blends of ultra low sulphur diesel and biofuels (FAME and HVO) in a Euro 5 small displacement passenger car diesel engine on combustion process, full load performance and part load emissions have been evaluated in this thesis. Moreover, a characterization of PM in terms of mass, chemical composition and particles number and size distribution was assessed as well.

In addition a comparison between two different FAME feedstocks, sourced by rapeseed and jatropha respectively was assessed running the engine at full and part load. At full load operating conditions, without any modifications to the ECU calibration, when fuelling the engine with blended (at 30% v/v blending ratio) and neat FAME a noticeable decrease (4% and 7% respectively) in the torque output was observed over almost the entire speed range due to the lower LHV of the biofuels that could not be fully compensated by the small increase in fuel density. Smoke levels measured under RME B30 blend operations were significantly lower in comparison with diesel operation, showing impressive FSN reductions. With an adjusted ECU calibration, the same torque levels measured under diesel operation could be obtained with the B30 blends, while with B100 blends a slight increase in torque output was achieved in medium-low load region, thanks to a shift of the compressor operating points which led to higher boost pressures. Smoke levels were found to be lower for both B30 and B100 in comparison with diesel fuel, for all tested operating points. This behavior highlights the potential for maintaining at least the same level of performance while achieving substantial emissions benefits. FAME blends were then evaluated at several part load operating conditions, representative of the New European Driving Cycle. With the adoption of a specific calibration a 4% on average rise of fuel consumption for B30 (12% on average for B100), on a mass basis, was highlighted at same fuel conversion efficiency and comparable CO_2 emissions; if fuel consumption are evaluated on a volume basis, as perceived by the final user, the higher biofuel density partially compensate its lower energy content, thus leading to volumetric fuel consumption increases of 2.5% and 7% for B30 and B100, respectively. Moreover, a noticeable increase of CO and HC emissions at low load could be noticed, along with a significant NO_x emissions decrease, and a considerable smoke emission reduction. As far as biodiesel feedstock effects are concerned, no significant emission variations could be highlighted between RME and JME blends, both B30 and B100, despite noticeable differences in terms of chemical properties, and in cetane number in particular. These results can be attributed, at least in part, to the use of a closed loop combustion control system, which therefore appeared to be robust enough to tolerate the changes in the fuel properties.

Recently, Hydrotreated Vegetable Oil (HVO), obtained by means of a refinery-based process that converts vegetable oils into paraffinic hydrocarbons, has been gaining an increasing attention. A comparison between HVO and RME B30 blends was therefore evaluated. At full load operating conditions, as far as the HVO B30 blend is concerned, levels of torque output comparable with reference diesel (with differences lower than 1% on average) could be observed over almost the entire speed range, while smoke emissions were generally still appreciably lower in comparison with diesel values. With an adjusted ECU calibration, the same torque levels measured under diesel operation could be obtained. At part load operating conditions, representative of the New European Driving Cycle, with the specifically adjusted calibration, a 4% average rise of fuel consumption, on a mass basis, at same fuel conversion efficiency and CO_2 emissions was found for the RME blend, while no significant variations were found for the HVO blend. CO and HC specific emissions were significantly reduced with both RME and HVO B30 blends at low and medium loads, while only modest or even insignificant variations were registered at higher loads. This behavior is more evident for the HVO blend, likely due to the better ignition quality of this fuel, and could therefore be emphasized when considering engine cold conditions (i.e. the conditions at the start of the relevant homologation testing procedures). NO_x emissions with the two biofuel blends were generally comparable with those of the reference diesel fuel, while a noteworthy reduction of smoke levels could generally be observed for medium and high load operating conditions, especially for the RME B30 fuel.

PM characterization in terms of PM mass, chemical composition and PN distributions for diesel, RME B30 and HVO B30 was then evaluated. Gravimetric analysis showed an increase of 30% of PM mass for RME B30 respect to diesel due to its higher distillation temperature, whereras HVO blend showed 30% lower specific PM emissions. At medium and high load condition, a noticeable reduction of PM for both RME and HVO respect to diesel was observed, due to local oxygen availability in RME molecule and lack of aromatics hydrocarbons in the case of HVO which led to lower soot emissions. PM gravimetric analysis at medium and high load operating points showed a good correlation with soot measurements carried out by means of standard laboratory equipment (i.e. smokemeters). On the contrary, at low loads, the same instrument underestimated the Soluble Organic Fraction (SOF) fraction of PM especially when biofuel was used. Thermo-gravimetric analysis confirmed the outcomes from gravimetric analysis: the significance of standard measurements which are commonly carried out during the engine calibration activity should therefore be carefully considered when biofuels are concerned. PM particles number and size distribution investigation carried out running the engine with conventional and bioderived fuels showed that with B30 blends negligible differences on PM particles number distributions were observed respect to diesel. On the contrary, when neat biodiesels were adopted, an appreciable reduction on PM particles number distribution was observed (45% on average) if compared to diesel fuel. Finally, different feedstocks led to similar PN distributions, i.e. the nature of the source of biodiesel did not affect PM emissions. Finally toxicological analysis on PM emitted when the engine was fuelled with diesel, RME B30 and HVO B30 showed an increase in biological activity, for samples sourced from HVO (B30) fuel respect to samples derived by diesel and RME fuels.

Bibliography

2008/692/EC. "Implementing and amending Regulation (EC) N. 715/2007 of the European Parliament and of the Council on type-approval of motor vehicles with respect to emissions from light passenger and commercial vehicles (Euro 5 and Euro 6)." July 18, 2008.

Abdul-Khalek, I. S., Kittelson, D. B. "The Influence of Dilution Conditions on Diesel Exhaust Particle Size Distribution Measurements." *SAE Technical Paper 1999-01-1142*, 1999.

Abdul-Khalek, I. S., Kittelson, D. B., Graskow, B. R., Wei, Q. "Diesel Exhaust Particle Size: Measurement Issues and Trends." *SAE Technical Paper 980525*, 1998.

Badami, M., Mallamo, F., Millo, F., Testa, D. "ICE Analyzer: a Data Acquisition System for Internal Combustion Engines." *National Instruments Automotive Users' Conference.* Turin, 2001.

Beatrice, C., Di Iorio, S., Guido, C., Mancaruso, E., Vaglieco, B.M., Vassallo, A. «Alternative Diesel Fuels Effects on Combustion and Emissions of an Euro4 Automotive Diesel Engine.» *SAE Tecnhical Paper 2009-24-0088*, 2009.

Bhave, A., Kraft, M., Montorsi, L., Mauss, F. "Sources of CO emissions in an HCCI engine: A numerical analysis." *Combustion and Flame* 144 (2006): 634-641.

Cisternino, M. "Influence of Mild Hybridization on Performance and Emission n a 4 Cylinder in-Line Common Rail Diesel Engine." *Directions in Engine Efficiency and Emissions Research (DEER) Conference.* Detroit, 2010.

Czarnowski, R. "Can Future Emissions Limits be Met with a Hybrid EGR System Alone?" Edited by Us Dept. of Energy. *Diesel Engine Emissions and Energy Reduction Conference (DEER).* Detroit, 2008.

De Filippo, A. "Characterization of carbonaceous nanoparticle size distributions (1-10 nm) emitted from laboratory flames, diesel engines and gas appliances." *Ph.D. Thesis.* 2009.

Dieselnet. *"Appendix: Biodiesel Composition and Properties of Components".* 2009. http://www.dieselnet.com/tech/fuel_biodiesel_app.php (accessed on January 2013).

—. *Emission Standards - Europe - Cars GHG - ACEA Agreements.* October 2010. http://dieselnet.com/standards/eu/ghg_acea.php (accessed January 2012).

—. *Emissions Standards - Europe - Cars and Light Trucks.* 2011. http://dieselnet.com/standards/eu/ld.php (accessed January 2012).

—. *Emissions Standards - USA - Cars and Light-Duty Trucks - Tier 2.* 2011. http://dieselnet.com/standards/us/ld_t2.php (accessed January 2012).

Dorenkamp, R. "Volkswagen's Exhaust Gas Aftertreatment Concepts to Meet the Lowest Emissions Standards." *FAD Conference.* Dresden, 2008.

EN 14907:2005. «Standard gravimetric measurement method for the determination of the PM2.5 mass fraction of suspended particulate matter.» s.d.

EPA, US. *"Air Quality Criteria Document for Particulate Matter" Volume I & II.* October 2004. http://www.epa.gov/oar/particlepollution/publications.htlm (accessed January 2012).

Herbert, A.J., and Russel, M.F. «Measurement of combustion noise in diesel engines.» *Mech. Eng. Technolology*, 1982.

Hulkkonen, T., Hillamo, H., Sarjovaara, T. and Larmi, M.,. «Experimental Study of Spray Characteristics between Hydrotreated Vegetable Oil (HVO) and Crude Oil Based EN 590 Diesel Fuel.» *SAE Techical Paper 2011-24-0042*, 2011.

Joergl, V. "Can Future Emissions Limits be Met with a Hybrid EGR System Alone?" *IAV MinNOx Conference.* Berlin, 2008.

Johnson, T.V. "Diesel Emission Control in Review." *SAE International Journal of Fuels and Lubricants* 02, no. 01 (October 2009): 1 - 12.

Johnson, T.V. "Diesel Emissions in Review." *SAE International Journal of Engines* 04, no. 01 (December 2011): 143 - 157.

Johnson, T.V. "Review of CO2 Emissions and Pertinent Powertrain Technologies." *SAE Technical Paper 2010-01-1276*, 2010.

Kittelson, D.B. "Engines and nanoparticles: a review." *Journal of Aerosol Science* 29, no. 05-06 (1998): 575 - 588.

Köerfer, T. "The Future Power Density of HSDI Diesel Engines with Lowest Engine out Emissions – A Key Element for Upcoming CO2 Demands." *FISITA Conference.* Munich, 2008.

Körfer, T., Lamping, M., Kolbeck, A., Pischinger, S. "Potential of Modern Diesel Engines with Lowest Raw Emissions - a Key Factor for Future CO2 Reduction." *SAE Technical Paper 2009-26-0025*, 2009.

Krüger, M., Cornetti, G., Greis, A., Weidmann, U., Schumacher, H., Ger, J. "Operational Strategies of a Diesel Hybrid Electric Vehicle with Focus on the Combustion Engine." *Aachen Colloquium.* Aachen, 2010.

Lüders, H., Krüger, M., Stommel, P., Lüers, B. "The Role of Sampling Conditions in Particle Size Distribution Measurements." *SAE Technical Paper 981374*, 1998.

Maricq, M., Giuliano, J., Szente, J., Tennison, P. "Effects of B20 versus ULSD Fuel on Diesel Engine PM Emissions and Aftertreatment Performance." *SAE International Journal of Engines* 03, no. 01 (August 2010): 581 - 596.

Mattes, W. "BMW Diesel - Engine Concepts for Efficient Dynamics." Edited by US Dept. of Energy. *Diesel Engine Emissions and Energy Reductions Conference (DEER).* Detroit, 2008.

Method 8030 B - Salmonella Microsomial Mutagenicity test. (2005).

Mikkonen, S., Hartikka, T., Kuronen M., Saikkonen, P. «HVO, Hydrotreated Vegetable Oil – A Premium Renewable Biofuel For Diesel Engines.» s.d.

Millo, F., Bianco, A., Grange, T., Voicu, I. «The effects of neat biodiesel usage on performance and exhaust emissions from a small displacement passenger car diesel engine.» *SAE Technical Paper 2010-01-1515*, 2010.

Millo, F., Bianco, A., Vezza, D. S., Vlachos, T., Ciaravino, C., Vassallo, A.,. «Biodiesel fuelling impact on performance and emissions of a Euro5 small displacement passenger car diesel engine.» *SEEP2010 Conference Proceedings.* Bari, 2010.

Millo, F., Ferraro, C.V., Vezza, D.S., Vlachos, T. «Analysis of Performance and Emissions of an Automotive Euro 5 Diesel Engine Fuelled with B30 from RME and JME.» *SAE Paper 2011-01-0328*, 2011.

Millo, F., Mallamo, F., Vlachos, T., Ciaravino, C., Postrioti, L., Buitoni, G. "Experimental Investigation on the Effects on Performance and Emissions of an Automotive Euro 5 Diesel Engine fuelled with B30 from RME and HVO." *SAE Tecnhical Paper 2013-01-1679*, 2013.

Mueller, C.J., Upatnieks, A. "Dilute clean diesel combustion achieves low emissions and high efficiency while avoiding control problems of HCCI." *11th Diesel Engine Emissions Reduction Conference (DEER).* Chicago (IL), 2005.

Postrioti, L., Grimaldi, C. N., Ceccobello, M., Di Gioia, R. «Diesel Common Rail Injection System Behavior with Different Fuels.» *SAE Paper 2004-01-0029*, 2004.

Sakono, T., Nakai, E., Kataoka, M., Takamatsu, H., Terazawa, Y. "Mazda SKYACTIV-D 2.2L Diesel Engine." *20th Aachen Colloquium Automobile and Engine Technology.* Aachen, 2011.

Sharp, C., Howell, S., Jobe, J. «The Effect of Biodiesel Fuels on Transient Emissions from Modern Diesel Engines.» *SAE Technical Paper 2000-01-1967*, 2000.

Sugiyama, K., Goto, I., Kitano, K., Mogi, K., and Honkanen, M. «Effects of Hydrotreated Vegetable Oil (HVO) as Renewable Diesel Fuel on Combustion and Exhaust Emissions in Diesel Engine.» *SAE Techical Paper 2011-01-1954*, 2011.

Tao, F., Liu, Y., Rempelewert, B.H., Foster, D.E., Reitz, R.D., Choi, D., Miles, P. "Modeling the effects of EGR and injection pressure on soot formation in a high-speed direct-injection (HSDI) diesel engine using a multi-step phenomenological soot model." *SAE paper 2005-01-0121*, 2005.

Tatur, M. "Future Directions in Engines and Vehicles." Edited by US Department of Energy. *Directions in Engine Efficiency and Emissions Research (DEER) Conference.* Detroit, 2010.

Tomoda, T., Ohki, H., Koyama, T., Fujiwara, K. "Study of Diesel Combustion Improvement for Ultra Low Compression Ratio." *Aachen Colloquium.* Aachen, 2010.

TSI. "Scanning Mobility Particle Sizer User Manual." 2006.

Van Gerpen, Jon H., Yang, David Y.,. «Determination of Particulate and Unburned Hydrocarbon Emissions from Diesel EnginesFueled with Biodiesel.» *SAE Technical Paper 982527*, 1998.

List of Publications

[1] Millo, F., Mallamo, F., Vlachos, T., Ciaravino, C., Postrioti, L., Buitoni, G., “Experimental Investigation on the Effects on Performance and Emissions of an Automotive Euro 5 Diesel Engine fuelled with B30 from RME and HVO”, Sae Technical Paper, 2013-01-1679, 2013.

[2] Millo, F., Iannielli, R., Mallamo, F., Vlachos, T., Ciaravino, C., “Effects of B30 and HVO30 on Performance and Emissions of a Euro 5 Small Displacement Automotive Diesel Engine”, Diesel Powertrain Conference, Rouen (France), June 2012.

[3] Millo, F., Vezza, D., Vlachos, T., Fino, D. et al., "Impact of Engine Operating Conditions on Particle Number and Size from a Small Displacement Automotive Diesel Engine", Sae Technical Paper 2012-01-0429, doi:10.4271/2012-01-0429, 2012.

[4] Millo, F., Vezza, D.S., Vlachos, T., De Filippo, A., Ciavarino, C., Russo, N., Fino, D., “Particle Number and Size Emissions from a Small Displacement Automotive Diesel Engine: bioderived vs. conventional fossil fuels”, Industrial & Engineering Chemistry Research, vol. 51, pp. 7565-7572, ISSN 0888-5885, 2012.

[5] Millo, F., Vezza, D.S., Vlachos, “Performance and emissions of a Euro5 small diesel engine fuelled with biodiesel.”, International Journal Of

Automotive Technology And Management, vol. 12 n. 3, pp. 252-272. - ISSN 1470-9511, 2012.

[6] Millo, F., Ferraro, C. V., Vezza, D.S., Vlachos, T., "Analysis of Performance and Emissions of an Automotive Euro 5 Diesel Engine Fuelled with B30 from RME and JME", Sae International Journal Of Fuels And Lubricants, vol. 4, pp. 9-22, ISSN: 1946-3952, DOI: 10.4271/2011-01-0328, 2011.

[7] Caroca, J. C., Millo, F., Vezza, D.S., Vlachos, T., De Filippo, A., Bensaid, S., Russo, N., Fino, D., "Detailed Investigation on Soot Particle Size Distribution during DPF Regeneration, using Standard and Bio-Diesel Fuels", Industrial & Engineering Chemistry Research, Vol. 50, n.5, pp.. 2650-2658, ISSN: 0888-5885, DOI: 10.1021/ie1006799, 2011.

[8] Millo, F., Vezza, D.S., Vlachos, T., Fino, D., Russo, N., De Filippo, A, "Particle Number and Size Distribution from a small displacement automotive diesel engine during DPF regeneration", Sae Technical Paper, Vol. 2010-01-1552, ISSN: 0148-7191, 2010.

[9] Millo, F., Vezza, D.S., Vlachos, T., "Effects of Rapeseed and Jatropha Methyl Ester on Performance and Emissions of a Euro 5 Small Displacement Automotive Diesel Engine", SAE Technical Paper 2011-24-0109, DOI: 10.4271/2011-24-0109, 2011.

[10] De Filippo, A., Ciaravino, C., Millo, F., Vezza, D.S., Fino, D., Russo, N., Vlachos, T., "Particle Number, Size and Mass Emissions of Different Biodiesel Blends Versus ULSD from a Small Displacement Automotive Diesel Engine", XXXIV Meeting of the Italian Section of the Combustion Institute, Rome, 24-26/10/2011.

[11] Caroca, J.C., Millo, F., Vezza, D., Vlachos, T., De Filippo, A., Bensaid, S., Fino, D., Russo, N., "Detailed Investigation on Soot Particle Size Distribution during DPF regeneration, using Standard and Bio-Diesel", Proceedings of the International Conference on Processes and Technologies for a Sustainable Energy (PTSE 2010): 33rd Event of Event of the Italian Section of The Combustion Institute and Second S4FE, Ischia, Naples (Italy) 30 June - 3 July 2010, 2010.

[12] Millo, F., Bianco, A., Vezza, D.S., Vlachos, T., Ciaravino, C., Vassallo, A., "Biodiesel fuelling impact on performance and emissions of a Euro5 small displacement passenger car diesel engine", 4th International

conference on sustainable energy & environmental protection, Bari 29 June - 2 July 2010, pp. 11, 2010.

[13] Millo, F., Vezza, D.S., Vlachos, T., Fino, D., Russo, N., De Filippo, A., "Particle Number and Size Distribution from a small displacement automotive diesel engine during DPF regeneration", Sae International Journal Of Fuels And Lubricants, vol. 3 n. 2, pp. 404-413. - ISSN 1946-3952, 2010

Appendix I – PM estimation on the basis of FSN measurements

I.1 Introduction

Contrary to gaseous diesel emissions, PM is not well defined. PM is traditionally divided into the following three main fractions: the solid fraction consisted mainly by elemental carbon and ashes, the soluble organic fraction (SOF) derived mainly from the fuel and the lubricating oil which condense and absorb on soot particles or directly nucleate to new PM particles and sulfate particulates (Figure I.1). Moreover, the properties of PM depend on the fuel, engine technology, operating conditions, and exhaust aftertreatment. Therefore, due to PM complexity does not exist a single absolute measure method for particulate matter.

Because of simple operability, the fast data availability and the clear indication of the emitted soot concentration in the exhaust gas of internal combustion engines, instruments which operate on the basis of in situ optical smoke measurement techniques such as the smokemeters have become the standard for engine test bed. In more detail smokemeters detect the fractional reduction in reflectance by a smoke filter due to the blackening of its surface by soot. Therefore for the estimation of PM emissions the effects of fuel and oil consumption and fuel sulphur content have to be taken into account as well.

In the following sections the estimation of PM emissions using the AVL and MIRA relationships will be presented. Both formulas calculate PM emissions on the basis of smoke measurements performed by means of smokemeters. It should be noticed that both methods adopt the same formula for estimating PM emissions, while the difference between methods is related to specific soot emissions calculation. In both cases PM emissions are estimated according the following expression:

$$PM\left[\frac{gr}{kWh}\right] = SOOT\left[\frac{gr}{kWh}\right] + 0.1 \cdot BSHC\left[\frac{gr}{kWh}\right] + \frac{0.09 \cdot BSFC\left[\frac{gr}{kWh}\right] \cdot S[\%]}{100} + 0.1 \cdot B_{oil}\left[\frac{gr}{kWh}\right]$$

Where SOOT is the specific soot emissions, BSFC and BSHC are the brake specific fuel consumption and HC emissions respectively, S is the fuel sulphur content and Boil is the oil consumption.

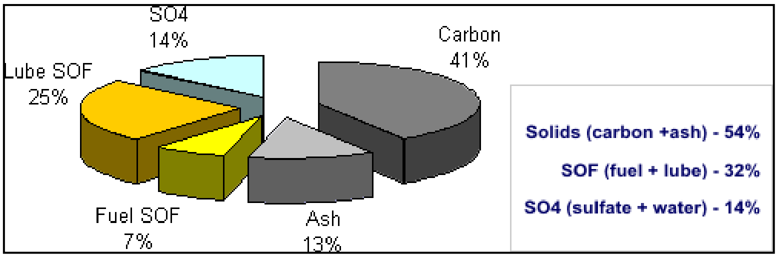

Figure I.1. An example of a typical chemical composition of PM

I.2 AVL relationship

According to AVL method, specific soot emissions could be estimated by means of the following formulas:

$$SOOT_{AVL}\left[\frac{gr}{kWh}\right] = \frac{SOOT_{AVL}\left[\frac{gr}{h}\right]}{P[kW]}$$

$$SOOT_{AVL}\left[\frac{gr}{h}\right] = \frac{SOOT_{ConcAVL}\left[\frac{mg}{m^3}\right] \cdot G_{exh}\left[\frac{gr}{h}\right]}{1.183 \cdot 10^{-3}}$$

Where P is the engine power, Gexh is the exhaust gases mass flow and $SOOT_{ConcAVL}$ is the concentration of SOOT calculated on the basis of FSN measurements as follows:

$$SOOT_{ConcAVL}\left[\frac{mg}{m^3}\right] = \frac{4.95 \cdot FSN \cdot e^{(0.38 \cdot FSN)}}{0.406}$$

I.3 MIRA relationship

In the case of MIRA method specific soot emission are calculated according to the following expressions:

$$SOOT_{MIRA}\left[\frac{gr}{kWh}\right] = \frac{SOOT_{MIRA}\left[\frac{gr}{h}\right]}{P[kW]}$$

$$SOOT_{MIRA}\left[\frac{gr}{h}\right] = SOOT[-] \cdot G_{exh}$$

Where Gexh is the exhaust gases mass flow while the variable SOOT is calculated as follows:

$$SOOT1 = 3.07 \cdot 10^{-5} \cdot FSN^5$$

$$SOOT2 = SOOT1 - 6.69 \cdot 10^{-5} \cdot FSN^4$$

$$SOOT3 = SOOT2 - 7.02 \cdot 10^{-4} \cdot FSN^3$$

$$SOOT4 = SOOT3 + 1.462 \cdot 10^{-2} \cdot FSN^2$$

$$SOOT = SOOT4 + 7.636 \cdot 10^{-3} \cdot FSN$$

I.4 AVL and MIRA methods comparison

Figure I.2 depicts the comparison between the abovementioned methods. It should be noticed that in a range of smoke emissions from 1 up to 5 FSN, MIRA method overestimates PM emission respect to AVL and viceversa for higher smoke emissions.

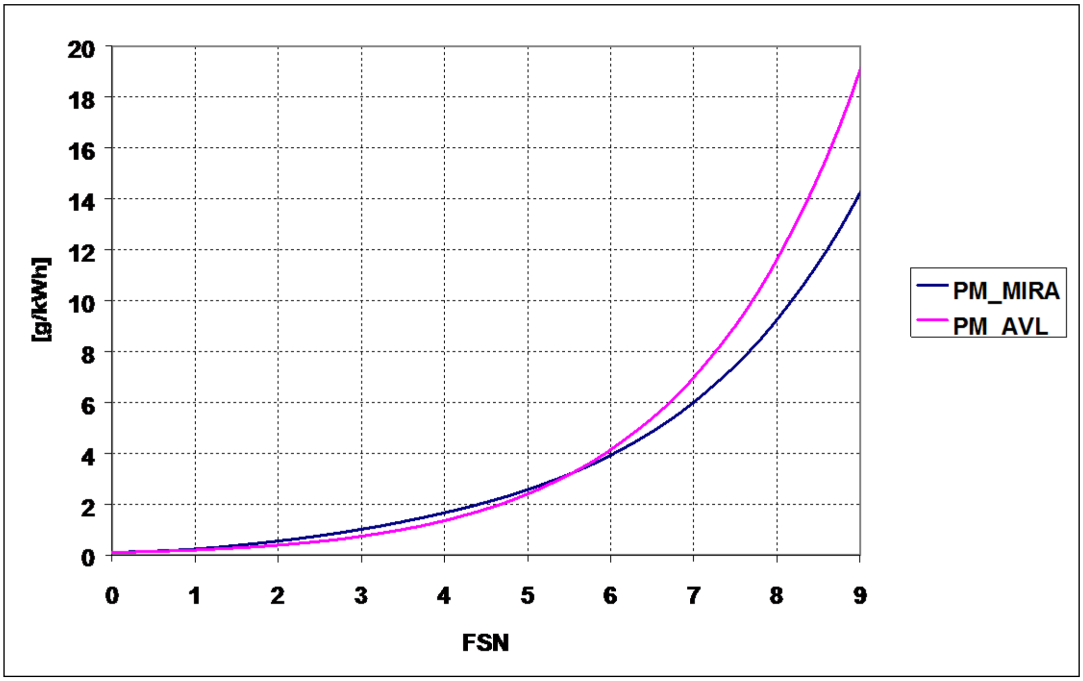

Figure I.2 Comparison between MIRA and AVL methods